

KERNFORSCHUNGSZENTRUM

KARLSRUHE

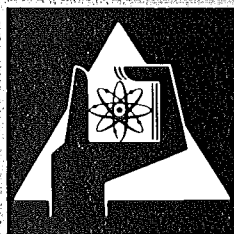
August 1977

KFK 2461

Institut für Angewandte Kernphysik

**Operation of the Karlsruhe Isochronous
Cyclotron in 1976**

F. Schulz, H. Schweickert



**GESELLSCHAFT
FÜR
KERNFORSCHUNG M.B.H.**

KARLSRUHE

Als Manuskript vervielfältigt

Für diesen Bericht behalten wir uns alle Rechte vor

GESELLSCHAFT FÜR KERNFORSCHUNG M. B. H.
KARLSRUHE

KERNFORSCHUNGSZENTRUM KARLSRUHE

KFK 2461

Institut für Angewandte Kernphysik

Operation of the Karlsruhe Isochronous Cyclotron
in 1976

F. Schulz and H. Schweickert

Gesellschaft für Kernforschung mbH, Karlsruhe

Abstract

The operation of the Karlsruhe Isochronous Cyclotron in 1976 is briefly surveyed. The status and the results of the following technical developments are briefly described:

- Computer aided cyclotron operation
- New correction coils for the cyclotron
- Non-intercepting measurement of the extraction rate
- Lambshift source for polarized deuterons
- Improvements of the ${}^6\text{Li}^{3+}$ -Penning ion source
- New beam line to an irradiation room for machine parts
- Nova 2 computer system for nuclear physics experiments
- Routine production of Iodine-123 for nuclear medicine

In the annual report 1975 we have included a section consisting of a series of brief reports on applied research in progress. This year we give a compilation of the current basic nuclear physics work at our cyclotron. The short papers prepared by the experimental groups are arranged according to the following topics:

- Experiments using the 156 MeV ${}^6\text{Li}^{3+}$ -beam
- Experiments using the 52 MeV polarized deuteron beam
- Further nuclear reactions
- Nuclear spectroscopy
- Measurements of nuclear magnetic moments
- Measurements with the neutron time-of-flight spectrometer

Zusammenfassung

Betrieb des Karlsruher Isochron Zyklotrons im Jahre 1976

Es wird ein kurzer Überblick über den Betrieb des Karlsruher Isochron Zyklotrons im Jahre 1976 gegeben. Ferner wird über den Stand und die Ergebnisse folgender Weiterentwicklungen an der Beschleunigeranlage berichtet:

- Rechnerunterstützung des Zyklotronbetriebes
- Neue Korrekturspulen für das Zyklotron
- Berührungslose Messung der Extraktionsrate
- Lambshiftquelle für polarisierte Deuteronen
- Verbesserungen an der ${}^6\text{Li}^{3+}$ -Penning-Ionenquelle
- Strahlführung in den Bestrahlungsraum für Verschleißmessungen
- Nova 2-Rechnersystem für kernphysikalische Experimente
- Routineproduktion von Jod-123 für die Nuklearmedizin

Nachdem wir im Jahresbericht 1975 einen Überblick über die anwendungsorientierte Forschung an dem Beschleuniger gegeben haben, werden in einem Anhang zu diesem Bericht die aktuellen kernphysikalischen Arbeiten beschrieben. Die Kurzberichte der Experimentatoren sind dabei in folgende Abschnitte eingeteilt:

- Experimente mit hochenergetischen (156 MeV) ${}^6\text{Li}^{3+}$ -Ionen
- Experimente mit polarisierten Deuteronen
- Sonstige Kernreaktionen
- Kernspektroskopie
- Messung von Kernmomenten
- Messungen am großen Flugzeitspektrometer

<u>TABLE OF CONTENTS</u>	Page
1. OPERATION SUMMARY F. Schulz, H. Schweickert	1
2. TECHNICAL DEVELOPMENTS	6
2.1 Computer Aided Cyclotron Operation W. Kappel, W. Karbstein, W. Kneis, J. Möllenbeck, H. Schweickert	6
2.2 New Correction Coils of the Cyclotron V. Bechtold, L. Friedrich, L. Wiss	10
2.3 New Computer Controlled Power Supplies for the Correction Coils of the Cyclotron W. Kappel, G. Klinger, E. Schönstein	14
2.4 Non-intercepting Measurement of the Extraction Efficiency at the Karlsruhe Cyclotron G. Haushahn, W. Maier, E. Röhrli	15
2.5 Present Status of the Karlsruhe Polarized Ion Source V. Bechtold, L. Friedrich, P. Ziegler	17
2.6 Improvements of the ${}^6\text{Li}^{3+}$ -Penning Ion Source J. Biber, H. Kuhn, F. Schulz	21
2.7 New Beam Line for Irradiation of Machine Parts G. Bauer, P. Kauther, Ch. Rämer	23
2.8 Nova-2-Computer-System for Nuclear Physics Experiments W. Karbstein, B. Kögel	26
2.9 First Attempts towards an Automatization of the Beam Guiding System W. Kneis	29
2.10 A Novel Method of ${}^{123}\text{J}$ -Routine-Production for Radio Diagnostical Purpose K.H. Assmus, F. Schulz, R. Schütz, H. Schweickert, F. Michel, H. Münzel	32
3. BASIC NUCLEAR PHYSICS AT THE CYCLOTRON	36
3.1 Experiments using the 156 MeV ${}^6\text{Li}^{3+}$ -Beam	36
3.1.1 Giant Resonance Excitation by 156 MeV ${}^6\text{Li}$ Scattering H.J. Gils, H. Rebel, J. Buschmann, H. Klewe-Nebenius	36
3.1.2 Investigation of the Compound Nuclear Reactions ${}^{191+193}\text{Ir}, {}^{197}\text{Au}({}^6\text{Li}, xn+yp)$ at $E_{\text{Li}} = 48 - 156$ MeV J. Kropp, H. Faust, J. Rieder, H. Klewe-Nebenius, H. Rebel, H.J. Gils, K. Wisshak	39
3.1.3 Scattering of ${}^6\text{Li}$ on ${}^{12}\text{C}, {}^{40}\text{Ca}, {}^{90}\text{Zr}, {}^{208}\text{Pb}$ at $E_{\text{Li}}=156$ MeV H.J. Gils, H. Rebel, J. Buschmann, S. Zagromski, H. Klewe-Nebenius, H. Faust	44

	Page
3.2 Experiments using the 52 MeV Polarized Deuteron Beam	48
3.2.1 Spin Determination of Selected Hole States by a Measurement of the Analysing Power of the (α , ^3He) Reaction H. Breuer, P. Doll, K.T. Knöpfle, G. Mairle, H. Riedesel, G.J. Wagner, V. Bechtold, L. Friedrich	48
3.2.2 Vector Analysing Power in d-p and d-d Elastic Scattering at 52 MeV V. Bechtold, L. Friedrich, M.S. Abdel-Wahab, J. Bialy, M. Junge, F.K. Schmidt	52
3.3 Nuclear Reactions with Unpolarized Deuterons and α -Particles	55
3.3.1 Decay Properties of Nuclear Hole States H. Breuer, P. Doll, K.T. Knöpfle, G. Mairle, H. Riedesel, K. Schindler, G.J. Wagner	55
3.3.2 Particle Decay from the Giant Resonance Region in ^{12}C H. Breuer, P. Doll, K.T. Knöpfle, G. Mairle, H. Riedesel, K. Schindler, G.J. Wagner	58
3.3.3 Nuclear Matter Sizes of $^{204,206,208}\text{Pb}$ from 104 MeV α -Particle Scattering H.J. Gils, H. Rebel, J. Buschmann, H. Klewe-Nebenius	61
3.3.4 Experimental Studies of Isoscalar Octupole Transition Rates and of Neutron Collectivities by α -Particle Scattering H.J. Gils, H. Rebel	64
3.3.5 ($\alpha, \alpha'\gamma$) Angular Correlation Measurements on sd-Shell Nuclei W. Eyrich, A. Hofmann, U. Scheib, S. Schneider, F. Vogler, H. Rebel	69
3.4 Nuclear Spectroscopy	72
3.4.1 Experimental Study of the Enhanced L=4 Transition in ^{140}Ce A. Hanser, H. Rebel, H. Buschmann, H.J. Gils, H. Klewe-Nebenius	72
3.4.2 Shape Factor Measurements on Short Lived β -Emitters W. Thies, H. Appel, R. Pesl, H. Behrens	76
3.5 Measurements of Nuclear Magnetic Moments	79
3.5.1 Determination of the Quadrupolemoment of the ($25/2^+$) Isomer in ^{117}Sb M. von Hartrott, K. Nishiyama, D. Quitmann, J. Rossbach, E. Weihreter	79
3.5.2 Spins and Magnetic Moments of Neutron Deficient Rb Isotopes by In-Beam Optical Pumping J. Collignon, F. Buchinger, R. Neugart, H. Schweickert	81

	Page
3.5.3 High Resolution Laser Spectroscopy of Radioactive Light Barium Isotopes G. Nowicki, K. Bekk, S. Göring, A. Hanser, H. Rebel, G. Schatz	83
3.5.4 Positron Trapping G. Gräff, D. Richter	86
3.6 Measurements with the Large Neutron Spectrometer	87
3.6.1 Isospin Mixing of $T = 3/2$ Isobaric Analog States in Light $T_z = 1/2$ Nuclei S. Cierjacks, I. Schouky	87
3.6.2 Precision Measurements of Fission Cross Section Ratios for ^{239}Pu and ^{240}Pu Relative to ^{235}Pu K. Kari, S. Cierjacks, D. Erbe, B. Leugers, G. Schmalz,	91
3.7 Measurements on Nuclear Fission	93
3.7.1 Determination of the Fission Barrier of ^{232}Pu from β -Delayed Fission D. Habs, H. Klewe-Nebenius, V. Metag, B. Neumann, H.J. Specht	93
PUBLICATIONS	96

1. OPERATION SUMMARY

F. Schulz, H. Schweickert

Institut für Angewandte Kernphysik/Zyklotron des
Kernforschungszentrums Karlsruhe

During the period of report the machine was in full operation (see table 1). The cyclotron beam was used for irradiations for 7722 hours, which amounts to 90.6 % of the total shift time. Since we needed no shut down time in this period and since the ratio of system failures to the total scheduled shift time decreased to 6.4 % the available beam time increased by 899 hours as compared to the past year. The present reduction of the unscheduled shut downs must partly be attributed to the cyclotron computer which is now in routine use. Again for approximately 12 % of the experimental time the axial injection system was used to study nuclear reactions with polarized deuterons (52 MeV) and high energy ${}^6\text{Li}^{3+}$ ions (156 MeV). Tables 1 to 4 show the operational statistic 1976 in a form similar to that of the previous reports ¹⁻²).

On the users' side (Table 3) now 47 % of our machine time is given to visitors from laboratories outside the Nuclear Research Center Karlsruhe.

It is in fact our policy to accommodate every experiment for which the facilities of this laboratory are particularly appropriate independent of questions of institutional affiliation. The use of the cyclotron for application oriented research projects amounted to about 50 % of the total time available for experiments. Because of the starting routine production of iodine-123 (~ 4 Ci in 1976) the amount of beam time for nuclear medicine increased from 316 h in 1975 to 570 h in 1976.

References

- 1) G. Schatz, F. Schulz, H. Schweickert, KFK-Ext. 18/75-1
- 2) F. Schulz, H. Schweickert, KFK 2298 (1976)

Cyclotron operational	with internal ion sources		with external ion sources		total	
for experiments	6087 h	82.9 %	796 h	67.3 %	6883 h	80.8 %
for beam development and testing new components	701 h	9.6 %	138 h	11.7 %	839 h	9.8 %
Total time of operation	6788 h	92.5 %	934 h	79.0 %	7722 h	90.6 %
Scheduled shut-down for maintenance, repair and installation	213 h	2.9 %	39 h	3.3 %	252 h	2.9 %
Unscheduled shut-down	338 h	4.6 %	209 h	17.7 %	547 h	6.4 %
Total shift time	7339 h	100 %	1182 h	100 %	8521 h	100 %

Table 1: Operation of the Karlsruhe Isochronous Cyclotron in 1976

Cyclotron

Axial injection including ion source	223 h	40.76 %
Radiofrequency system	64 h	11.70 %
Internal ion source	46 h	8.41 %
Extraction	36 h	6.58 %
Vacuum system (including all leaks)	30 h	5.48 %
Magnet power supplies	8 h	1.46 %
Others	23 h	4.20 %
	<hr/>	<hr/>
Cyclotron total	430 h	78.61 %

Additional equipment

Targets (including target transport, cooling, automatic target handling)	50 h	9.14 %
Internal deflector for neutron time-of-flight experiments	27 h	4.93 %
External beam handling system	23 h	4.20 %
Safety control system	9 h	1.64 %
Others	3 h	0.55 %
	<hr/>	<hr/>
Additional equipment total	112 h	20.47 %
Loss of machine time due to high radiation level	5 h	0.92 %
	<hr/>	<hr/>
Grand total	547 h	100 %

Table 2: Main causes of unscheduled shut-down in 1976

GfK - Karlsruhe users

Institut für Angewandte Kernphysik	1168 h	17.0 %
Projekt Schneller Brüter	1166 h	17.0 %
Labor für Isotopentechnik	589 h	8.5 %
Institut für Radiochemie	402 h	5.8 %
Institut für Experimentelle Kernphysik	277 h	4.0 %
Institut für Heiße Chemie	23 h	0.3 %
Institut für Material- und Festkörperforschung	6 h	0.1 %
	<hr/>	<hr/>
	3631 h	52.7 %

External users

Universität Saarbrücken	852 h	12.4 %
Freie Universität Berlin	547 h	7.9 %
MPI für Kernphysik Heidelberg	390 h	5.7 %
Techn. Universität München	324 h	4.7 %
Kernforschungsanlage Jülich	223 h	3.2 %
Universität Heidelberg	198 h	2.9 %
Deutsches Krebsforschungszentrum Heidelberg	184 h	2.7 %
Universität Erlangen	170 h	2.5 %
Universität Mainz	120 h	1.7 %
Universität Konstanz	93 h	1.3 %
Nuklearmedizinische Klinik München	75 h	1.1 %
Universität Clermont	42 h	0.6 %
Universität Gießen	20 h	0.3 %
Universität Ulm	8 h	0.1 %
Universität Münster	3 h	0.1 %
Universität Stuttgart	3 h	0.1 %
	<hr/>	<hr/>
	3252 h	47.3 %

Grand total	6883 h	100 %
-------------	--------	-------

Table 3: User statistics for 1976

Nuclear reactions	1653 h	24.0 %
Neutron physics	1166 h	17.0 %
Materials research	1017 h	14.7 %
Solid state physics	957 h	13.9 %
Engineering	686 h	10.0 %
Nuclear medicine	570 h	8.3 %
Nuclear spectroscopy	480 h	7.0 %
Nuclear chemistry	311 h	4.5 %
Others	42 h	0.6 %
	<hr/>	<hr/>
	6882 h	100 %

Table 4: User statistics for 1976

Period	Numbers of persons	Total dose (man-rem)	Mean dose (rem)
1968	12	8.77	0.73
1969	18	27.98	1.55
1970	18	33.83	1.88
1971	15	21.61	1.44
1972	15	16.06	1.07
1973	15	19.27	1.28
1974	15	16.22	1.08
1975	14	15.11	1.08
1976	25	18.67	0.75

Table 5: Total radiation dose received by operation personnel

2. TECHNICAL DEVELOPMENTS

2.1 Computer Aided Cyclotron Operation

W. Kappel, W. Karbstein, W. Kneis, J. Möllenbeck, H. Schweickert
Institut für Angewandte Kernphysik/Zyklotron des Kernforschungszentrums
Karlsruhe

In the last year a first description of our computer controlled beam diagnostic and logging system has been given ^{1,2)}. In the meantime the system has proved to be very helpful for the routine operation of the cyclotron, especially for the quick, reproducible and accurate measurement of beam properties and for the detection of imperfect parameter settings. A number of new programs has been added to the CICERO-system (fig. 1). In the following we will give short descriptions of some of these.

DATE 2/ 3/1977	TIME 12:45:37	DATE 2/ 3/1977	TIME 12:46: 6	DATE 2/ 3/1977	TIME 12:46:39
----- PAGE 1		----- PAGE 2		----- PAGE 3	
0	- STATUS INJECTION 1	0	- PHASE WIDTH INTERNAL	0	- EMITTANCE POSITION OF REST
1	- STATUS INJECTION 2	1	- PHASE WIDTH EXTERNAL	1	- EMITTANCE EXTERNAL BEAM
2	- STATUS IONSOURCE	2	- PHASE POSITION PHI=F(R)	2	- BEAM SCANNER EU
3	- STATUS CYCLOTRON	3	- 3:1 PULSING	3	- BEAM SCANNER C1
4	- STATUS MAGNETIC FIELDS	4	- 'QUITMANN'-PULSING	4	- BEAM SCANNER C5
5	- STATUS EXTERNAL BEAM	5	- ABSOLUTE ENERGY	5	- BEAM MATCHING C5
6	- FREE	6	- TEST PHOTOMULTIPLIER	6	- FREE
7	- FREE	7	- FREE	7	- FREE
8	- FREE	8	- FREE	8	- FREE
9	- MONITOR	9	- FREE	9	- FREE
-----		-----		-----	
'RET'	- NEXT PAGE	'RET'	- NEXT PAGE	'RET'	- NEXT PAGE
2	- PREVIOUS PAGE	2	- PREVIOUS PAGE	2	- PREVIOUS PAGE
2	- BACK TO CICERO	2	- BACK TO CICERO	2	- BACK TO CICERO
-----		-----		-----	

Fig. 1: Lists of measurement programs ready for use as displayed on the television screen in the control room. The cyclotron operator selects the diagnostics program required by input of a number via a keyboard. The computer subsequently executes this program and displays the result on the television screen.

Emittance measurement

The emittance measurement described earlier ^{1,2)} has been extended by a further evaluation section named SIGMAFIT. This program is automatically started after measurement. A fit for the best ellipse representation of the measuring points is made and displayed on the TV-screen as shown in fig. 2.

```

FROM 27/12/1976      TIME 17:12:32
HB= 5.704      UB= 4.99      I= 90%
XMAX      3.165      YMAX      10.647
ALPHA     -1.410     OALPHA     5.246
X'MAX     1.847     Y'MAX     5.334
X0        -2.375     Y0         4.375
EX/PI     5.533     EY/PI     18.378
    
```

HORIZONTAL VERTICAL



Fig. 2: Results of an emittance measurement performed by the computer at the extracted 52 MeV deuteron beam. Horizontal and vertical emittance ellipses are fitted by the new program SIGMAFIT

Absolute energy measurement

For some applications of the cyclotron, especially for the investigations of wear of machine parts, it is important to know the energy of the external beam precisely. Since in practice the beam energy depends on the operating conditions of the cyclotron it is desirable to have a simple beam energy monitor. The time-of-flight technique used (figs. 3 and 4) consecutively measures the time of arrival of prompt γ -rays from two graphite targets with respect to a timing signal from the accelerating frequency.

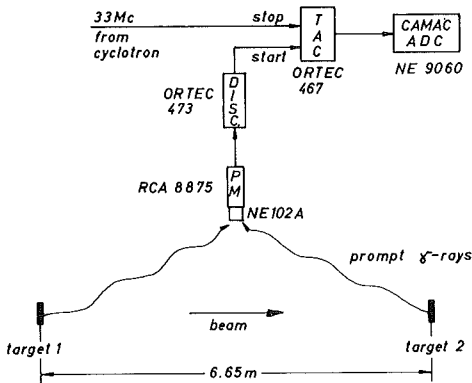


Fig. 3: Schematic diagram of the energy determination for the extracted beam by a time-of-flight technique. The accuracy achieved is ± 50 keV at 52 MeV

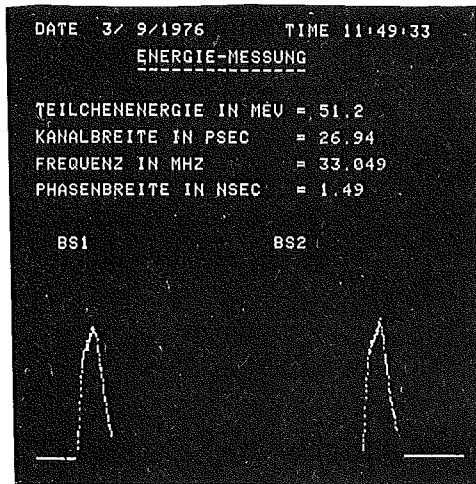


Fig. 4: Typical result of an energy measurement at the external 52 MeV deuteron beam. As in similar programs the computer tracks the operator through the procedure up to this final TV-picture. The time used is 60 sec.

Adjusting the currents of the correction coils

The installation of the new CAMAC controlled power supplies for the correction coils ³⁾ gives the possibility to decouple the corrections for isochronism and the centering of the beam. In fig. 5 the geometrical arrangement of the correction coils is shown.

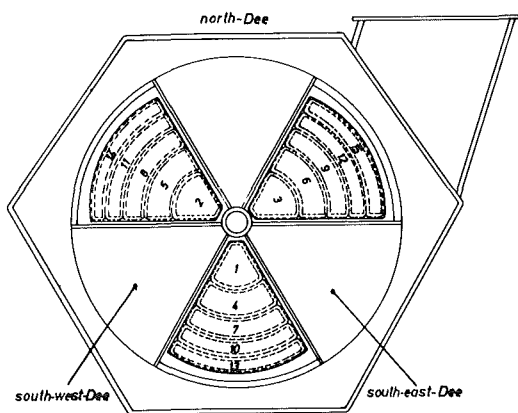


Fig. 5: Geometrical arrangement of the existing correction coils on the pole faces of the hill sectors. It consists of 15 individual pairs of coils each powered by a separate supply

According to the philosophy represented in fig. 6 it is possible to adjust and monitor the isochronism correction ($\sum I_c$), the amplitude (K) and angle (ϕ) of a first harmonic for the five radii (fig.7) independently of each other at the control console.

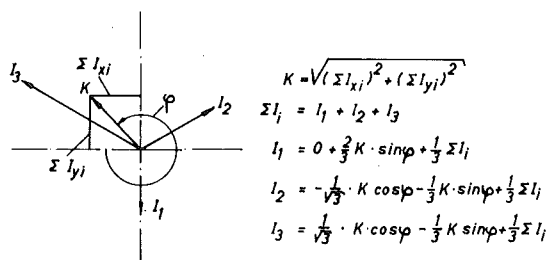


Fig. 6: Definition of the adjustment parameters: $\sum I_c$ = sum current; K = amplitude of the first harmonic and ϕ = angular direction of the first harmonic.

DATUM 2/ 3/1977 ZEIT 8:21:56
 KORREKTURSPULENWERTE FUER DEUTERONEN
 STROEME IN (10*MA), WINKEL IN (GRAD)

	SP1	SP2	SP3	SUMME	KEIL	Ø
1:	-24	-41	-55	-120	27	118
2:	28	0	0	28	28	90
3:	125	-43	-164	-82	251	115
4:	-121	243	-119	3	363	210
5:	147	52	61	260	91	85



Fig. 7: Typical display picture during the adjustment of the correction currents. The isochronous correction and the first field harmonic (K, ϕ) can be varied independently from the console. Measured actual values are displayed.

Quality of the 3:1 beam suppression

During operation of the fast neutron time-of-flight spectrometer it is often necessary to test the quality of the 3:1 beam suppression. The hardware for this measurement has been described in detail elsewhere⁴⁾, so it is sufficient to show the final display picture (fig. 8).

Beam scanner

The first two rotating beam scanners⁵⁾ have been tested in connection with the computer (fig. 9).

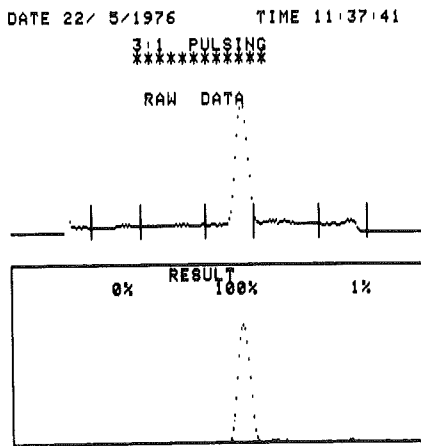


Fig. 8: TV-screen of the computer after the measurement of the 3:1 beam suppression. For demonstration a situation with a poor suppression is chosen

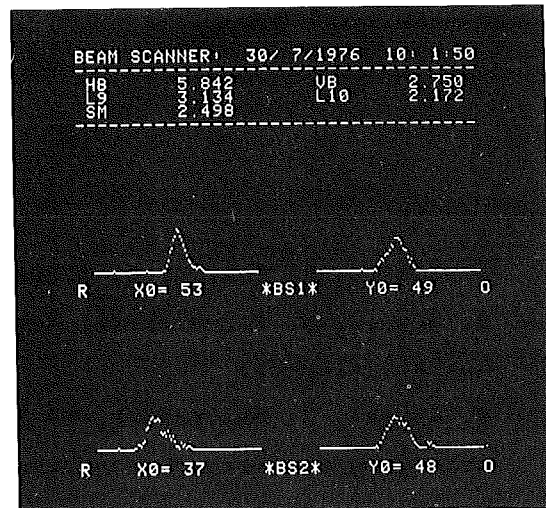


Fig. 9: Display of the beam profile and center taken with the fast quasi-non-intercepting devices. Currents down to 300 nA can be measured; below this limit the sliding contacts used give noise problems

Iodine-123 quality control

For isotope production a program has been added which controls the activity and quality of the produced ¹²³J⁶⁾. The γ -spectrum of the NaJ solution is measured by means of a 27 cm³ Ge(Li) detector and a NE 9060 CAMAC ADC. A quality control certificate accompanies the batches to be sent to the hospitals (fig. 10).

```
JOD-MESSUNG 1/3/1977 20:50:0
-----
START      : 20:50:0
STOP       : 21:01:0
MESSZEIT   : 352 [SEC]
AKTIVITÄT : 129.54 [MCi] RH: 1.37 [%]
```

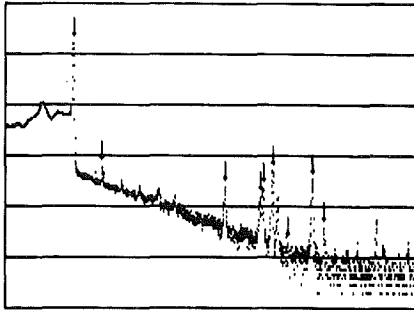


Fig. 10: Results of the quality control of the iodine-123 production. This picture is part of a detailed quality control certificate and shows a typical sample of 129 mCi and a iodine-124 impurity of 1.3 % at the time of measurement

References

- 1) G. Schatz, F. Schulz, H. Schweickert; Report KFK-Ext. 18/75-1 (1975)
- 2) F. Schulz, H. Schweickert; Report KFK 2298 (1976)
- 3) Contribution 2.3
- 4) W. Kappel, J. Möllenbeck, H. Schweickert; Proc. Sixth International Cyclotron Conference, Vancouver, July 1972 (American Inst. of Physics, New York, 1972) p.358
- 5) G. Bauer, K. Heidenreich, G. Klinger, Ch. Rämmer, R. Schütz; Report KFK 2233 (1975) p. 101
- 6) Contribution 2.10

2.2 New Correction Coils of the Cyclotron

V. Bechtold, L. Friedrich, L. Wiss

Institut für Angewandte Kernphysik/Zyklotron des Kernforschungszentrums
Karlsruhe

After the decision in 1975 to build a new set of trim coils for the cyclotron numerical calculations were done to investigate whether a suitable new configuration of trim coils is able to accelerate ${}^3\text{He}^{2+}$ and H^+ -ions in addition to the $e/m = 1/2$ particles. These calculations led to a trim coil configuration consisting of six coils per plate with summing fields ¹⁾.

According to these calculations a prototype coil was designed. Several changes in the project for the cooling plate resulted in a simpler and less expensive design. A prototype is now under construction.

The coil conductor is a copper band of $7 \times 0.7 \text{ mm}^2$ in cross section which will be wound tightly around aluminium forms. The power dissipated in the coil windings is transported through a thin insulation layer on the copper band, a thin glass silk (0.1 mm) and a thin layer of epoxy resin with quartz to a copper plate on each side of the coil. These plates are cooled by water flowing through a rectangular cooling channel inserted into the plates. Fig. 1 shows a top view of the copper plate and the layout of the cooling channel. The copper plate is only 3 mm thick and the cooling channels are $12.5 \times 2.5 \text{ mm}$ with $11.5 \times 1.5 \text{ mm}^2$ inner cross section.

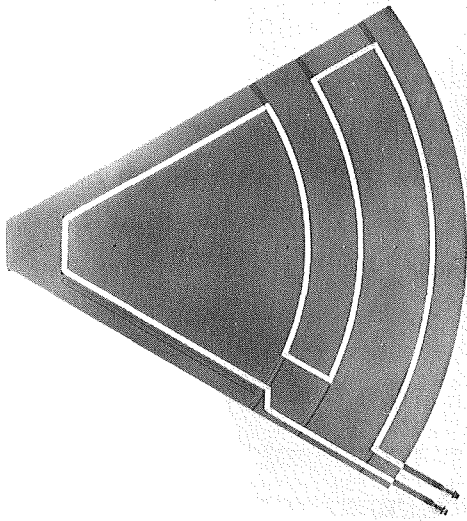


Fig. 1: Top view of the copper plate with layout of the cooling channel. The plate is 3 mm thick and the inner cross section of the cooling channels is $11.5 \times 1.5 \text{ mm}^2$

The all over thickness of the trim coil is 13.3 mm. Fig. 2 shows a cross section of the coil with cooling plates on either side.

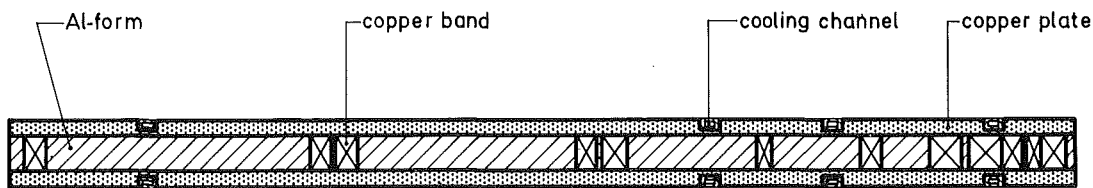


Fig. 2: Cross section of a trim coil with cooling plates on each side.

To get the desired field correction currents up to 50 A per coil are necessary, producing a power density of 1 W/cm^2 . To transport this power loss quickly to the cooling plates a good thermal conductivity is necessary. The thermal conductivity depends on the distance and the medium between windings and cooling plate.

The distance is minimized by pressing the whole winding of the coils. The trim coil set is then completely filled with epoxy resin and the cooling plates are pasted on each side. This leads on one hand to a good mechanical

stability of the coil, on the other hand to an improvement of the thermal conductivity between windings and plates by appropriate selection of the epoxy resin.

We tried two epoxy resins from Ciba namely Araldit F and Araldit F doted with quartz powder. The measured thermal conductivity for both epoxy resins is

$$\lambda = 0.58 \cdot 10^{-3} \frac{\text{cal}}{\text{cm sec } ^\circ\text{C}} \text{ for Araldit F}$$

$$\lambda = 1.45 \cdot 10^{-3} \frac{\text{cal}}{\text{cm sec } ^\circ\text{C}} \text{ for Araldit F doted with quarz powder}$$

The thermal conductivity λ for the doted resin is a factor of 2.5 higher than for the resin without quartz. The processing of the epoxy resin at 70°C was done in vacuum to ensure a proper outgassing. The hardening was made at 100°C while simultaneously pressing the whole trim coil set. This is done in vacuum, too. The arrangement for this procedure is shown in fig. 3.

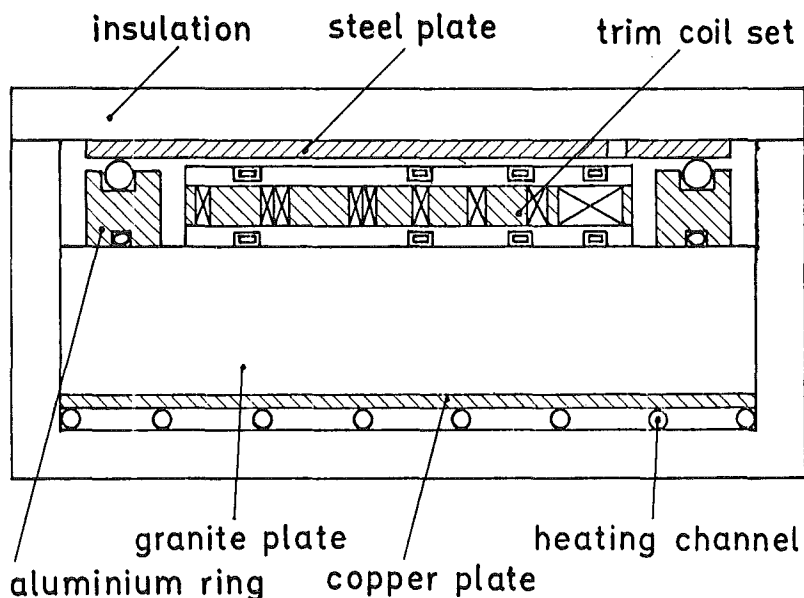


Fig. 3: The arrangement for pressing and outgassing the whole trim coil set during the hardening time of the epoxy resin by means of vacuum. The whole set-up can be heated to 100°C

The basis is a granite plate (150 x 150 x 20 cm) which can be heated up to 100°C by means of heating channels at the bottom. The surface of the granite plate is manufactured with an accuracy of 1-5 μ and a parallelism of 1/10 mm. This surface quality will not change while heating up the plate to 100°C. A vacuum chamber is built up with an aluminium ring on the surface of the plate. A steel plate will close this chamber. The whole trim coil set will be inserted into this chamber and can be heated. By properly dimensioning the height of the aluminium ring it is possible to press the trim coil set between the steel plate and the granite plate by evacuating the chamber. In this way the trim coil set is fixed during the hardening time of the epoxy resin.

For the high currents up to 50 A a special vacuum tight feed through was designed. This feed through consists of an epoxy flange into which hard silver plated copper bolts and copper pipes are soldered. Each coil plate will be supplied separately with current and water so that six epoxy flanges are needed. The flange with the arrangement of the current and water connections is drawn to scale in fig. 4.

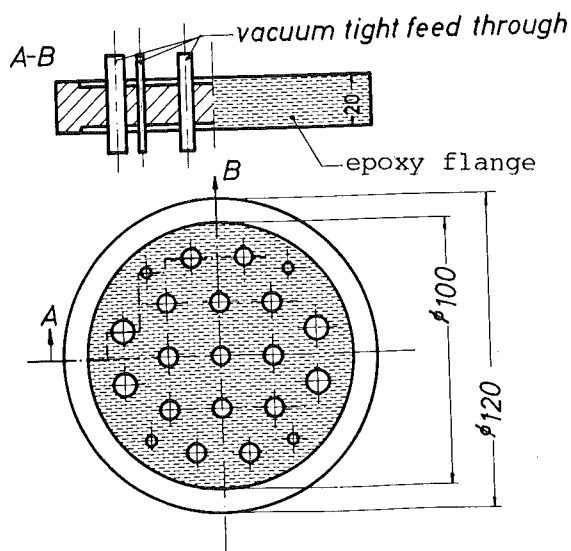


Fig. 4: Epoxy flange with the arrangement of the 13 current and 4 water connections supplying one coil plate. The flange is a special feed-through for high currents

In the middle of 1977 a prototype of the trim coil will be ready for the test bench. If all experimental investigations and tests are satisfying the new trim coils will be available at the end of 1978.

References

- 1) F. Schulz, H. Schweickert; Report KFK 2298 (1976) p.15

2.3 New Computer Controlled Power Supplies for the Correction Coils of the Cyclotron

W. Kappel, G. Klinger, E. Schönstein

Institut für Angewandte Kernphysik/Zyklotron des Kernforschungszentrums Karlsruhe

The 12 years old power supplies for the correction coils have been replaced by new ones which are controlled and monitored via CAMAC by our Nova 2/10 computer. The principle of this set up is shown in fig. 1.

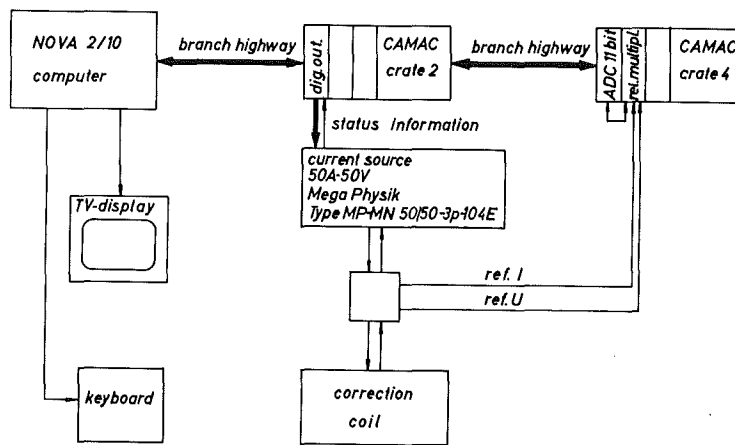


Fig. 1: Simplified block diagram of the circuitry for the new computer controlled power supplies for the correction coils

Each coil is supplied by a separate current source with a built in 12 bit BCD digital-to-analog converter. The digital input of this DAC is defined by a register incorporated in a special CAMAC modul (fig. 2). The register can be loaded and read either by a standard CAMAC dataway operation or in the case of manual operation by an up/down counter. Two clock rates, 2 Hz and 200 Hz, are provided. An additional 3 bit register, which is read by the dataway, serves as a status register for alarm situations at the high current power supplies. The long line transmitter circuits to the power supplies are equipped with optoelectronic coupling boards to give a high noise suppression. The computer control also enables us to check the mechanical and electrical quality of the correction coils by monitoring the applied voltages and circulating currents.

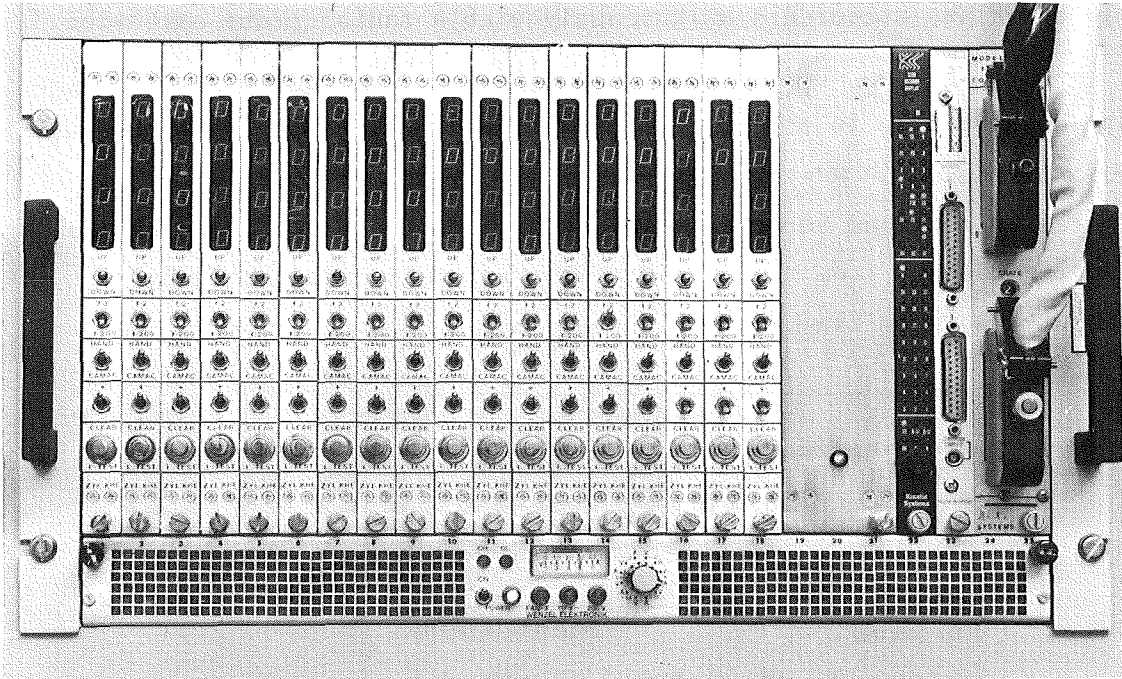


Abb. 2: Photograph of the CAMAC moduls controlling the power supplies for the correction coils

2.4 Non-intercepting Measurement of the Extraction Efficiency at the Karlsruhe Cyclotron

G. Haushahn, W. Maier, E. Röhr1

Institut für Angewandte Kernphysik/Zyklotron des Kernforschungszentrums Karlsruhe

The aim of the capacitive internal beam probe described below is to measure the extraction efficiency of the Karlsruhe Isochronous Cyclotron without interrupting the beam. Last year we reported about a simple capacitive probe at the external beam line using the second harmonic (66 MHz) of the ion beam pulses to suppress the noise background ¹⁾. A similar technique is now applied to an internal capacitive probe located just in front of the extraction elements in the north east hill sector. A cross section of the very carefully shielded probe is shown in fig.1. In order to increase the pick-up signal from the

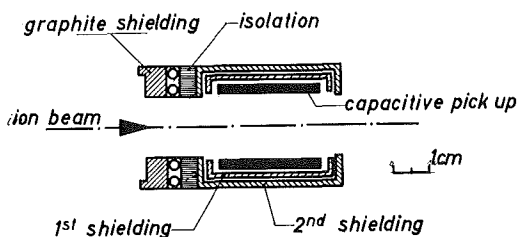


Fig. 1: The triply shielded internal capacitive probe. The probe length in radial direction is 40 mm to increase the signal induced by the beam

ion beam, 30 turns are measured simultaneously with a radial probe extension of 40 mm.

In contrary to the probes in the external beam line the rf-suppression by use of the second harmonic (66 MHz) is not sufficient, since the pick-up voltage is contaminated by a second harmonic originating from the stray field of the dees. This noise voltage from the acceleration system is compensated by a special circuit shown in fig. 2.

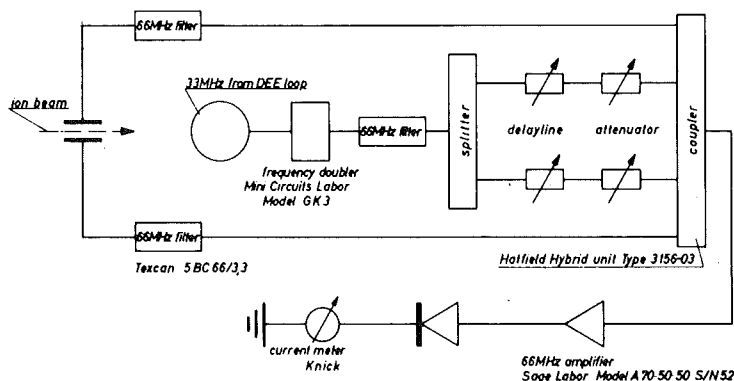


Fig. 2: A block diagram of the non-intercepting internal beam current monitor working on the second harmonic. A compensation technique is used to suppress the pick up of the second harmonic from the rf-system.

By using this technique a suppression of the second harmonic component of approximately 50 dB has been realized. Thus ion beam currents down to $0.1 \mu\text{A}$ can be measured (fig. 3).

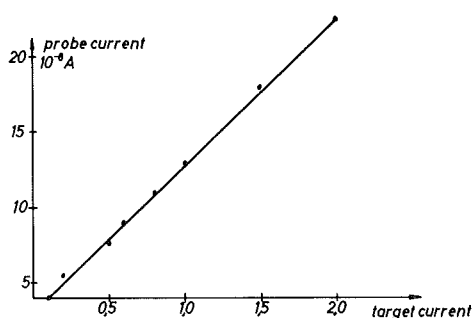


Fig. 3: Calibration curve of the new internal non-intercepting current probe. Currents down to $0.1 \mu\text{A}$ can be measured very reliably

Up to now there are some difficulties in the long term stability of the necessary rf-compensation for the internal probe. It turned out that the stray-field of the dee's is strongly dependent on some cyclotron parameters. Nevertheless this probe together with an external capacitive probe in the beam line gives the operators a continuous information on the extraction efficiency. For that purpose the output voltages of the two probes are compared in a ratiometer (Ortec 5047) and displayed at the control console.

1) G. Haushahn, K. Heidenreich, E. Röhrl; KFK 223 (1975) p.97

2.5 Present Status of the Karlsruhe Polarized Ion Source

V. Bechtold, L. Friedrich

Institut für Angewandte Kernphysik/Zyklotron des Kernforschungszentrums
Karlsruhe

P. Ziegler, Institut für Experimentelle Kernphysik, Universität Karlsruhe

The Lambshift source C-LASKA (fig. 1) producing polarized deuterons from charge exchange of metastables with iodine is in operation at the Karlsruhe isochronous cyclotron since the beginning of 1974. The source is installed in the basement of the experimental hall, separated from the cyclotron vault by 3m of shielding. The distance between the axial injection system and the source is 11 m. Thus the magnetic strayfield of the cyclotron is eluded. In addition the source can be handled, when the cyclotron is in operation. The source delivers 0.8 μA vector polarized deuterons with an emittance of $1.1 \text{ cm rad eV}^{1/2}$. Of this, 5 % could be extracted from the cyclotron.

Source current		Current in scattering chamber	
vector pol.	tensor pol.	vector pol.	tensor pol.
0.8 μA	0.6 μA	40 nA	30 nA

Two important improvements have been achieved in 1976:

1. To protect the bearings and the oil of the turbopumps from the very aggressive iodine, evaporated in the source, a low iodine pressure in the forevacuum has been maintained by liquid nitrogen traps. The consumption of the liquid nitrogen was high and every three hours a refilling of the traps led to an interruption of 10 minutes. These traps have been replaced by an iodine condensor, which is cooled by alcohol at -80°C . The source can now be operated continuously for more than 150 h.
2. Accelerating a polarized beam in a cyclotron without depolarization requires the spin alignment axis to be parallel to the cyclotron magnetic field. In this case the general formula for the cross section for scattering or reaction with polarized deuterons amounts to:

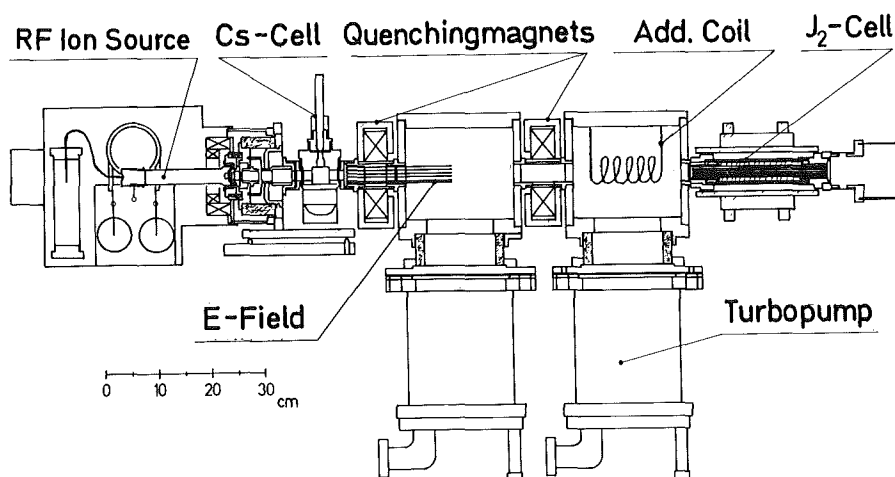
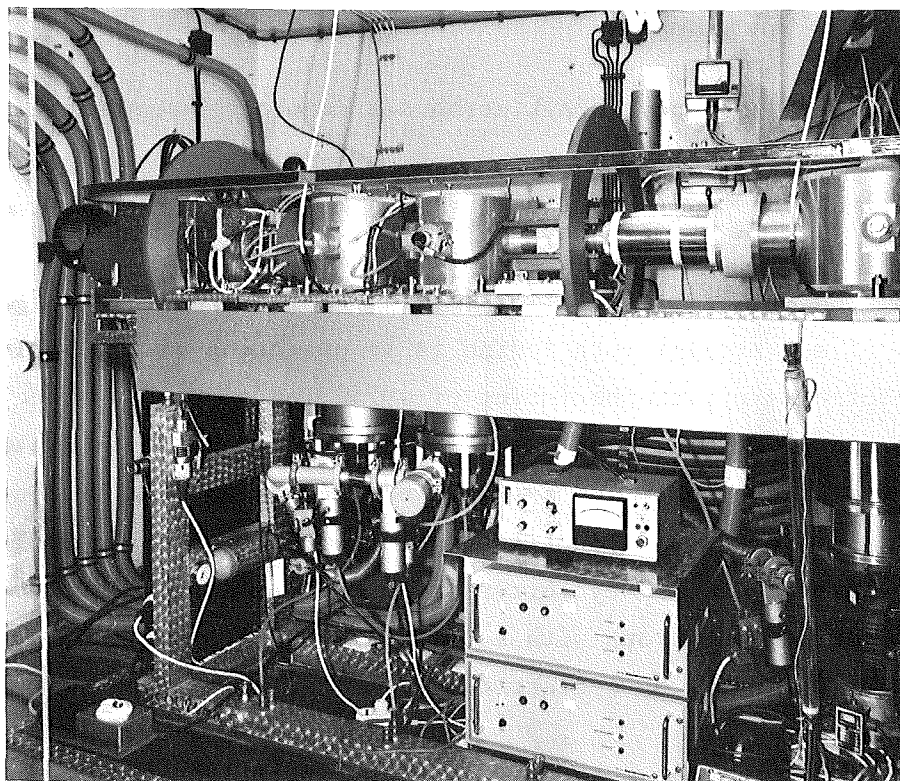


Fig. 1: The Lambshift source C-LASKA in the basement of the experimental hall. A section of the source is drawn to scale in the figure below. The deuterons produced in the rf-source are partially neutralized in cesium by the charge exchange reaction $D^+ + Cs \rightarrow D(2S) + Cs^+$. The metastable atoms are polarized by running through a special magnetic field of two quenching magnets. Then the ionization takes place in a charge exchange cell with iodine. The 1 keV polarized beam produced this way is accelerated in two steps to 10 keV by tube lenses.

$$\sigma(\theta) = \sigma_o(\theta) \left\{ 1 + \frac{3}{2} \cos \beta \cdot P_3 \cdot A_y(\theta) + \frac{1}{2} \sin^2 \beta \cdot P_{33} \cdot A_{xx}(\theta) + \frac{1}{2} \sin^2 \beta \cdot P_{33} \cdot A_{yy}(\theta) \right\}$$

$\sigma_o(\theta)$ is the cross section measured with unpolarized beam. With a polarized beam the cross section depends on the angle β between the (vertical) spin alignment axis and the normal $n = K_{in} \times K_{out}$ of the scattering plane. The simplest method to determine the vector analysing power $A_y(\theta)$ and the tensor analysing power $A_{xx}(\theta)$ and $A_{yy}(\theta)$ uses two detectors mounted symmetrically in a scattering chamber with equal scattering angles θ . It was shown by König et al. that 8 counting rates have to be taken, namely the "right" and "left" counting rate in the horizontal scattering chamber and the "below" and "above" counting rate in the vertical scattering chamber with "spin up" and "spin down" respectively ¹⁾.

In a modified version of this method we used the mixed and pure vector polarized beam of C-LASKA both with spin flip to get the analysing powers A_y and A_{yy} in a horizontal scattering experiment. An effective method to flip the spin was achieved in the following way.

To get a transverse polarized beam, a transverse magnetic field is produced in the charge exchange cell (fig. 2). This field is compensated electrically to avoid quenching of the metastables and broadening of the beam. For this purpose

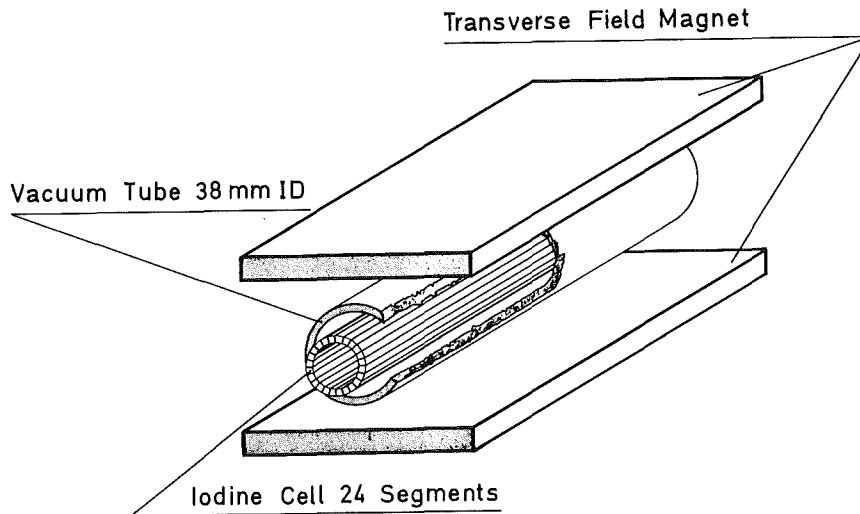


Fig. 2 : The charge exchange cell with the transverse field magnet. The sliced iodine cell is able to compensate the transverse field

the cell (18 mm diameter and 200 mm length) has been sliced into 24 segments which are operated at different potentials. The polarization of the metastable atoms is rotated to transverse direction by superimposing the outgoing field of the second quenching magnet and the strayfield of the iodine cell. Shaping of this field is achieved by an additional coil.

The polarization is flipped by simultaneously reversing the magnetic and electrical field. This results in small changes of the beam direction, which have to be corrected carefully because the acceptance of the cyclotron depends very critically on the beam direction. This is done by compensating separately the magnetic field for both directions. In addition a transverse field magnet is applied at the exit of the cell, which also can be excited separately for both directions. This magnet looks like the stator of an electric motor. Careful adjustment gives equal intensity for both directions. The measured vector polarization P_3 for spin "up" and "down" as a function of time is given in fig. 3. The direction of the polarization can be automatically controlled by the data acquisition system of the experiment,

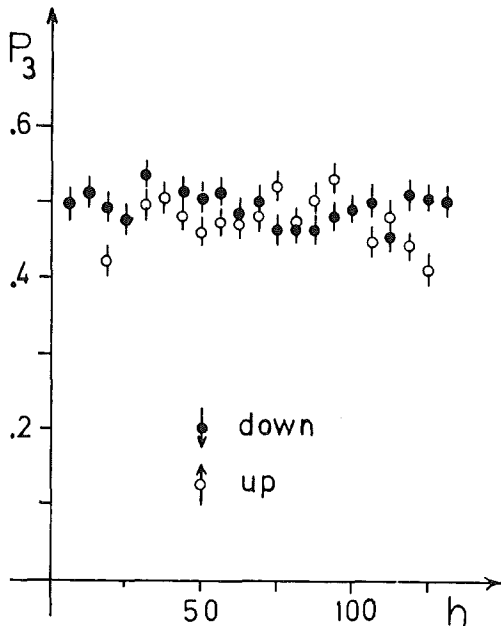


Fig. 3: The vector polarization P_3 measured during a period of 100 hours for "spin up" and "spin down"

References

- 1) V. König, W. Gruebler, P.A. Schmelzbach; Jahresbericht 1976, Laboratorium für Kernphysik ETH Zürich, p.138
- 2) J. Bruinsma and R. van Wageningen, preprint, to be published in Nucl. Phys.

2.6 Improvements of the ${}^6\text{Li}^{3+}$ -Penning Ion Source

J. Biber, H. Kuhn, F. Schulz

Institut für Angewandte Kernphysik/Zyklotron des Kernforschungszentrums
Karlsruhe

Since 1973 the external hot filament Penning ion source ¹⁾ is used at the Karlsruhe axial injection system for basic nuclear physics experiments. The improvement in this time can be seen in table 1.

	mean current in scattering chamber	max. current in scattering chamber
1973	-	10 pA
1974	30 pA	50 pA
1975	150 pA	1 nA
1976	5 nA	15 nA

Table 1: Numbers showing the improvement of the ${}^6\text{Li}^{3+}$ -source

Though no essential modification of the source has been carried out, the external ${}^6\text{Li}^{3+}$ -beam current increased by a factor of 1500. There are a number of small technical improvements at the source leading to this success. Fig. 1 shows the actual configuration of our source. In the first place, the position of the plasma was adjusted closer to the extraction slit by appropriate shim rings

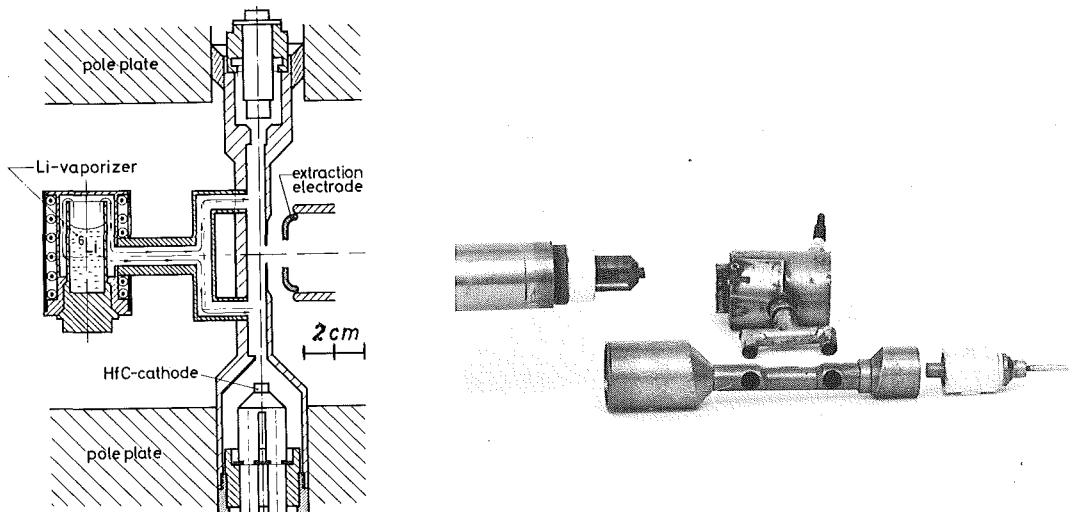


Fig. 1: Actual mechanical structure of the external ${}^6\text{Li}^{3+}$ hot filament Penning source together with a photograph of a source disassembled for cathode exchange.

around the bore in the magnet. In order to reduce impurities inside the source volume, the source is now excited without any buffer gas. The gas inlet is connected to the diffusion pump. The operation conditions of the source are as follows:

- temperature of the Li-oven about 600⁰C at 12-15 A heating current
- cathode heating current for start-up 500 A (300 V) and in operation 100 A
- arc conditions for 3 μ A of ⁶Li³⁺ (250e μ A of ⁶Li²⁺) in the injection line are $I_A = 1,2-1,4$ A and $U_A = 400-500$ V
- average life time about 36 h
- preparation time after spare parts replacement about 4 h

Based on the investigations on our test bench a new external Penning source with a higher magnetic field of 8 kG has been built up and is now tested. A recent photograph of this arrangement is shown in fig. 2

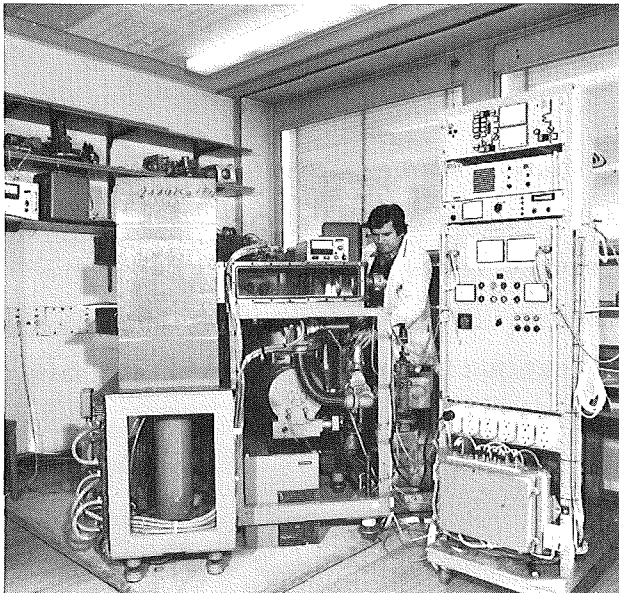


Fig. 2: A recent photograph of the new external Penning ion source. Strong plasma compression will be achieved by a homogeneous magnetic field of 8 kG

References

- 1) G. Schatz, F. Schulz; KFK-Ext. 18/73-1 (1973)

2.7 New Beam Line for the Irradiation of Machine Parts

G. Bauer, P. Kauther, Ch. Ramer

Institut fur Angewandte Kernphysik/Zyklotron des Kerforschungszentrums
Karlsruhe

In previous years about 500-700 h of irradiation time had been utilized annually to activate machine parts ^{1,2)}. Since these irradiations had to be performed in our large experimental hall, quite a number of nuclear physics experiments suffered from the background generated. Also, in many cases the space available was not sufficient to set up the components to be activated, some of them being rather large in size (e.g. motor engines). For this reason, it became necessary to build a separate room for experiments for this purpose.

Since mid-1976 this room together with a control room, both installed at the western side of the experimental hall, have become available. The beam line in channel I was extended by about 5 m. This made necessary the installation of additional beam handling elements to meet the requirements of the users (100 % transmission from extraction to target position, beam spot < 5 mm ϕ). The optimum beam handling system was determined by our analog particle track computer. The best solution to be realized without major modifications is represented in fig. 1.

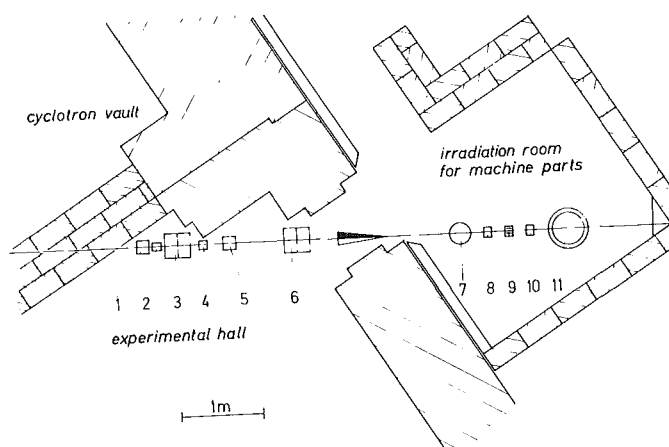
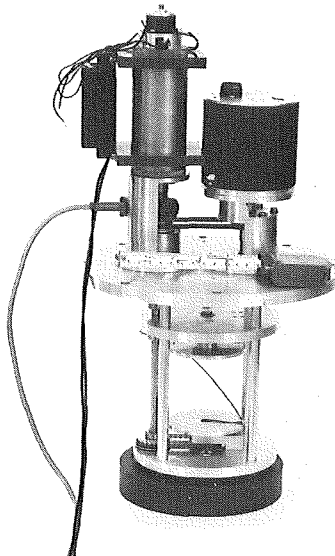


Fig. 1: Layout of the new irradiation room for wear measurements on machine components outside the main experimental hall; (1), (5) x-y-bending elements, (3),(6) quadrupol doublet lenses, (7) diffusion pump, (2),(10) diagnostic boxes, (4),(8) beam scanners, (9) capacitive beam monitor, (11) machine parts

Besides the two quadrupole doublets the following additional devices for beam transport have been installed:

- two bending magnets to correct the beam direction by $\pm 0.2^\circ$ both horizontally and vertically
- two ZnS screen + beam stop units preceding the first doublet and the target position, respectively, for visual control of the beam and for measurement of the beam current
- two computer controlled X-Y beam scanners to measure the beam position (fig. 2)
- one capacitive current monitor in front of the target position for the measurement of the relative intensity (current integral) during irradiation. The usual current measurement in a Farady cup is not possible here since the beam is shot through a thin vacuum sealing foil into air and then hits the target (fig. 3).

A valve behind the pumping system (oil diffusion pump) allows to replace the foil without vacuum brake down in the whole beam line. A fast-closing valve for all channels in front of the switching magnet protects the cyclotron in case of foil rupture.



```
BEAM SCANNER: 27/12/1976 17:56:54
-----
HB      5.690      L1      5.186
UB      1.460      L2      0.000
SM      2.458      L3      0.000
-----
```

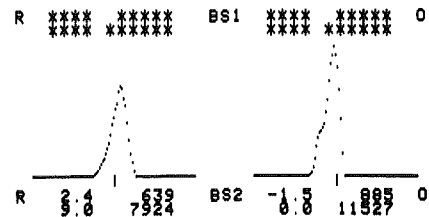


Fig. 2: X-Y-Beam scanner driven by a DC-motor. The position is taken via an incremental position encoder. The right side shows a typical beam profile measurement with this unit

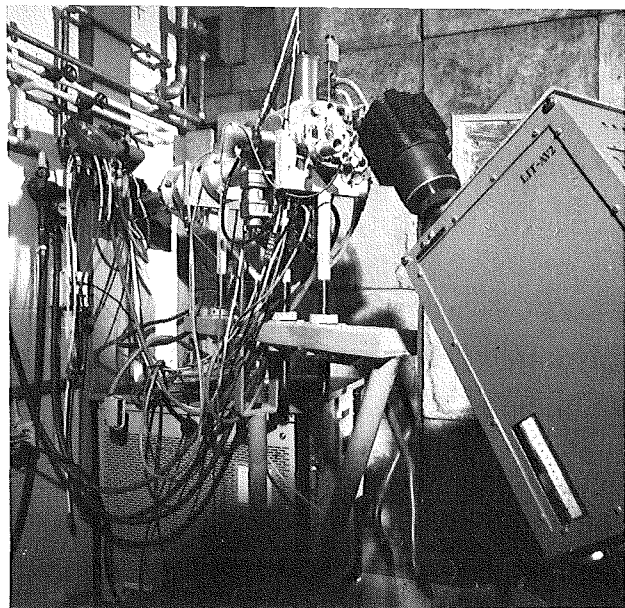


Fig. 3: Typical irradiation set-up
for activation of a pinion

With this new beam line to the irradiation room, the experimental conditions in the large experimental hall have been considerably improved. Further improvement will be achieved by shielding this beam line in the experimental room.

References

- 1) F. Schulz, H. Schweickert; Operation Summary of the Karlsruhe Isochronous Cyclotron Annual Report KFK 2379
- 2) A. Gerve, G. Schatz; Applications of Cyclotrons in Technical and Analytical Studies 7. Intern. Conf. on Cyclotrons and their Applications, Zürich, August 19-22, 1975

2.8 Nova-2-Computer-System for Nuclear Physics Experiments

W. Karbstein, B. Kögel

Institut für Angewandte Kernphysik/Zyklotron des Kernforschungszentrums
Karlsruhe

A new computer configuration is now available to all experimentalists at the Karlsruhe cyclotron for on line data acquisition. The following hard- and software description gives an survey on the possibilities of the system.

Hardware

The hardware configuration is shown fig. 1. An ADC multiparametric system and data display allows the operator to choose the mode of operation and representation of data by hardware switches. The CAMAC branch offers a practically unlimited expansion possibility for all CAMAC devices which are available today. Since modular and computer independent ADC interfaces in CAMAC were not available we decided to develop the concept of a hardware multiparametric system which was built by Laben. Fig. 2 shows the system schematically together with the computer and increment unit in order to illustrate the operation of the whole system.

Software

Much convenience in programming and program-development is achieved by use of Data Generals' Real Time Disk Operating System (RDOS) ²⁾. Some of its features are: An interactive (via console) Command Line Interpreter (CLI) ³⁾, which includes all necessary utilities for program-development (like editors, macroassembler, relocatable loaders, compilers etc.), intensive file handling, and the use of high level programming languages (FORTRAN, BASIC).

User programs are written in BASIC or FORTRAN. Besides these standard programming possibilities there exist a lot of fast assembler subroutines for the nonstandard peripheral equipment (CAMAC ⁴⁾, Data Display ⁵⁾, Increment Unit ⁶⁾. These subroutines can be used within BASIC by the CALL-mechanism.

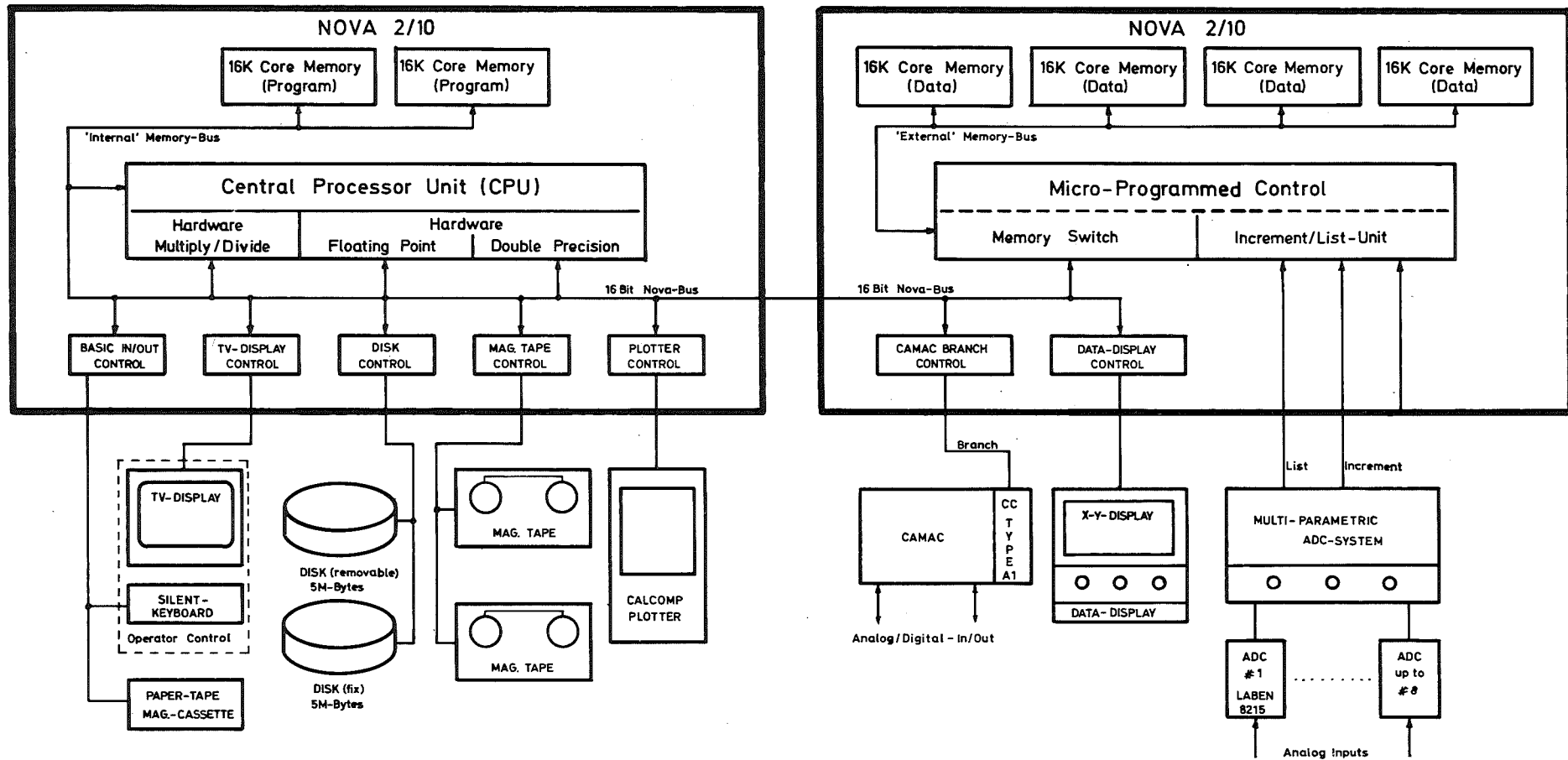


Fig. 1: The left computer with 32 K of core memory (normally max. for Nova 2), hardware multiply/divide - and floating point processor, conventional input/output devices (console, 2 disks, 2 magnetic tapes, paper tape station, incremental plotter) represents a complete computing center for program development and data evaluation. The right one with the experimental periphery can be regarded as a multichannel analyser. Both computers are connected by their central busses, and so the second computer also serves as an expansion chassis for the additional 64 K core memory (data memory) as well as for other controllers (part of them are home made) for connecting on-line electronic devices (CAMAC branch, data display, ADC multiparametric system). Instead of a CPU, the second computer has as an essential part a microprogrammed double controller which operates as a memory switch and increment unit ¹⁾.

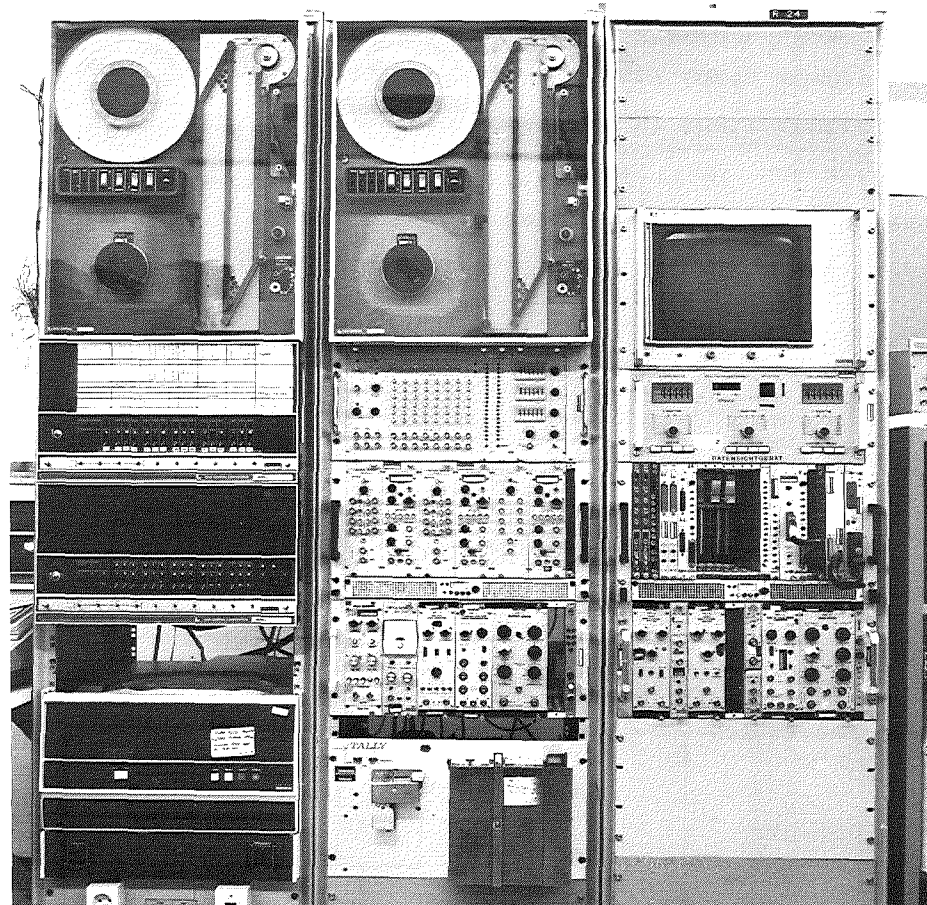
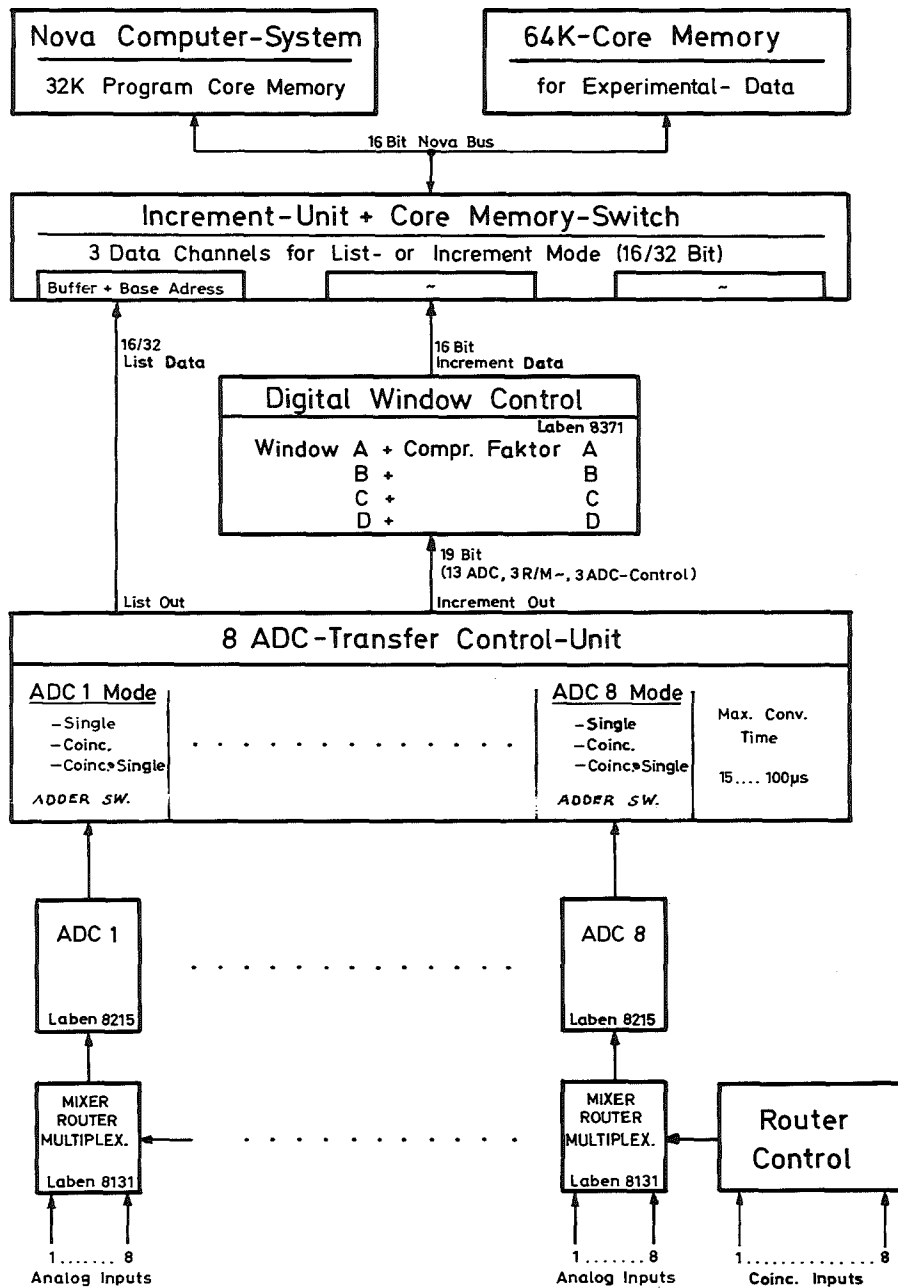


Fig. 2: The ADC multiparametric system as connected to the NOVA computers via the increment unit 1). This is a special NOVA controller, which allows the connection of additional 64 K-core memory and also opens three data channels in increment and list mode (16 or 32 bit each). The ADC multiparametric system uses one list channel for the coincidence data and one increment channel for the single spectra. A recent photograph of the whole system is shown on the right side

References

- 1) G. Ehret, H. Hanak; Report KFK 2183, p.99
- 2) Data General Corp.: Realtime Disk Operating System, Ref. Man. 093-000075
- 3) Data General Corp.: RDOS-Command Line Interpreter, Ref. Man. 093-000109
(with further references to other standard software)
- 4) G. Ehret, W. Karbstein, W. Kneis; BASIC Subroutines for CAMAC on NOVA 2 Computers, 2. Intern. Symposium on CAMAC, Brüssel, 14-16 Oct. 1975
- 5) W. Karbstein; BASIC CALL's for the display, Internal. Report, März 1977
- 6) G. Ehret, B. Volk, Subroutine CALL's, to be published

2.9 First Attempts towards an Automatization of the Beam Guiding System

W. Kneis

Institut für Angewandte Kernphysik/Zyklotron des Kernforschungszentrums
Karlsruhe

Attempts towards automatization and optimization of parameter settings in beam guiding systems are characterized by the problem of minimization of a variety of functions describing beam properties. The minimization is made by the variation of a number of parameters influencing these functions. This can be done either by theoretical simulation, by a more or less empirical treatment applying numerical optimization and least-squares techniques to measured beam data or by an appropriate combination of both methods. Since in our laboratory a variety of beam diagnostic tools like emittance measurement, beam-scanners etc. are ready for use ¹⁾ it is therefore necessary to provide the theoretical simulation facilities too.

Many computer programs for simulation of beam transport systems have been developed over the past decades. Compared with former programs ^{1,2)} running on batch computers and printing long lists and matrices of beam lines, the programs offered today emphasize the graphic presentation of results and the provision of facilities allowing the user to interact with the program ^{3,4)}. The need for this can be understood by the fact that for all but the simplest problems there is no unique solution for beam optimization. So the user must have the means to impose the right constraints - also during the run - to his optimization to arrive at acceptable solutions. The possibility to interact with the program is also advantageous for finding initial values for iteration .

The beam optics design system, BOD, implemented on a Nova 2 computer consists of three programs:

- BODIO - System Input/Output
- BODIGA - Graphic Package
- BODEONI - Optimization Program

The three programs available under BASIC are connected to each other by a common data base and are controllable via a switchboard with 24 individual switches (fig. 1). The system allows to describe a beam guiding system consisting of drift spaces, quadrupoles (electrical or magnetic), bending elements, edge angles, and coordinate rotation and to display either the resulting phase space ellipses (fig. 2) for the x- and y-subspaces at the desired point of the

```

BODIO: 9/ 9/1976 17: 4:33
-----
B O D I O  S W I T C H E S
-----
1 - INPUT OF NEW PROBLEM
2 - DESCRIPTION OF 'BODEONI'
3 - INPUT ELLIPSE FOR START
4 - INPUT NOMINAL ELLIPSE AT END
5 - ELLIPSE CONSTRAINTS FOR NOMINAL
6 - INPUT OPTICAL ELEMENTS
7 - INPUT VARIABLE OPTICAL ELEMENTS
8 - CHANGE OPTICAL ELEMENTS
9 - =0 - INSERT
10 - PRINT PROBLEM CHARACTERISTIC
11 - START ITERATION -> 'BODEONI'
12 - BATCH MODE
13 - INPUT FROM DISK
14 - OUTPUT TO DISK
15 - PRINT DISK FILES

BODIO: 9/ 9/1976 17:52:15
-----
B O D I G A  S W I T C H E S
-----
1 - =0 - DISPLAY ELLIPSE AT END
2 - =1 - DISPLAY BEAM ENVELOPE
3 - DISPLAY ELLIPSE AT START
4 - SETTING OF VARIABLE OPTICAL
  ELEMENTS
5 - PRINT RAY TRACING
6 - UNIT: EKG (SLAC)
7 - EKG (CM) FOR Q, EKG FOR B
8 - CALLED BY PROGRAM
9 - BACK TO 'BODIO' (BATCH MODE)
10 - OUTPUT TO DISK

BODIO: 9/ 9/1976 18: 7:55
-----
B O D E O N I  S W I T C H E S
-----
1 - DISPLAY ELLIPSE AT END
2 - DO NOT PRINT ITERATIONS
3 - PRINT V.A.T.U.
4 - PRINT IN SUBROUTINE 4000
5 - PRINT RAY TRACING
6 - FIT WITH BOUNDARY CONSTRAINTS
7 - SHORT TERM PRINT OUTPUT
8 - STOP IMMEDIATELY
9 - PRINT ELLIPSE AT END
10 - PRINT VARIABLE OPTICAL ELEMENTS
11 - NO AUTOMATIC STOP IF DIVERGENT
12 - STOP ONLY IF CHIGU<1%
13 - CALLED BY PROGRAM
14 - BACK TO 'BODIO' (BATCH MODE)
15 - OUTPUT TO DISK AUTOMATICALLY
16 - PRINT DISK FILES
    
```

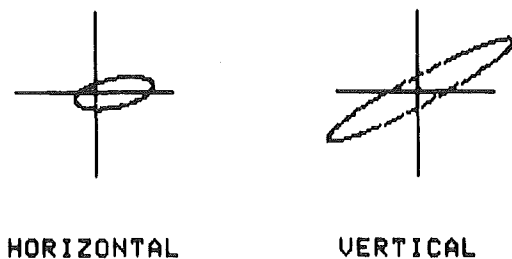
Fig. 1: Function switches for the control of the BOD-systems.

- a) program BODIO
- b) program BODIGA
- c) program BODEONI

```

BODIGA: 9/ 9/1976 22:47: 2
-----
IN:TK5M4 ** [KGI] - SLAC **
-----
XMAX 4.9903 * 1 END 0.000
ALPHA .4199 * 19 KEY 250
OUMAX 1.9800 20 * CHANGE END *
X0 0.2433
Y0 0.2433
YMAX 11.9906
ALPHA .4199
OUMAX 6.3081
Y0 1.0071
Y0 1.0071
    
```

Fig. 2: Specification and display of the horizontal and vertical phase space ellipses



z-axis or to show the beam envelopes in x and y along the beam guiding system (fig. 3). Furthermore it allows to optimize the settings of the optical elements by a least squares iteration method via nominal constraints of the phase space ellipse or boundary constraints. Ray tracing is performed by application of the conventional first order 4 x 4 transfer matrices ¹⁾ to the phase space ellipses. The elements of the phase space ellipse σ are:

$$\sigma = \begin{pmatrix} \sigma_{11} & \sigma_{12} & & \\ & \sigma_{12} & \sigma_{22} & \\ & & & 0 \\ & & 0 & \sigma_{33} & \sigma_{34} \\ & & & \sigma_{34} & \sigma_{44} \end{pmatrix}$$

$$\begin{aligned} \text{with } \sigma_{11} &= XMAX^2 & \sigma_{33} &= YMAX^2 \\ \sigma_{12} &= ALPHA \times XMAX \times X'MAX & \sigma_{34} &= ALPHA \times YMAX \times Y'MAX \\ \sigma_{22} &= X'MAX^2 & \sigma_{44} &= Y'MAX^2 \end{aligned}$$

(see fig. 2 and 3).

The desired coordinate system can be chosen by the specification of a beam centroid shift and a reference angle in the bending elements.

References

- 1) K.L. Brown, S.K. Howry; Report SLAC 91 (1970)
- 2) W. Gardner, D. Whiteside; Rutherford High Energy Laboratory, Report NIRL/M/21 (1961)
- 3) B.W. Davis; Nucl. Inst. Meth. 105 (1972) 477
- 4) D.V. Amundson, J.W. Dawson; Particle Accelerators 4 (1972) 19

are routinely available. The best target found is enriched tellurium (96 %) dioxide ¹⁾ irradiated behind the first electrostatic deflector. Fig. 1 shows the TeO₂-target on a platinum backing inside a so-called water target ²⁾ head. The beam passes through a 0.1 mm CuBe window and a 0.1 mm water film onto the target.

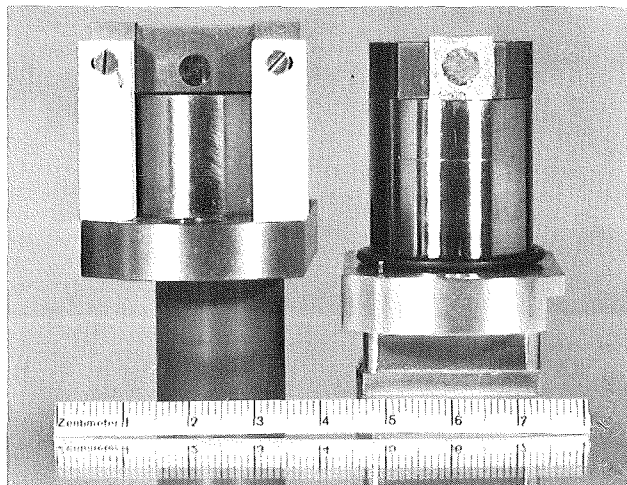
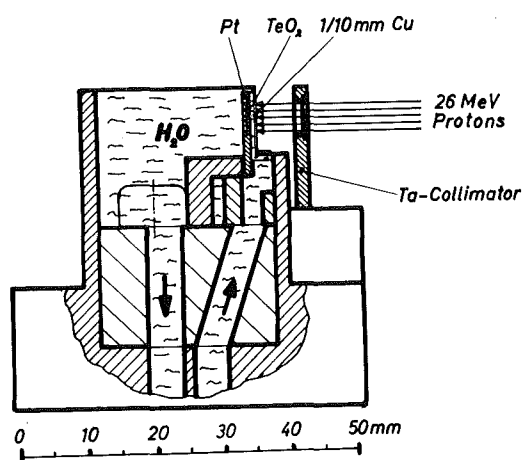


Fig. 1: Principle and photograph of the irradiation set-up for ¹²³J production. The glassy 150 mg/cm² TeO₂ (¹²⁴Te 96 %) is melted into a thin platinum metal backing. The energy loss in the target is about 5 MeV. We have tested this kind of target several times at beam currents of 20 μA of protons without any problems

The extraction of iodine is achieved by dry distillation at 820°C in a glovebox (fig. 2).

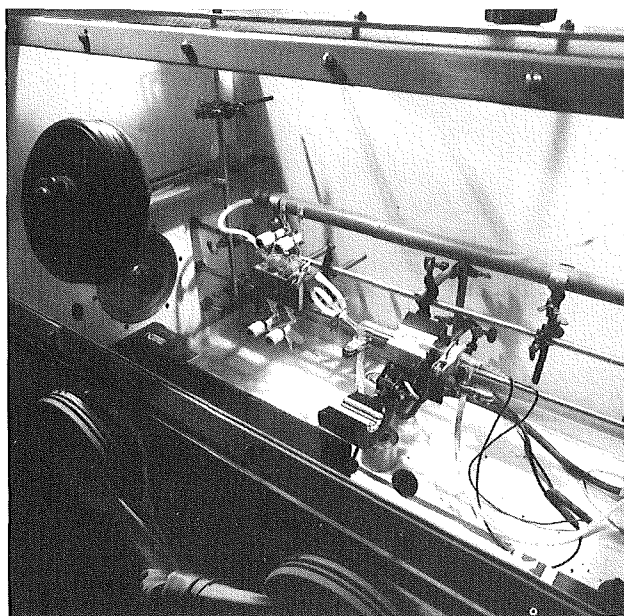
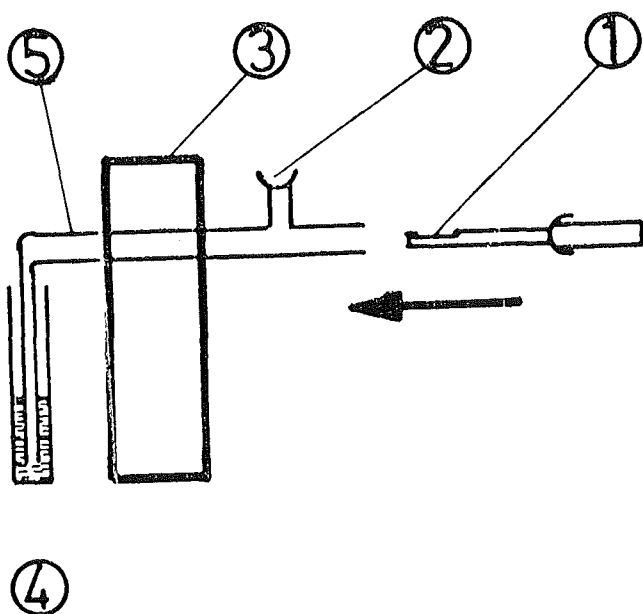


Fig. 2: Apparatus for separation of iodine from the irradiated TeO₂ target:
 (1) platinum with TeO; (2) O₂ gas flow (20 ml/min); (3) oven (820°C);
 (4) 0.001 M NaOH solution; (5) quartz tubes

Typically, a 1 h bombardment at 10 μ A of protons yields 85 mCi Iodine-123 after chemical separation. The contamination of Iodin-124 is <1.2 % at E.O.B. (end of bombardement). The radionuclidic purity of the NaJ-solution is analyzed using a 27 cm^3 Ge(Li) detector and the following relativ activities normalized to E.O.B. were found:

Iodine	$T_{1/2}$ [h]	Concentration [% of I-123]
120	1.35	$< 7 \cdot 10^{-3}$
121	2.12	0.2
123	13.2	100
124	99.6	1.03
126	312.0	< 0.02
128	0.42	4.1
130	12.4	< 0.03

Since the middle of 1976 this production scheme has proved to be very reliable in a pilot study together with the Nuklearmedizinische Klinik rechts der Isar in München and the Deutsche Krebsforschungszentrum Heidelberg. A summary of Iodine-123 production figures for 1976 is given in table 1.

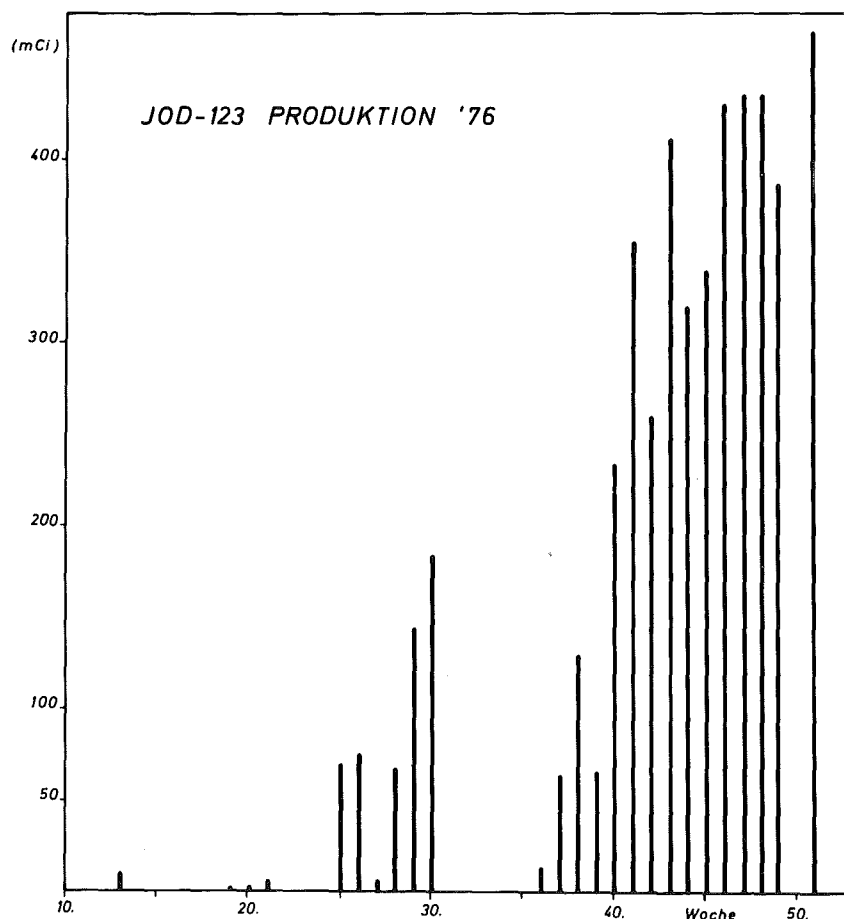


Table 1: ^{123}J -production at Karlsruhe, 1976

References

- 1) R. van de Bosch, J.J.M. de Goeig, J.A. van der Heide, J.F.W. Terlolen, H.M.J. Theelen, C. Zegers; Eindhoven, private communication (1976)
- 2) F. Schulz, H. Bellemann; Report KFK 685 (1967)

3. BASIC NUCLEAR PHYSICS AT THE CYCLOTRON

3.1 Experiments using the 156 MeV ${}^6\text{Li}^{3+}$ -Beam

3.1.1 Giant Resonance Excitation by 156 MeV ${}^6\text{Li}$ Scattering

H.J. Gils, H. Rebel, J. Buschmann

Institut für Angewandte Kernphysik des Kernforschungszentrums Karlsruhe

H. Klewe-Nebenius

Institut für Radiochemie des Kernforschungszentrums Karlsruhe

Recent investigations of electron and hadron scattering have revealed a new type of giant resonance in nuclei which is ascribed to an isoscalar quadrupole oscillation. Generally the corresponding peak in the spectra of inelastically scattered particles occurs at 2 MeV lower in excitation energy than the well established giant dipole resonance. In (p,p') , (d,d') , (τ,τ') and (α,α') spectra it has been observed as a broad bump superimposed upon a considerable continuum background. This background arising from more complicated processes such as quasielastic reactions and preequilibrium decay is the origin of difficulties of the quantitative interpretation of the measured spectra.

As part of a general study of ${}^6\text{Li}$ induced reactions at bombarding energies up to 156 MeV we report the observation of the giant quadrupole resonance (and possibly some components of different multipolarities hidden in the broad bump observed) excited by scattering of ${}^6\text{Li}$ projectiles on ${}^{208}\text{Pb}$. The excitation of highly excited states by inelastic scattering of more complex projectiles may be assumed to provide advantages concerning the reduction of the continuum background in the scattering spectra. ${}^6\text{Li}$ projectiles ($T = 0$) seem to be of particular interest since - in contrast to heavier projectiles - ejectile excitation is suppressed due to the low lying α -d break-up threshold. In this experiment we used the 156 MeV ${}^6\text{Li}$ beam of the Karlsruhe Isochronous Cyclotron. The inherent acceleration conditions require a charge to mass ratio $e/m = 1/2$ so that ${}^6\text{Li}^{3+}$ ions injected from an external Penning ion source have to be accelerated ¹⁾. This implies severe restrictions to the beam current which was limited to about 30 nA in the present measurements. The measurements were done in a scattering chamber (130 cm \emptyset) installed behind a deflecting magnet operated in non-dispersive mode. Because of the restricted intensity the ${}^6\text{Li}$ beam has not been energy-analyzed, but the magnet provides some advantages for preparing a clean beam. The energy width of the beam was approximately 500 keV (FWHM). The particles scattered from a ${}^{208}\text{Pb}$ target (thickness 8 mg/cm²,

isotopic enrichment 99.2 %) were detected with several surface barrier detectors telescopes which allowed to distinguish ${}^7\text{Li}$ and ${}^6\text{Li}$ particles from each other and from all other reaction products. Despite of the limited beam intensity the giant resonance bump could be detected very quickly as a distinct peak at the expected energy position ⁴⁾, clearly separated from peaks due to target impurities and with the correct kinematic behaviour when varying the scattering angle. Without any background subtraction fig. 1 displays the interesting

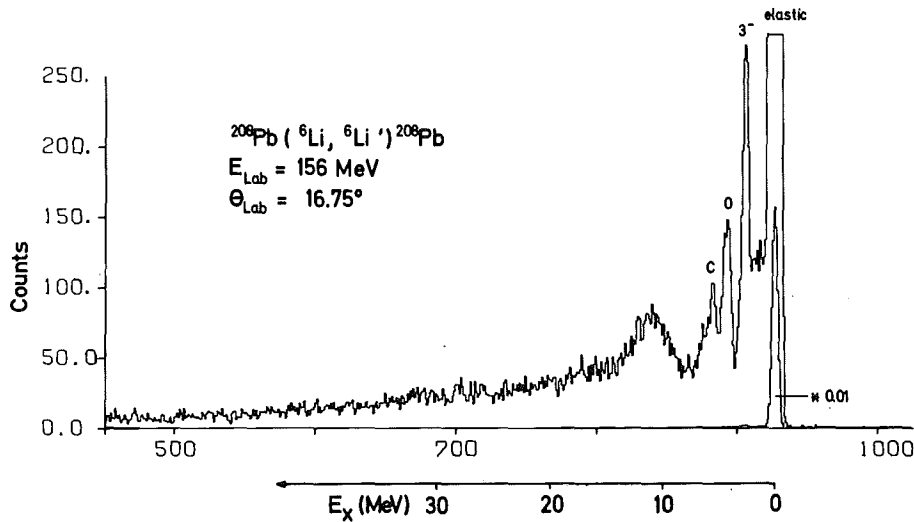


Fig. 1: Spectrum of inelastically scattered ${}^6\text{Li}$ ions of 156 MeV from ${}^{208}\text{Pb}$ showing the giant resonance region

part of one (${}^6\text{Li}, {}^6\text{Li}'$) spectrum revealing the giant resonance bump as convincingly as in more tedious α -particle decay-particle coincidence experiments ²⁾. Approximating the background linearly we extracted the giant resonance cross sections (for excitation energies $E_x = 7.5 - 16 \text{ MeV}$) for several scattering angles. The values obtained are compared to theoretical predictions on the basis of the phenomenological collective model for the quadrupole giant resonance centered around $E_x = 11 \text{ MeV}$ (fig. 2). The coupled channel calculations which have been performed in a 0^+-2^+ (GQR)-coupling scheme utilized the optical potential derived from elastic scattering of 156 MeV ${}^6\text{Li}$ particles from ${}^{208}\text{Pb}$ ³⁾. The $\beta_2 R$ -value was adopted from α -particle scattering results ⁴⁾. In general, complex coupling has been used with equal coupling parameters for real and imaginary part (the latter assumption $\beta^{\text{Real}} = \beta^{\text{Imag}}$ does not influence the results very strongly). For the purpose of our exploratory calculations

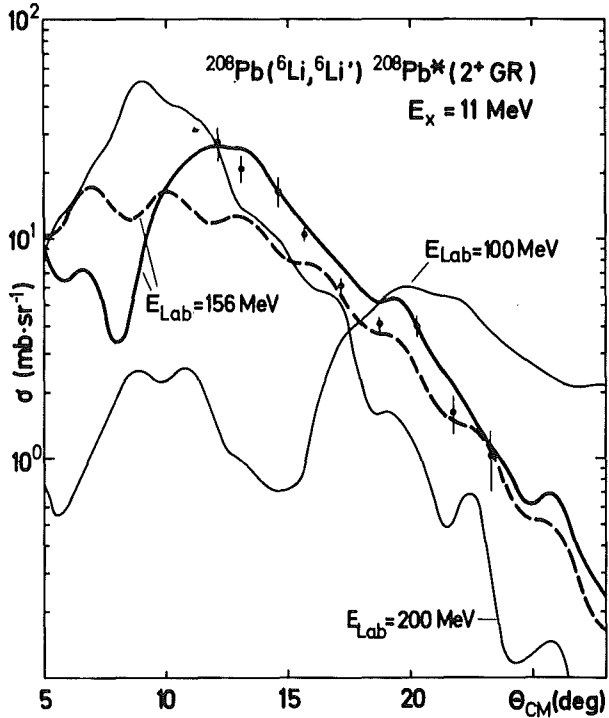


Fig. 2: Differential cross sections for the excitation of the observed giant resonance in ^{208}Pb ($7.5 < E_x < 16$ MeV) compared to the theoretical cross sections of quadrupole transitions for different projectile energies. The solid curves were obtained by complex coupling, the dashed curve corresponds to real coupling

a spin-orbit term of the optical potential has been ignored. The calculations indicate that the cross sections are strongly decreasing at energies $E_{\text{Li}} < 100$ MeV. The experiment demonstrates that ^6Li scattering at sufficiently high bombarding energy and with improved beam quality appears to be an excellent tool for more detailed studies of shape, components and multi-polarities of giant resonance excitation peaks.

References

- 1) F. Schulz and H. Schweickert, KFK-Report 2298 (1976)
- 2) K.T. Knöpfle and G.J. Wagner, private communication
- 3) H.J. Gils, H. Rebel, J. Buschmann, H. Faust, H. Klewe-Nebenius and S. Zagromski, to be published
- 4) D.H. Youngblood, J.M. Moos, C.M. Rozsa, J.D. Bronson, A.D. Bacher and D.R. Brown, Phys. Rev. C13 (1976) 934

3.1.2 Investigation of the Compound Nuclear Reactions $^{191+193}\text{Ir}, ^{197}\text{Au}(^6\text{Li}, xn+yp)$ at $E_{\text{Li}} = 48 - 156$ MeV

J. Kropp, H. Faust, J. Rieder, Physikalisches Institut der Universität Heidelberg

H. Klewe-Nebenius, Institut für Radiochemie des Kernforschungszentrums Karlsruhe

H. Rebel, H.J. Gils and K. Wisshak, Institut für Angewandte Kernphysik des Kernforschungszentrums Karlsruhe

Studies of the compound nuclear reactions $^{191+193}\text{Ir}, ^{197}\text{Au}(^6\text{Li}, xn+yp)$ at the 156 MeV ^6Li -beam by means of in-beam γ -ray spectroscopy ¹⁾ have been continued and the analyses of the data have been extended especially to reactions with charged particles in the exit channel. Experimental excitation functions for a variety of compound nuclear reactions have been compared to predictions of a more refined preequilibrium model (hybrid model ²⁾), which - in contrast to models used previously - is able to calculate absolute cross sections, too. In fig. 1 experimental excitation functions (drawn as smooth curves through the experimental points) are compared to theoretical predictions. The calculated excitation functions reproduce shapes and thresholds of the experimental curves in most cases well, but show strong discrepancies in absolute cross sections. The reduction factors by which the theoretical curves have to be divided, have values up to 7 for $(^6\text{Li}, xn)$ -reactions, but they are considerably smaller for the reactions with outgoing protons $(^6\text{Li}, xn+1(2)p)$.

Target							
^{197}Au	R	5n	7n	9n			
	F	6.5	6.5	6.5			
	R	5n+p	7n+p	9n+p	11n+p		
	F	2.2	2	2.8	3.5		
$^{191+193}\text{Ir}$	R	6n+2p	7n+2p	8n+2p	9n+2p	10n+2p	11n+2p
	F	0.15	0.3	0.4	0.9	1.8	3.7
$^{191+193}\text{Ir}$	R	(3+5)n(4+6)n	(5+7)n	(6+8)n	(7+9)n	(9+11)n	(10+12)n (11+13)n
	F	6.5 7	6.9	6.8	5.1	6.9	6.8 7.7
$^{191+193}\text{Ir}$	R	(3+5)n+p	(5+7)n+p				
	F	2	2.2				

Table 1: Reduction factors F for adjusting the calculated cross sections to the experimental excitation functions for all reactions R studied

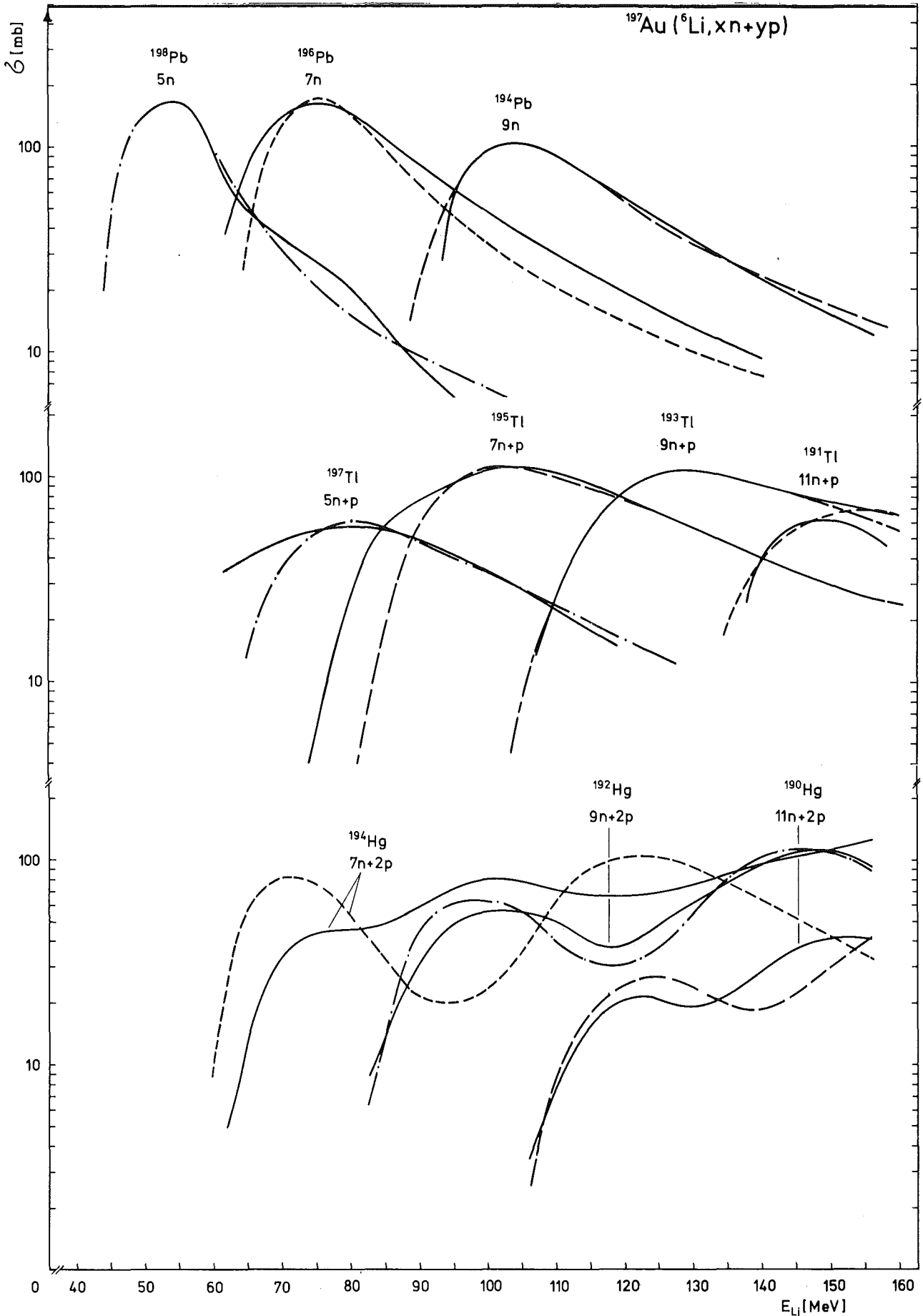


Fig. 1: Examples of the measured (—) excitation functions compared to the theoretical predictions. The theoretical cross sections have been reduced by the factors given in table 1

Since for (α, xn) reactions ³⁾ no such discrepancies were observed, the strong deviations for the $({}^6\text{Li}, xn)$ reactions are probably due to a strong reaction channel correlated with the ${}^6\text{Li}$ projectile which is not taken into account when calculating the total compound nucleus formation cross sections in theory.

We started, therefore, an investigation of ${}^6\text{Li}$ break-up which is expected to have a large cross section. Particle specific spectra obtained from the analysis of data measured with an E- Δ E telescope are shown in fig. 2. Broad α -particle, deuteron, and proton bumps are observed, with maxima at energies corresponding to the velocity of the primary projectiles, clearly indicating

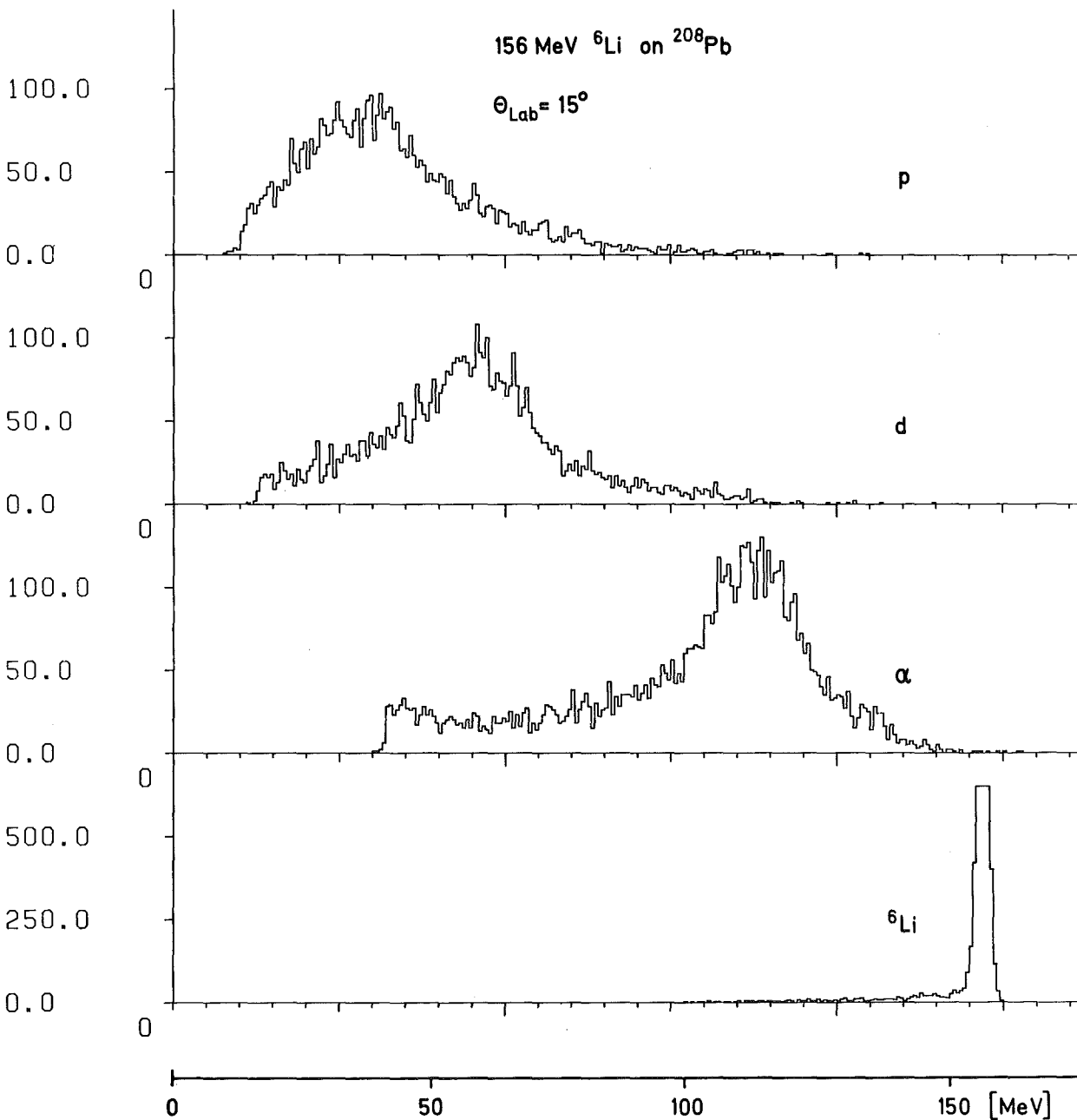


Fig. 2: Particle specific spectra from the reactions ${}^{208}\text{Pb}({}^6\text{Li}, p)$, $({}^6\text{Li}, d)$, $({}^6\text{Li}, \alpha)$, $({}^6\text{Li}, {}^6\text{Li}')$ measured at $E_{\text{Li}} = 156$ MeV and $\theta_{\text{Lab}} = 15^\circ$

the strong influence of the α -d-cluster structure of ${}^6\text{Li}$. The angular distributions of protons, deuterons and α -particles ejected from a ${}^{208}\text{Pb}$ target are displayed in fig. 3.

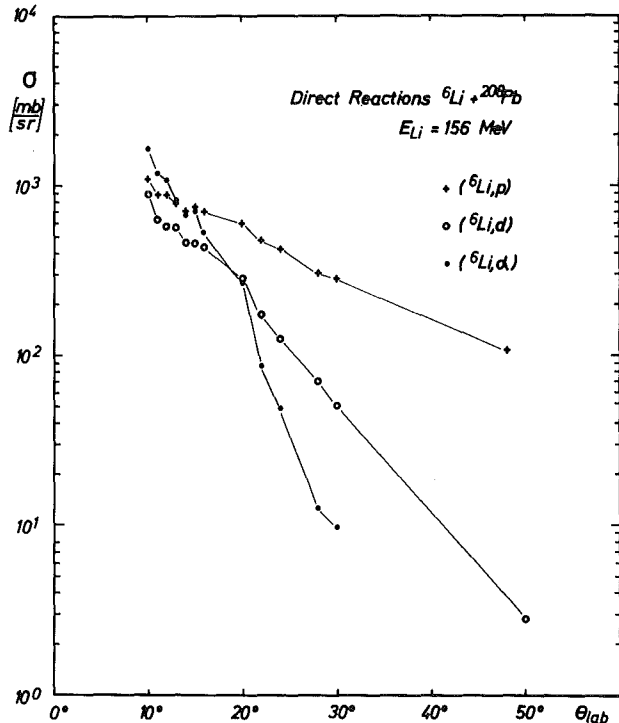


Fig. 3: Measured cross sections of the reactions $({}^6\text{Li},p)$, $({}^6\text{Li},d)$, and $({}^6\text{Li},\alpha)$ on ${}^{208}\text{Pb}$

Comparing the cross sections of the α -particle and d-bumps at very forward direction there are conspicuously more α -particles than deuterons, an observation suggesting some contribution of the three particle break-up ${}^6\text{Li} \rightarrow \alpha + p + n$. At more backward angles, however, this behaviour changes and we observe more deuterons than α -particles. The reason for this behaviour is not yet completely understood, but it may, at least partly, originate from a "cluster transfer into highly excited states". This effect described in the following may also explain the enhancement of the $({}^6\text{Li},xn+1(2)p)$ -reactions as compared to $({}^6\text{Li},xn)$ reactions discussed above. The ${}^6\text{Li}$ penetrating the nuclear field not completely loses the memory of its original structure and occupies with some preference cluster configurations in the beginning of the equilibration process from where one of the clusters is emitted by a direct stripping process while the other cluster and the target nucleus are fusing to a highly excited compound nucleus. With this view a $({}^6\text{Li},xn+pn)$ reaction e.g. may be regarded to contain a component of an $(\alpha,(x-1)n)$ compound nuclear reaction accompanied by emission of a spectator deuteron (or n-p pair). These reaction ways - being probable in particular when the ${}^6\text{Li}$ projectile is penetrating deeply into the target nucleus and when therefore the second cluster is emitted under larger scattering angles - enhance the probability for $({}^6\text{Li},xn+1(2)p)$.

A further investigation of these processes which is necessary to clarify these hypotheses, is planned for the near future by measuring e.g. the coincidences between break-up particles and γ -rays of the final nuclei of compound nuclear reactions.

References

- 1) J. Kropp, J. Buschmann, H. Klewe-Nebenius, H. Rebel, H. Faust, H.J. Gils, K. Wisshak, KFK-Report 2223 (1975) 42;
Z. Phys. A280 (1977) 61
- 2) M. Blann, Phys. Rev. Lett. 28 (1972) 757
- 3) P. Jahn, H.J. Probst, A. Djaloeis, W.F. Davidson, C. Mayer-Böricke, Nucl. Phys. A209 (1973) 333

3.1.3 Scattering of ${}^6\text{Li}$ on ${}^{12}\text{C}$, ${}^{40}\text{Ca}$, ${}^{90}\text{Zr}$, ${}^{208}\text{Pb}$ at $E_{\text{Li}} = 156 \text{ MeV}$

H.J. Gils, H. Rebel, J. Buschmann, S. Zagromski

Institut für Angewandte Kernphysik des Kernforschungszentrums Karlsruhe

H. Klewe-Nebenius

Institut für Radiochemie des Kernforschungszentrums Karlsruhe

H. Faust

Physikalisches Institut der Universität Heidelberg

Up to now information on phenomenological interaction parameters for high-energetic ${}^6\text{Li}$ -projectiles is very scarce. In order to obtain realistic optical potentials for ${}^6\text{Li}$ -interaction with nuclei scattering experiments with the 156 MeV ${}^6\text{Li}$ beam have been started at the Karlsruhe Isochronous Cyclotron. The experiments used the big scattering chamber (130 cm \emptyset) installed at beam line 5 which includes the monochromator magnet. In order not to lose intensity in the external beam transport system the monochromator magnet was used in non-dispersive mode. Thus the energy spread of the primary beam amounted to about 500 keV FWHM. The beam spot on the target had a diameter of about 2 mm and the beam divergence was estimated to be less than 0.2° FWHM. The beam current on the target varied between 1 and 30 nA.

Scattered particles with masses between 6 and 9 amu were detected by four ΔE -E telescopes of Si surface barrier detectors mounted on the same movable arm in the scattering chamber with angular distances of 1.5° between each other. Each telescope consisted of one ΔE detector of 300 μm thickness and one E detector of 4 mm thickness being sufficient to stop ${}^6\text{Li}$ ions up to their maximum energy. The electronic set-up consisting of standard NIM-modules enabled a preselection of ${}^6\text{Li}$, ${}^7\text{Li}$ and Be events. The data were accumulated and stored on magnetic tape event by event. Final particle identification was performed by an off-line method ¹⁾ after the measurements. Natural targets of C (8.3 mg/cm^2) and of Ca (7.8 mg/cm^2) and highly enriched targets (> 99 %) of ${}^{90}\text{Zr}$ (3.8 mg/cm^2) and of ${}^{208}\text{Pb}$ (8.0 mg/cm^2) were used. In fig. 1 some particle specific spectra are displayed for the ${}^{12}\text{C}$ and the ${}^{208}\text{Pb}$ target, respectively. Angular distributions of elastic scattering were measured between $\theta_{\text{Lab}} = 10\text{-}30^\circ$ (${}^{12}\text{C}$, ${}^{90}\text{Zr}$, ${}^{208}\text{Pb}$) and between $\theta_{\text{Lab}} = 7\text{-}45^\circ$ (${}^{40}\text{Ca}$) in steps of 0.5° .

Fig. 2 shows preliminary results of the measured cross sections for ${}^{12}\text{C}$ and ${}^{40}\text{Ca}$. The solid curves are the results of conventional optical model calculations with 6-parameter Saxon-Woods potential fitted to the measured data.

A spin-orbit term has not yet been included. The resulting parameter values

of the optical potential are compiled in tab. 1.

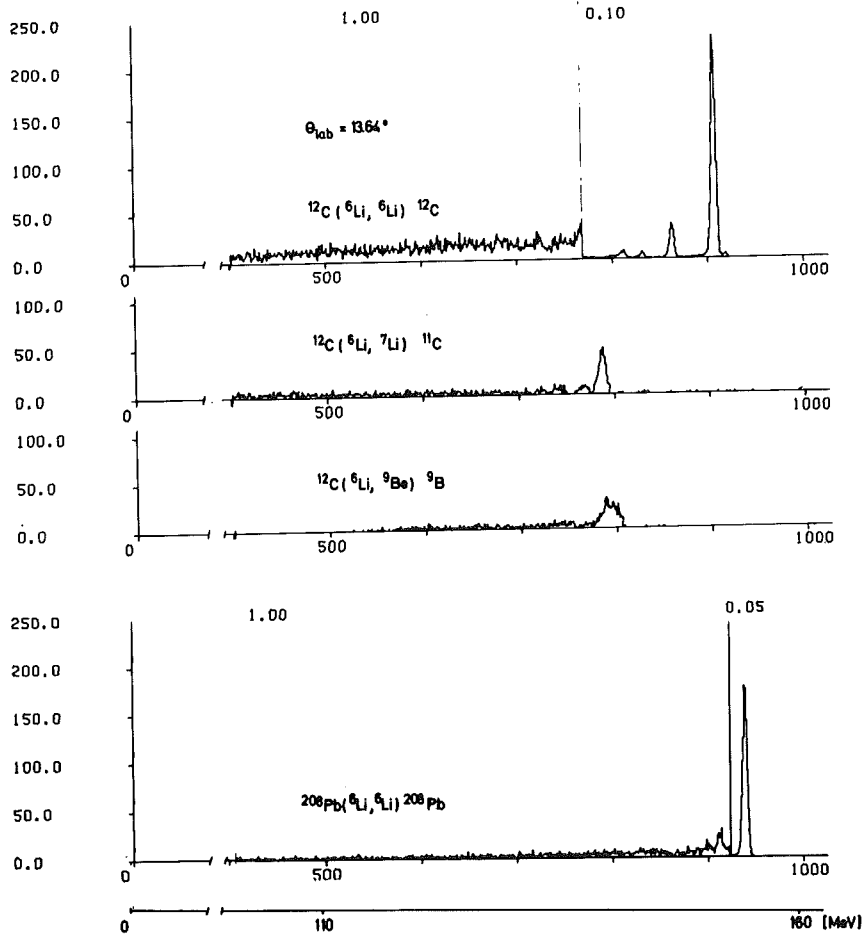


Fig. 1: Particle specific spectra of ${}^6\text{Li}$ induced nuclear reactions on ${}^{12}\text{C}$ and ${}^{208}\text{Pb}$ targets, respectively

Target	V (MeV)	r_v (fm)	a_v (fm)	W (MeV)	r_w (fm)	a_w (fm)
${}^{12}\text{C}$	129.	1.21	0.89	28.	1.67	0.97
${}^{40}\text{Ca}$	170.	1.22	0.89	29.	1.73	0.90
${}^{90}\text{Zr}$	145.	1.19	0.93	19.	1.75	0.83
${}^{208}\text{Pb}$	180.	1.22	0.78	20.	1.57	0.97

Tab. 1: Resulting parameters of Saxon-Woods optical potential for elastic ${}^6\text{Li}$ scattering resulting from fit calculations. For ${}^{208}\text{Pb}$ the depth of the real potential was fixed

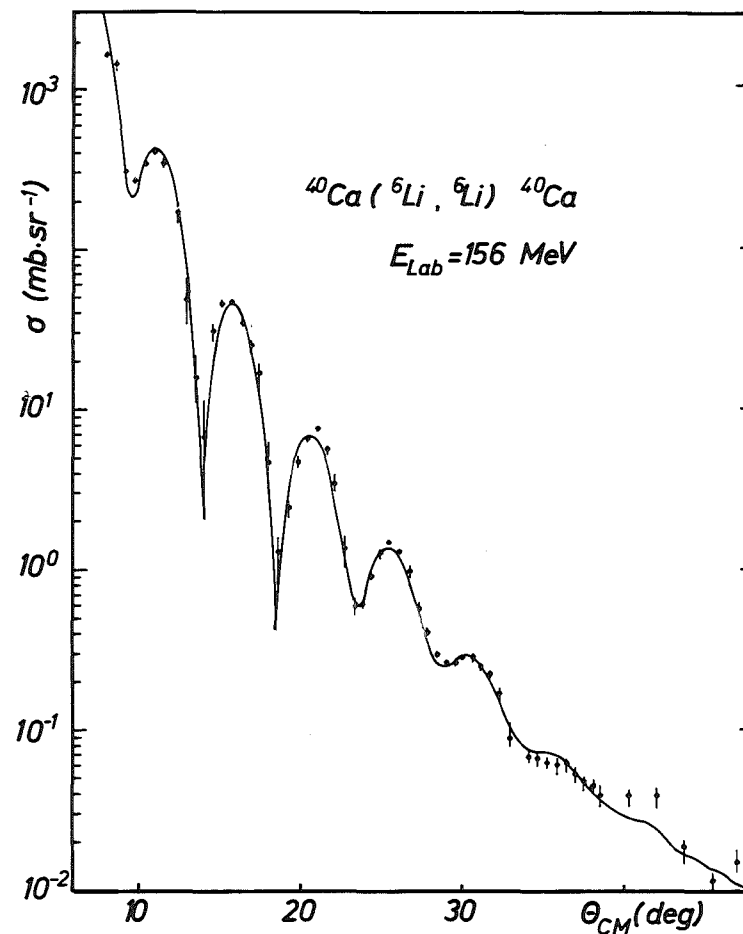
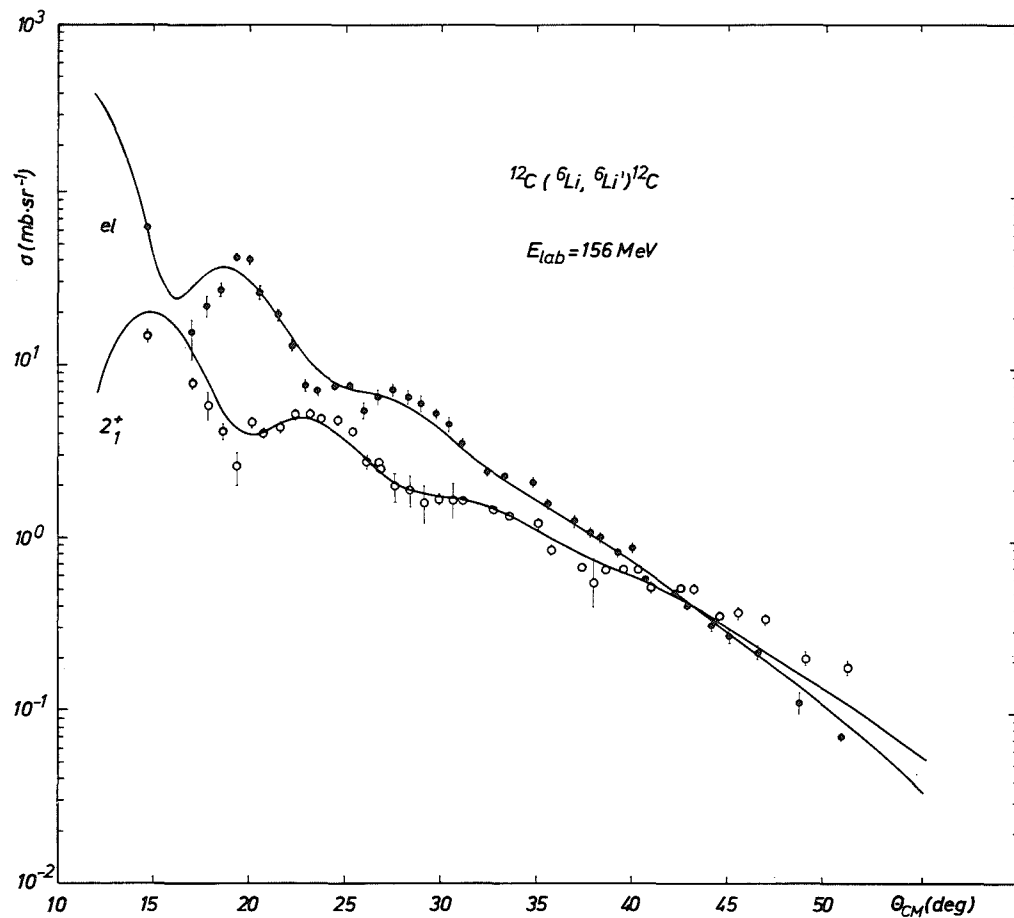


Fig. 2: Measured cross sections of elastic and inelastic ${}^6\text{Li}$ scattering on ^{12}C and ^{40}Ca . The solid curves through the elastic scattering points are the result of an optical model fit calculation. The curve of inelastic scattering to the 2_1^+ -state of ^{12}C is a coupled channel prediction with $\beta_2=0.4$ based on the elastic scattering optical potential parameters

For the heavier nuclei ^{90}Zr and ^{208}Pb the potential depth could not be determined unambiguously. The radius and diffuseness parameters of the real potential, however, are well determined and are nearly the same for all nuclei. One should note that the resulting diffuseness parameters of the imaginary part are rather large, which possibly can be ascribed to the influence of the strong ^6Li -break-up channel.

Using these parameters and adopting a value of $\beta_2 = 0.4$ the inelastic scattering angular distribution of the 2^+ -state in ^{12}C was calculated by the coupled channel method. The result is in good agreement with the experimental points.

References

- 1) F.S. Goulding, D.A. Landis, J. Cerny and R.H. Pehl,
Nucl. Instr. Meth. 31 (1964) 1

3.2 Experiments using the 52 MeV Polarized Deuteron Beam

3.2.1 Spin Determination of Selected Hole States by a Measurement of the Analysing Power of the ($\vec{d}, {}^3\text{He}$) Reaction

H. Breuer, P. Doll, K.T. Knöpfle, G. Mairle, H. Riedesel and G.J. Wagner
Max-Planck-Institut für Kernphysik, Heidelberg

V. Bechtold, L. Friedrich

Institut für Angewandte Kernphysik des Kernforschungszentrums Karlsruhe

The investigation of neutron and proton pick-up reactions which we performed in the past has yielded valuable spectroscopic information such as occupation numbers, separation energies and transferred ℓ -values. Unique assignments to the transferred spin j have become possible now by means of the vector-polarized d-beam of 52 MeV. We shall demonstrate in a few selected cases which are of particular importance for the structure of light nuclei how spins are determined from measuring the vector analysing power of the reaction products.

1. ${}^{16}\text{O}(\vec{d}, {}^3\text{He}){}^{15}\text{N}$

In addition to the strongly populated $1p_{1/2}$ and $1p_{3/2}$ hole states at 0 and 6.32 MeV, two other $1p$ hole states have been observed ¹⁾ at 9.94 and 10.71 MeV. Depending on their spins being $1/2^-$ or $3/2^-$, the $1p$ spin-orbit splitting could range between 4.32 and 6.88 MeV. By comparing the vector analysing powers of the states of unknown spins with the known ones (fig. 1), we conclude that $J = 3/2$ for both the 9.94 and 10.71 MeV states leading to a $1p$ spin-orbit splitting of 6.88 MeV. Difficulties of the DWBA calculations to describe the analysing powers are evident.

2. ${}^{28}\text{Si}(d, {}^3\text{He}){}^{27}\text{Al}$

In this reaction performed with unpolarized deuterons, two strong $\ell = 1$ transitions to states at 4.05 and 5.16 MeV in ${}^{27}\text{Al}$ have been known long since ^{2,3)}. Originally attributed to the pick-up from the essentially empty $2p$ shell ²⁾, the systematics of $1p$ proton separation energies revealed their $1p$ origin ⁴⁾. The spins of the two states, however, remained undetermined, though their knowledge is essential for the deformation of the ${}^{16}\text{O}$ core in ${}^{27}\text{Al}$ and the $1p$ spin-orbit splitting ⁵⁾. They are determined now from the analysing powers as $1/2^-$ (4.05 MeV) and $3/2^-$ (5.16 MeV); see fig. 2.

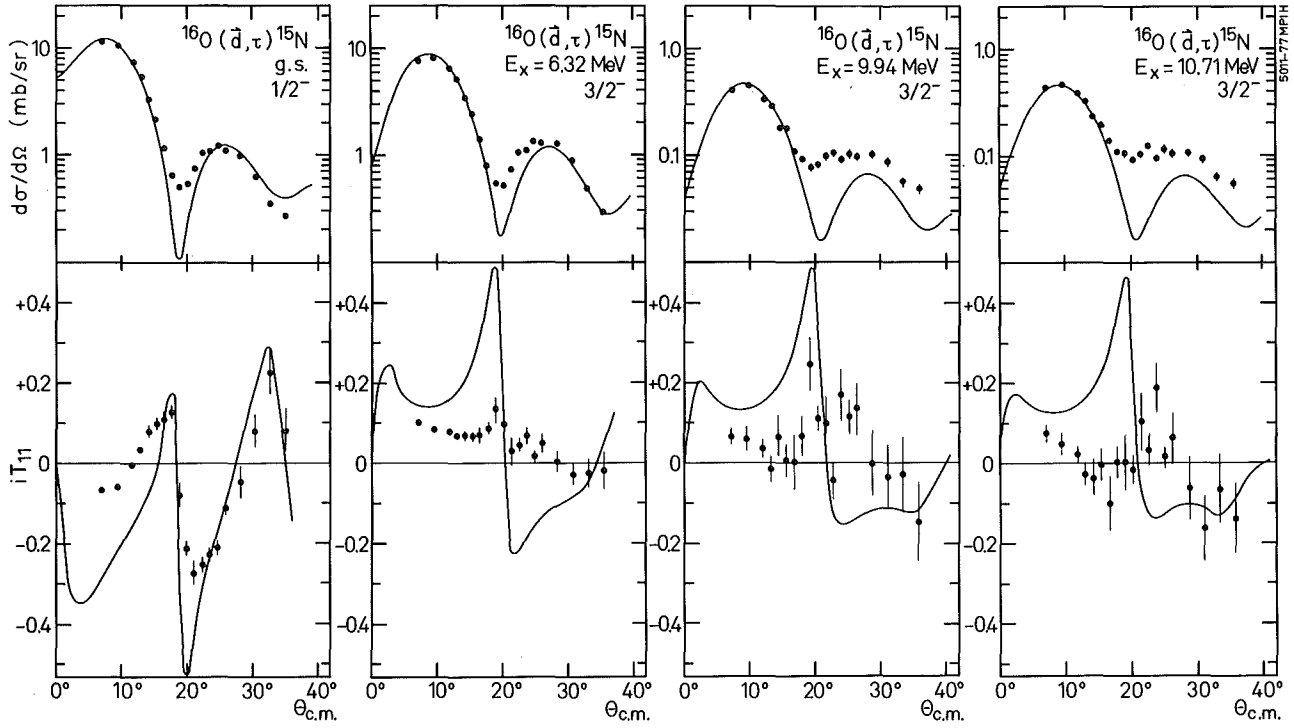


Fig. 1: Measured angular distributions (top) and analysing powers (bottom) together with DWBA calculations

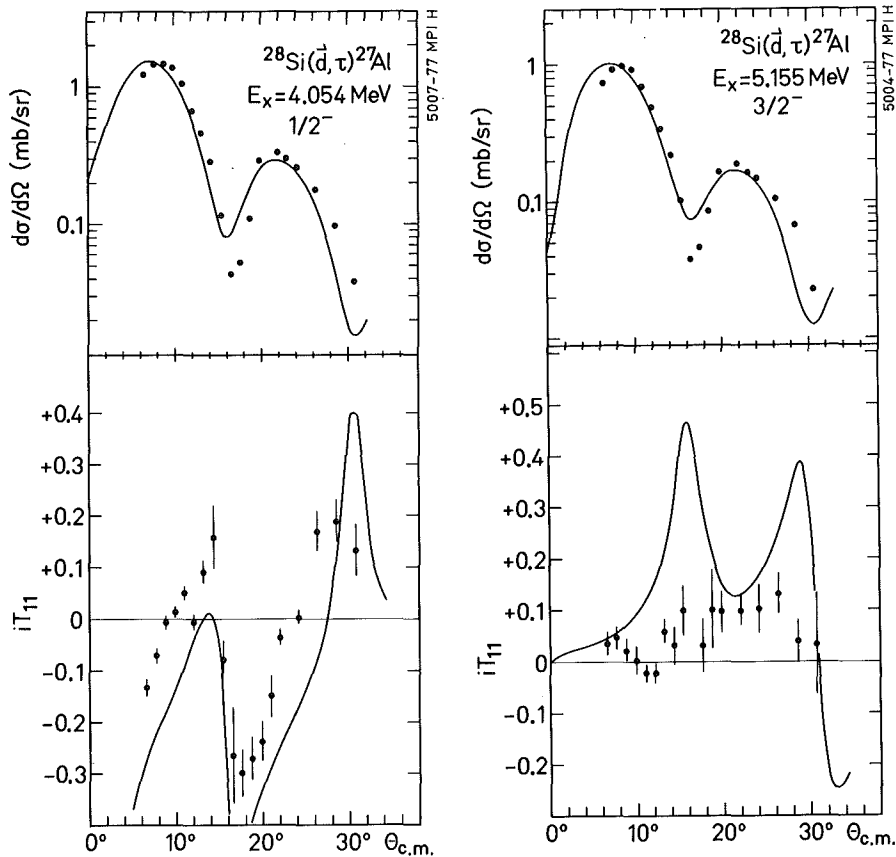


Fig. 2: Measured angular distributions (top) and analysing power (bottom) together with DWBA calculations

The absence of Q-value effects and the typical behaviour of the analysing powers for states of known spins is demonstrated in Fig. 3.

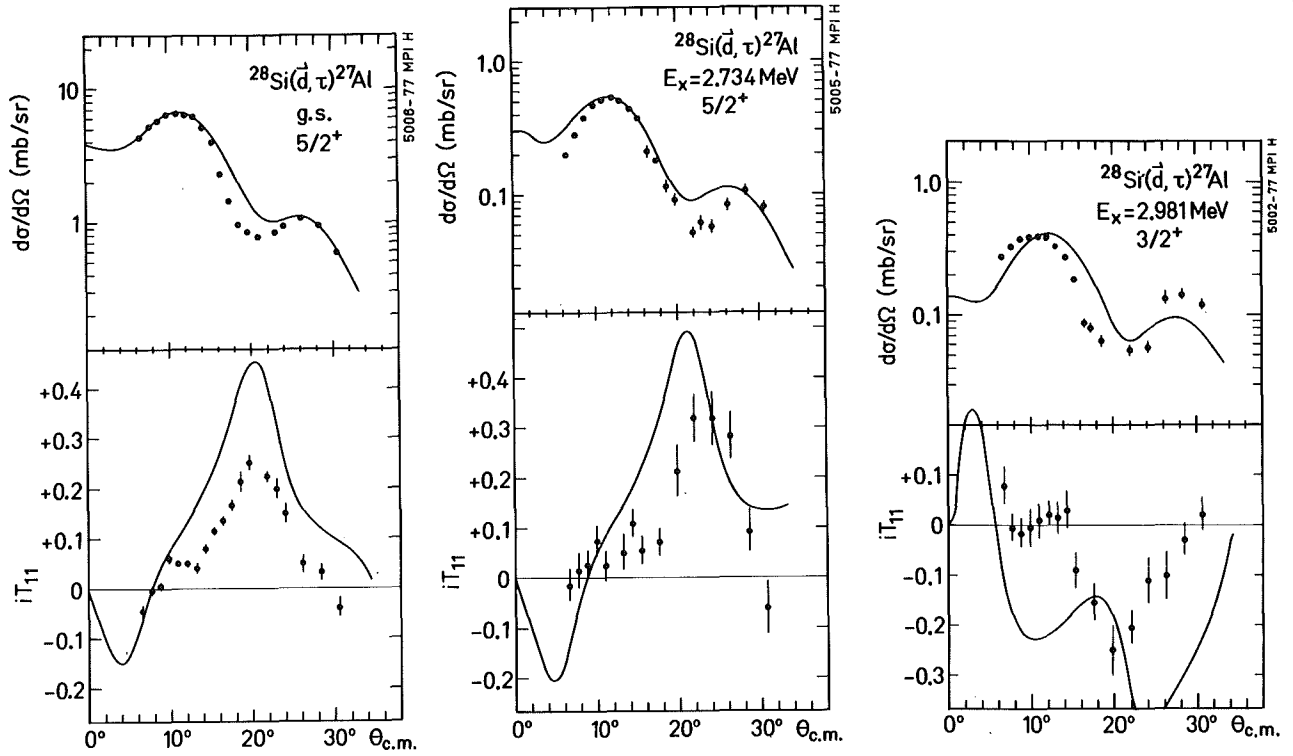


Fig. 3: Measured angular distributions (top) and analysing powers (bottom) together with DWBA calculations

3. $^{40}\text{Ca}(d, ^3\text{He})^{39}\text{K}$

Besides a strong g.s. transition, which corresponds to pick-up from the $1d_{3/2}$ shell, many $\ell = 2$ transitions are observed ⁶⁾ above 5 MeV in ^{39}K , which were interpreted as pick-up from the $1d_{5/2}$ shell on the basis of shell model arguments. On the other hand, Seth attributes ⁷⁾ a spin $3/2^+$ to a state at 6.322 MeV close to the energy where we observed a strong $\ell = 2$ transition. According to the measured analysing power, the states at 5.27, 5.61 and 6.34 MeV (the strongest $\ell = 2$ states in this energy range with $C^2S > 0.6$) have spins $5/2^+$.

References

- 1) G. Mairle and G.J. Wagner, Z. Physik 258 (1973) 321
- 2) B.H. Wildenthal and E. Newman, Phys. Rev. 167 (1968) 1027
- 3) H. Mackh, G. Mairle and G.J. Wagner, Z. Physik 269 (1974) 354
- 4) G.J. Wagner, Phys. Lett. 19 (1968) 1027
- 5) G. Mairle and G.J. Wagner, Phys. Lett. 50B (1974) 252
- 6) P. Doll, G.J. Wagner, K.T. Knöpfle and G. Mairle,
Nucl. Phys. A263 (1976) 210
- 7) K.K. Seth, private communication on the basis of a $^{41}\text{K}(p,t)$
experiment

3.2.2 Vector Analysing Power in d-p and d-d Elastic Scattering at 52 MeV

V. Bechtold, L. Friedrich

Institut für Angewandte Kernphysik des Kernforschungszentrums Karlsruhe

M.S. Abdel-Wahab, J. Bialy, M. Junge, F.K. Schmidt

Institut für Experimentelle Kernphysik des Kernforschungszentrums Karlsruhe

The investigation of nuclear reactions involving few nucleons only are of considerable interest, since it provides a direct access to the nucleon-nucleon interaction. Its importance is increasing even now since on the one hand polarization observables can be measured to a high degree of accuracy using polarized ion sources, on the other hand the theoretical treatment has been highly successful in the recent past¹⁻³⁾. Especially, calculations of the three body problem have been made starting from the Fadeev equations. They give information about the N-N-Interaction beyond that obtainable from two body investigations alone when they are compared to the experimental results. Using potentials, which included both P-wave interactions and tensor forces, Doleschall could demonstrate that the nucleon vector polarization in the elastic d-N-scattering was sensitive to the tensor part of the interaction. The experimental data that are available till now³⁻⁶⁾, namely the angular distributions of the nucleon polarization and the deuteron vector analysing power show a remarkable agreement with the theoretical predictions with regard to the structure. The still existing deviations in the magnitude should disappear with further refinement of the potential. The four body problem of the elastic d-d-scattering cannot be treated theoretically in such an exact way. Even if approximate calculations are tried difficulties arise because of the low break up threshold. Nevertheless from an experimental point of view it seems meaningful to measure the energy dependence of the deuteron vector analysing power, that shows unexpected large values with increasing energy⁷⁾.

The measurements of the deuteron vector analysing power in d-p and d-d elastic scattering reported here were carried out at a deuteron energy of 52 MeV. Thus the energy range investigated up to now is extended to higher energies. The deuteron beam of about 20 nA was purely vector polarized ($P_y = 0.45$). Gas targets were used in the main scattering chamber. In a second chamber the beam polarization was continuously monitored by counting the deuterons elastically scattered from ^{12}C at a lab. angle of 47° . The analysing power iT_{11} at this angle was taken to be $0.314 \pm 10\%$ ⁸⁾. NaJ scintillations detectors

were used. The particle identification was achieved by means of a time of flight method.

The results are shown graphically. The errors indicated there include those arising from counting statistics and background subtraction. The beam polarization uncertainty is not taken into account.

The angular distribution of the d-p-vector analysing power as shown in fig. 1 partly confirms the trend, that is already observed in the Berkeley data.

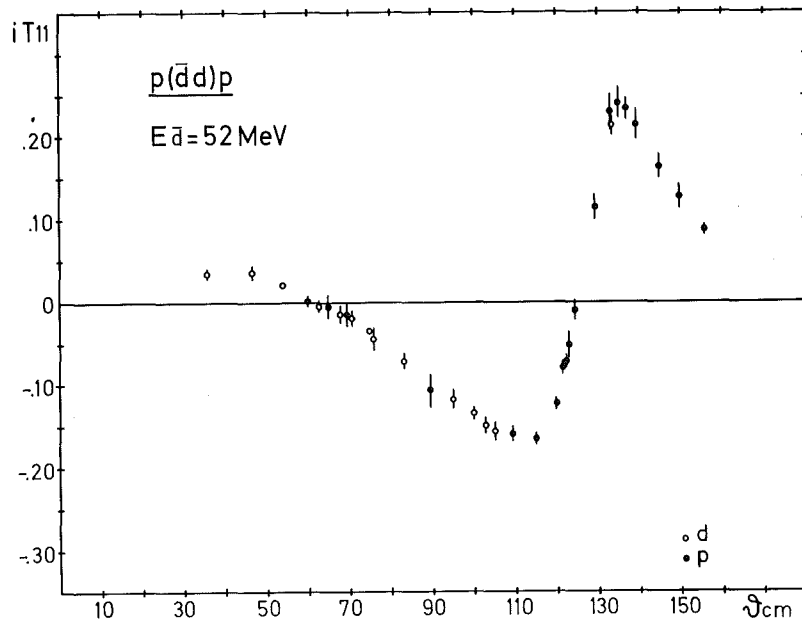


Fig. 1: The deuteron analysing power iT_{11} in the elastic deuteron-proton scattering at $E_d = 52$ MeV

With increasing deuteron energy the minimum of the distribution has become deeper as compared to the maximum value and its position has been shifted to larger angles. The peak value $iT_{11} = 0.25$ is the same as that measured at 45.4 MeV. Comparing the d-d distribution in fig. 2 to the Berkeley data taken at several lower energies a similar behavior is observed. The strong increase of the maximum analysing power between 20 and 40 MeV does not continue. Within the errors the value $iT_{11} = 0.32$ at 52 MeV agrees with that at 40 MeV. However at 52 MeV a second peak in the distribution seems to come into existence at forward angles.

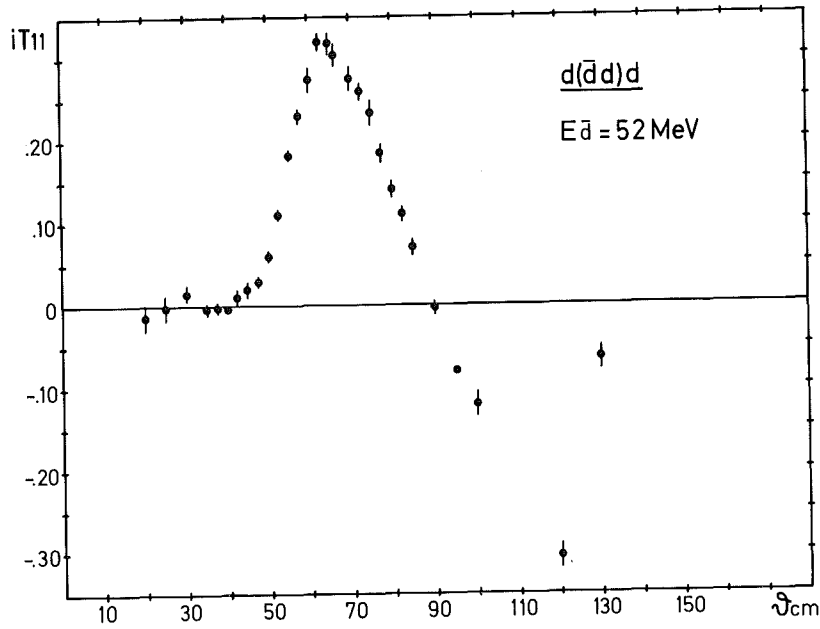


Fig. 2: The vector analysing power iT_{11} in the elastic deuteron-deuteron scattering at $E_d = 52 \text{ MeV}$

The authors wish to acknowledge the helpful assistance of P. Ziegler in operating the Lambshift-Source C-Laska.

References

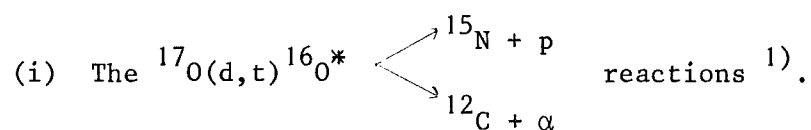
- 1) P. Doleschall, Nucl. Phys. A201 (1973) 264
- 2) P. Doleschall, Nucl. Phys. A220 (1974) 491
- 3) P. Doleschall, Proc. of the Fourth Intern. Symposium on Pol. Phenomena in Nucl. Reactions, Zürich, 1975, p. 51
- 4) J.C. Faivre, D. Garreta, J. Jungermann, A. Papineau, J. Sura and A. Tarrats, Nucl. Phys. A127 (1969) 169
- 5) J.S.C. McKee, H.E. Conzett, R.M. Larimer, and Ch. Leemann, Phys. Rev. Lett. 29 (1972) 1613
- 6) F.N. Rad, J. Birchall, H.E. Conzett, S. Chintalapudi, and R. Roy. Phys. Rev. Lett. 33 (1974) 1227
- 7) H.E. Conzett, W. Dahme, R.M. Larimer, Ch. Leemann, and J.S.C. McKee, Proc. of the Fourth Intern. Symposium on Pol. Phenomena in Nucl. Reactions, Zürich, 1975, p. 566
- 8) E. Seibt and Ch. Weddigen, Nucl. Inst. Meth. 100 (1972) 253

3.3 Nuclear Reactions with Unpolarized Deuterons and α -Particles

3.3.1 Decay Properties of Nuclear Hole States

H. Breuer, P. Doll, K.T. Knöpfle, G. Mairle, H. Riedesel, K. Schindler
and G.J. Wagner, Max-Planck-Institut für Kernphysik Heidelberg

The decay of nuclear hole states through coupling (i) with the continuum and (ii) with more complicated configurations in the A-1 nucleus has been investigated. To that aim, we have measured (i) the charged particle decay of highly excited hole states in ^{16}O and (ii) the systematics of hole strength distributions in the Ca-region.



The $^{17}\text{O}(d,t)$ reaction ²⁾ at 52 MeV strongly populates particle-hole states in ^{16}O of the dominant configuration $|1d_{5/2} \otimes 1p^{-1}|_{J^\pi, T}$; ($J^\pi = 1^-, \dots, 4^-$; $T = 0, 1$). In a coincidence experiment using a miniature gas cell we have now measured the protons and α -particles emitted from these states. The spectra of the decay products, identified by their time-of-flight, are given in fig. 1. The α -emission of states identified ²⁾ as $T = 1$ by a comparison with $^{17}\text{O}(d, ^3\text{He})^{16}\text{N}$ spectra reveals their isospin impurity. In-plane angular correlations yielding Γ_p/Γ and Γ_α/Γ branching ratios have been taken. With the total widths Γ measured in a high-resolution $^{17}\text{O}(^3\text{He}, \alpha)^{16}\text{O}$ experiment ³⁾, also reduced widths γ_p^2 and γ_α^2 were extracted. By comparison with DWBA angular correlation calculations, informations on spins and relative $1p_{1/2} : 1p_{3/2}$ (d,t)-transition amplitudes were obtained.

The coincidence requirement has revealed the existence of a strongly populated $(2,4)^-$ state at 17.78 MeV, which was masked by the $^{16}\text{O}(d,t)^{15}\text{O}$ (6.18 MeV) contaminant group in Ref. ²⁾. An interesting result is the observation of a P_o -decay of the $(4)^-, 1$ state at 18.97 MeV (see fig. 1). This dominant $|1d_{5/2} \otimes 1p_{3/2}^{-1}| \rightarrow 1p_{1/2}^{-1}$ transition represents the first observation of a nuclear Auger effect. The corresponding reduced width of only $\gamma_p^2 \approx 5$ keV is understood by treating the coupling with the $g_{9/2}$ -continuum as a small perturbation.

(ii) $1d_{5/2}$ hole states in Ar, Ca and Ti-nuclei

The $1d_{5/2}$ hole strength for Ar and Ca target nuclei is spread among many final states ⁴⁾. The intermediate structure of the strength distributions is understood ⁵⁾ from the decay of the $1d_{5/2}$ hole state into collective doorway states

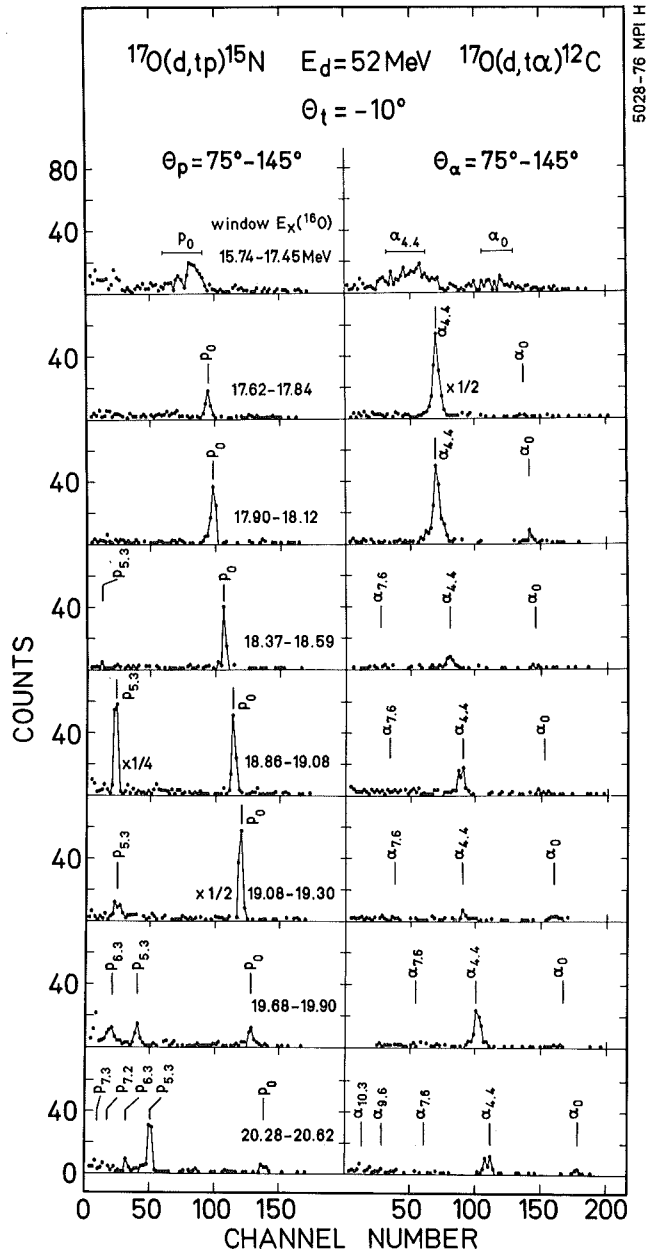


Fig. 1: Energy spectra of protons (left) and α -particles (right) emitted from $1d_{5/2}$ - $1p$ particle-hole states in ^{16}O

of the nature $|2^+ \otimes (2s, 1d)^{-1}|_{5/2^+}$, where 2^+ represents the lowest quadrupole phonon state. We have continued the study by measuring the $^{46,48,50}\text{Ti}(d, ^3\text{He})$ reactions at 52 MeV up to excitation energies of 30 MeV. There, also $|3^- \otimes f 7/2^{-1}|_{5/2^+}$ configurations contribute to the decay. The measured $1d$ -hole strength distributions averaged by folding with a Gaussian of 300 keV width are given by solid curves in fig. 2. The dashed curves result from a model calculation⁶⁾ with the $1d_{5/2}$ single particle energy as a free parameter. This calculation allows to study how single-particle properties depend on the unobservable high-energy tails of the strength distributions. E.g., deviations of up to 2 MeV (depending on the collectivity of the 2^+ phonon) of the observed centroid energy from the "true" $1d_{5/2}$ model energy are found.

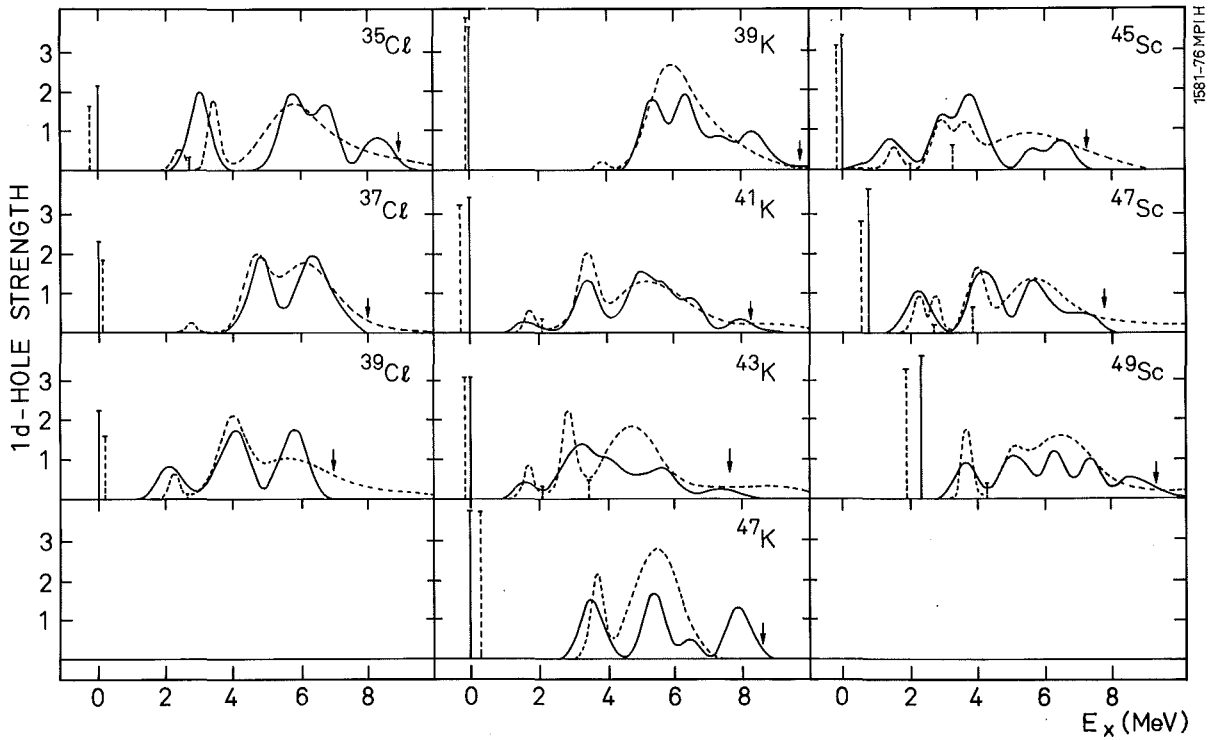


Fig. 2: Experimental (solid curve) and model dashed curve) $1d_{5/2}$ proton hole strength distributions versus excitation energy in the residual nucleus. Measured and calculated $1d_{3/2}$ spectroscopic factors are denoted by solid and dashed bars, respectively. The arrows indicate experimental energy limits

References

- 1) H. Breuer, thesis, Heidelberg (1976)
- 2) G. Mairle and G.J. Wagner, Phys. Lett. 50B (1974) 252
- 3) P. Doll, J.L.C. Ford, M. Goldschmidt, K.T. Knöpfle, G. Mairle, S.T. Thornton, G.J. Wagner and C.A. Wiedner, Proc. Int. Conf. on "Nuclear Structure and Spectroscopy", Amsterdam (1974), eds. H.P. Blok and A.E.L. Dieperink, Vol. 2, p. 181
- 4) P. Doll, H. Mackh, G. Mairle and G.J. Wagner, Nucl. Phys. A230 (1974) 329
P. Doll, G.J. Wagner, K.T. Knöpfle and G. Mairle, Nucl. Phys. A263 (1976) 210
- 5) G.J. Wagner, P. Doll, K.T. Knöpfle and G. Mairle, Phys. Lett. 57B (1975) 413
- 6) P. Doll and G.J. Wagner, to be published

3.3.2 Particle Decay from the Giant Resonance Region in ^{12}C

H. Breuer, P. Doll, K.T. Knöpfle, G. Mairle, H. Riedesel, K. Schindler,
G.J. Wagner, Max-Planck-Institut für Kernphysik Heidelberg

While the existence of an isoscalar giant resonance (GR) exhausting an appreciable fraction ($\sim 50\%$) of the isoscalar E2 energy weighted sum rule (EWSR) has been reported ¹⁾ for light nuclei down to ^{14}N , in the case of ^{12}C no appreciable concentration of E2 strength was observed in 150 MeV inelastic α scattering ($<(16 \pm 5)\%$ at $E_x \sim 27$ MeV). This result is at variance with 96 MeV inelastic α scattering data ²⁾ where a resonance structure around 27 MeV, which would exhaust 30-50% of the E2 EWSR, is observed. In order to clarify this discrepancy, we have measured the $^{12}\text{C}(\alpha, \alpha')$ reaction at $E_\alpha = 100$ MeV. The spectra (Fig. 1a) are in complete agreement with the 96 MeV data, but we observed a dependence of the shape of the GR structure on scattering angle, which indicates either the existence of different multipolarities or unaccounted variations of the large underlying α continuum with angle.

Since the origin of this effect cannot be determined uniquely from our singles spectra, we started an investigation of the charged particle decay from the GR region. The inelastically scattered α particles were measured at 17° , the maximum of the $L = 2$ angular distribution, while the decay products were detected in four surface barrier counters, which were moved in the reaction plane between -50° and -150° . Evaluation of the data is still in progress, but we can already state the following interesting conclusions:

(i) The coincidence requirement improves the peak-to-background ratio in the GR region considerably (fig. 1b), which results in a clean picture of the isoscalar GR in ^{12}C . In particular, we note a significant change of shape of the GR compared to the singles spectrum.

(ii) The origin of this change becomes evident from fig. 1c which shows that α particles from the $^{12}\text{C} + \alpha \rightarrow ^{11}\text{C} + ^5\text{He} \rightarrow ^{11}\text{C} + \alpha + n$ and $^{12}\text{C} + \alpha \rightarrow ^{11}\text{B} + ^5\text{Li} \rightarrow ^{11}\text{B} + \alpha + p$ reactions emerge with a final energy which equals that of inelastically scattered α particles from the GR region. In the singles spectra, these two processes cannot be separated, which may have simulated a large sum rule value ²⁾. In our coincidence experiment, both processes are easily disentangled

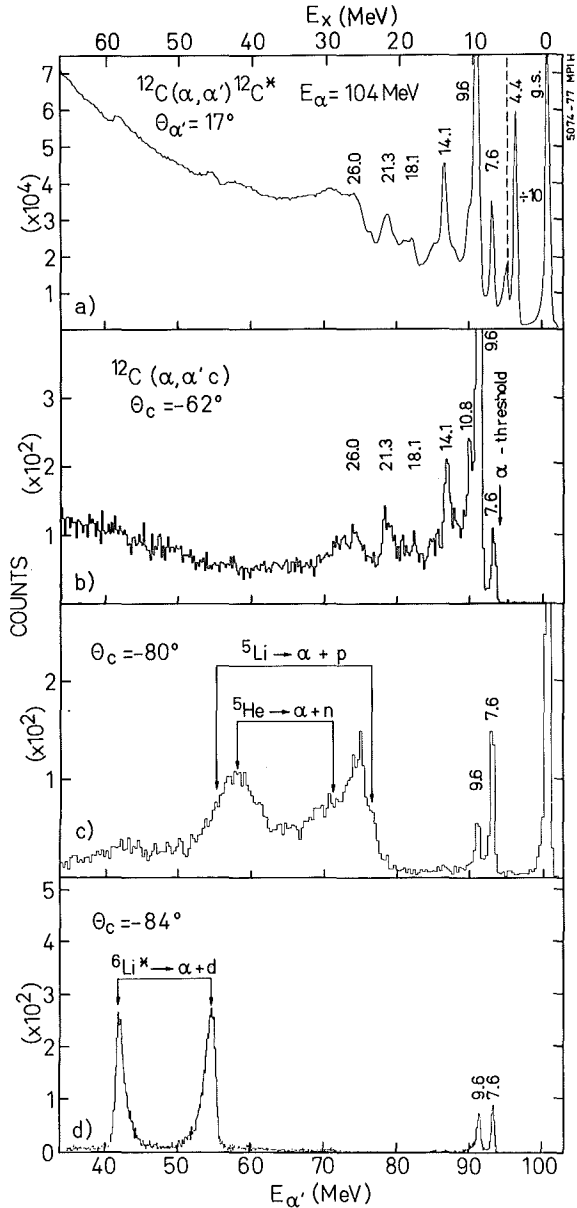
Fig. 1a:

Spectrum of the $^{12}\text{C}(\alpha, \alpha')$ reaction taken at 17° and at an incident energy of 104 MeV

1b: Spectrum of the $^{12}\text{C}(\alpha, \alpha'c)$ reaction taken in coincidence with all charged decay products $c(Z=1,2)$

1c: α spectrum of the $^{12}\text{C} + \alpha \rightarrow ^{11}\text{B} + ^5\text{Li} \rightarrow ^{11}\text{B} + \alpha + p$ and $^{12}\text{C} + \alpha \rightarrow ^{11}\text{C} + ^5\text{He} \rightarrow ^{11}\text{C} + \alpha + n$ reactions measured by kinematic coincidence with the respective recoil nuclei ^{11}B and ^{11}C

1d: α spectrum of the $^{12}\text{C} + \alpha \rightarrow ^{10}\text{B} + ^6\text{Li}^* \rightarrow ^{10}\text{B} + \alpha + d$ reaction measured by kinematic coincidence with the ^{10}B recoil nucleus



by a kinematic coincidence with the respective ^{11}C and ^{11}B recoil nuclei. (In case of 150 MeV α scattering, the energy of the α particles from ^5He and ^5Li decay corresponds to higher excitations in ^{12}C and thus does not affect the analysis of the 27 MeV excitation region.)

(iii) Via similar kinematic coincidences we were able to explain a large part of the underlying continuum. Besides processes mentioned in (ii), there are also contributions from the $^{12}\text{C} + \alpha \rightarrow ^{10}\text{B} + ^6\text{Li}^* \rightarrow ^{10}\text{B} + \alpha + d$ (Fig. 1d), $^{12}\text{C} + \alpha \rightarrow ^{10}\text{C} + ^6\text{He}^* \rightarrow ^{10}\text{C} + \alpha + 2n$ and $^{12}\text{C} + \alpha \rightarrow ^{10}\text{Be} + ^6\text{Be}^* \rightarrow ^{10}\text{Be} + \alpha + 2p$ reactions.

The final analysis of our measured angular correlation functions for the different decay products should enable us to determine uniquely the spins and the partial decay widths of the observed highly excited ^{12}C states, which will give important information on their microscopic structure.

References

- 1) K.T. Knöpfle et al., Phys. Lett. 64B (1976) 263 and
Annual Report of the MPI Heidelberg 1976
- 2) D.H. Youngblood, Proc. Intern. Symp. on Highly Excited States
in Nuclei, Jülich 1975, Vol. II, p. 51

3.3.3 Nuclear Matter Sizes of $^{204,206,208}\text{Pb}$ from 104 MeV α -Particle Scattering

H.J. Gils, H. Rebel, J. Buschmann

Institut für Angewandte Kernphysik des Kernforschungszentrums Karlsruhe

H. Klewe-Nebenius

Institut für Radiochemie des Kernforschungszentrums Karlsruhe

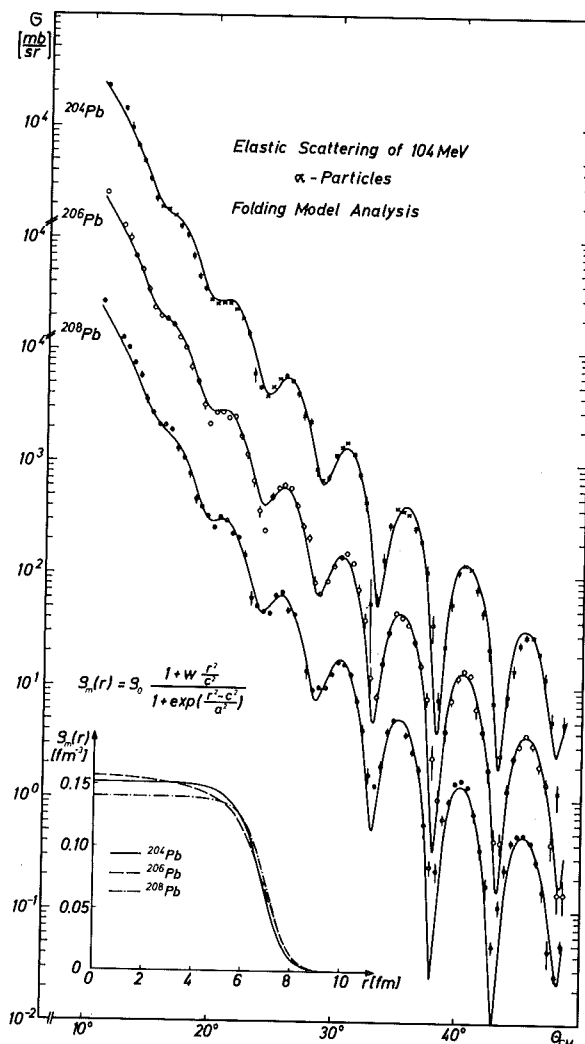
Gross properties of nuclei such as size, nucleon distribution or binding energy are of great importance for testing microscopic nuclear structure models. From electron scattering and mounic X-rays we have accurate information on charge and proton distributions, respectively. The experimental knowledge about neutron or total nucleon distributions, however, is scarce and less certain. In particular for heavier nuclei with a large neutron excess differences between proton and neutron distributions ¹⁾ may be expected. Hence a direct and unambiguous determination of neutron or total nucleon distributions is of great general interest.

Among the various methods which have been proposed for such an investigation α -particle scattering is a very promising approach. Due to the strong absorption in nuclear matter medium energy α -particle scattering has proved to be an excellent total for studying the nuclear surface. By folding models ²⁾ which relate the interaction potential to the nucleon density a reliable reaction model is provided. Recent systematic studies and analyses ³⁾ on the basis of such a model have shown that for lighter (not neutron rich) nuclei ($A \leq 60$) the extracted rms radii and higher moments of nuclear matter are in excellent agreement with other investigations so that this method can be applied to heavy nuclei with some confidence.

With this view the differential cross sections for elastic α -particle scattering from $^{204,206,208}\text{Pb}$ have been measured using the scattering facilities at the Karlsruhe Isochronous Cyclotron. The sharp diffraction pattern in the forward hemisphere ($\theta_{\text{CM}} < 50^\circ$) has been measured with high angular accuracy ($\Delta\theta < 0.1^\circ$) and in small angular steps (0.5°) which is important for the intended analyses.

The experimental results were analysed on the basis of the semimicroscopic folding model in order to determine the nucleon distributions at the nuclear surface using several phenomenological parametrizations of the densities. Fig. 1 shows the measured differential cross sections and the results of analyses with 3-parameter modified Gaussian distributions which reproduce the

Fig. 1: Folding model analyses of elastic α -particle scattering from $^{204,206,208}\text{Pb}$. The parameters c, a, w of the modified Gaussian nucleon distribution have been fitted to the measured data. The inset shows the resulting nucleon densities



experimental cross sections well. The corresponding nucleon distributions are inserted into the graph. Considering all analyses with different parametrization of the densities ^{4,5)} the following rms radii of the total nucleon distributions were obtained:

$$\begin{aligned}
 {}^{204}\text{Pb} \quad \langle r^2 \rangle_m^{1/2} &= 5.55 \pm 0.06 \text{ fm} \\
 {}^{206}\text{Pb} \quad \langle r^2 \rangle_m^{1/2} &= 5.57 \pm 0.06 \text{ fm} \\
 {}^{208}\text{Pb} \quad \langle r^2 \rangle_m^{1/2} &= 5.63 \pm 0.05 \text{ fm}
 \end{aligned}$$

From that one can calculate differences between neutron and proton distributions using e.g. the results of very precise electron scattering experiments ⁶⁾. The absolute values of the differences between neutron and proton density rms radii obtained by that way apparently depend on the particular procedure applied ^{4,5,7)}. But in any case there remains a small "neutron skin" at the

nuclear surface of 0.05 to 0.30 fm thickness. This is in fair agreement with laborious Hartree-Fock calculations ¹⁾ performed for the case of ^{208}Pb predicting the radius of the neutron density to be 0.23 fm larger than that of the proton density.

References

- 1) J.W. Negele; Comments Nucl. Part. Phys. 6 (1974) 15
- 2) H. Rebel, Proceedings of the Int. Summer School of Nucl Phys. (Predeal Sept. 1974); KFK-Report 2065 (1974)
- 3) H.J. Gils and H. Rebel, KFK-Report 2127 (1975);
Z. Physik A274 (1975) 259
- 4) H.J. Gils and H. Rebel, Phys. Rev. C13 (1976) 2159
- 5) H.J. Gils, H. Rebel, J. Buschmann, H. Klewe-Nebenius, G.P. Nowicki, and W. Nowatzke, Z. Physik A279 (1976) 55
- 6) H. Euteneuer, J. Friedrich, and N. Voegler, Phys. Rev. Lett. 36 (1976) 129
and private communications
- 7) E. Friedman and C.J. Batty, preprint (1977)

3.3.4 Experimental Studies of Isoscalar Octupole Transition Rates and of Neutron Collectivities by α -Particle Scattering

H.J. Gils and H. Rebel

Institut für Angewandte Kernphysik des Kernforschungszentrums Karlsruhe

The usual tests of the validity of nuclear structure models relate to excitation energies, electromagnetic transition rates, multipole moments, and inelastic electron scattering form factors. Electromagnetic quantities, however, are dominated by the proton configurations. In general, for more extended tests of microscopic descriptions of nuclei additional information on the neutron configurations is of extreme interest. In particular for heavy nuclei with different proton and neutron numbers a different collective behavior of protons and neutrons may be expected. The current methods for investigating such features are particle scattering and reaction experiments.

As well known, α -particle scattering provides great advantages when investigating collective features of nuclei. Different from electromagnetic methods, this method is not only sensitive to neutron configurations but at medium high energies the penetrability of α -particles is sufficient to probe the tails of the transition densities. The strong absorption situation leads to a simplified and reliable reaction model ¹⁾ providing the required information comparable to electromagnetic results. This is not often the case when working with strongly interacting probes.

We report here some studies of the strong collective 3_1^- -states of the even stable Pb isotopes $^{204,206,208}\text{Pb}$, especially of the 3_1^- -state of ^{208}Pb ($E_x = 2.615$ MeV) based on recent measurements of inelastic scattering of 104 MeV α -particles ²⁾. The experiments were motivated by the search for differences in collective proton and neutron properties and aim at a determination of isoscalar octupole transition rates and transition radii ($R_{\text{trans}} = |\langle r^{L+2} \rangle / \langle r^L \rangle|^{1/2}$).

The $^{204,206,208}\text{Pb}$ (α, α') cross sections have been analysed by the coupled channel method including Coulomb excitation in a $0^+ - 3_1^-$ -coupling scheme. The coupling potentials were generated by the folding procedure using various different functional forms for the transition densities $\rho_{\text{tr}}(r)$: ^{*)}

^{*)} Details of the procedures are given in refs. 2,3.

(i) The standard functional form used was a phenomenological parametrization of the matter transition density ρ_{if}^m according to the vibrational model (first derivate of a Fermi shape) following the procedure proposed for extracting isoscalar transition rates ^{4,5}. The values of the radius parameter c_m , diffuseness parameter a_m and the "normalization" β_3^m have been adjusted by fitting the data. The results of this standard procedure are given in tab. 1.

Target	$B(IS3;0^+ \rightarrow 3^-)$ ($10^5 e^2 fm^6$)	(s.p.u.)	R_{trans} (fm)
204	5.52 ± 0.35	31.9 ± 2.0	7.52 ± 0.06
206	6.11 ± 0.43	34.6 ± 2.4	7.50 ± 0.06
208	6.18 ± 0.68	34.3 ± 3.8	7.56 ± 0.08

Table 1: Transition probabilities $B(IS3;0^+ \rightarrow 3^-)$ and radii R_{trans} derived by the standard procedure (vibrational-model form of the mass transition density)

The experimental and the theoretical scattering cross sections obtained by procedure (i) are displayed in fig. 1 for ²⁰⁶Pb as example.

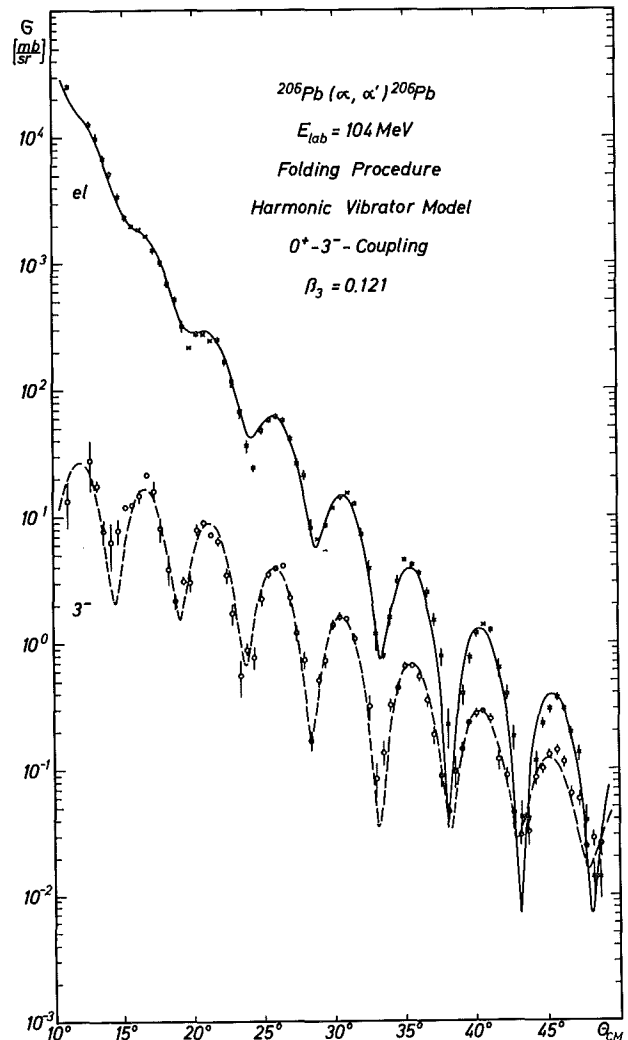


Fig. 1: Measured differential cross sections ²⁰⁶Pb (α, α') at $E_\alpha = 104$ MeV. The theoretical curves represent the results of a coupled channel analysis with the standard folding model

In view of our interest in proton-neutron differences the parametrization of the transition density by a common form for the proton and neutron part is less consistent and may obscure the information.

(ii) In order to decouple proton and neutron parts the quantity ρ_{if} has been split into $\rho_{if} = \rho_p + \rho_n$, and both parts have been treated independently. Generally such a procedure improves the description of the measured cross sections. Confining our interest to the case of ^{208}Pb we have adopted the proton part from a "model independent evaluation" of inelastic electron scattering data ⁶⁾. For the form of the neutron part of the transition density again the vibrational model form has been taken.

Applying this "modified vibrational model" procedure we obtained the neutron transition density shown in fig. 2 revealing a larger transition radius compared to the proton part.

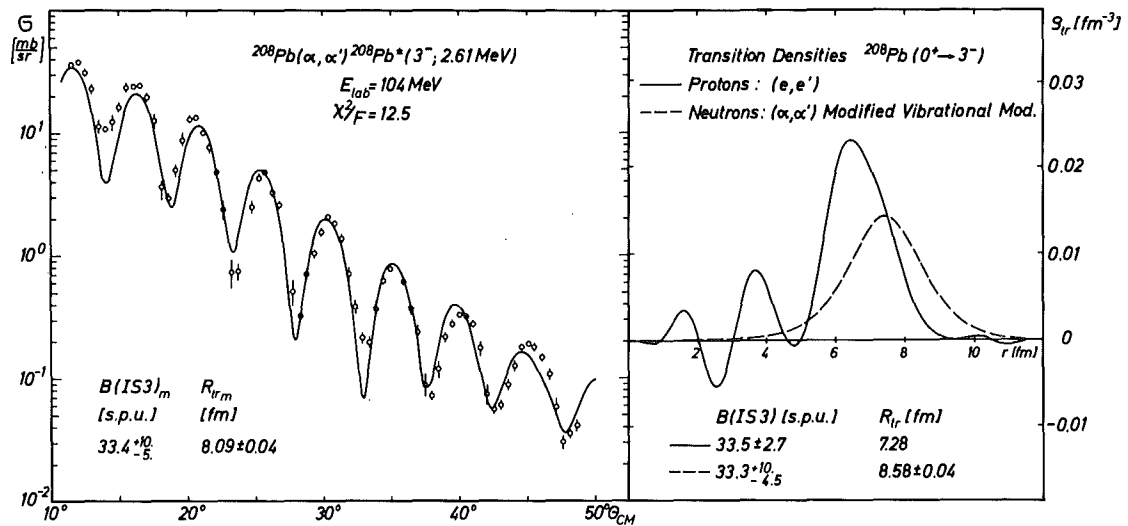


Fig. 2: Result of the 3^- -state cross section analysis adopting the proton transition density from a "model independent" analysis of (e,e') scattering (ref. 6) and fitting the phenomenologically parametrized neutron density to the experimental (α, α') cross sections

Table 2 compiles the octupole transition rates and transition radii calculated for mass, proton and neutron transitions from the various results of $\rho_{if}(r)$ including results of microscopic nuclear structure calculations ^{7,8)}.

The values of the neutron transition radii indicate significant differences to the proton value.

As can be seen in tab. 2 the neutron collectivities seem to be underestimated by theoretical results. In order to discuss our experimental cross sections more directly in the light of the theoretical predictions of ρ_{if} we introduce

Transition density $\rho_3(r)$		G_3 [s.p.u.]			$R_{\text{trans}} = \langle r^{L+2} \rangle / \langle r^L \rangle ^{1/2}$ [fm]		
		m	p	n	m	p	n
$(e, e')^{6)}$			33.5 ± 2.7			7.28	
(α, α')	ST	34.3 ± 3.8			7.65 ± 0.08		
	MVN	33.4	(33.5)	33.3	8.09	(7.28)	8.58
Theory	Speth ⁷⁾	31.1	34.0	29.3	7.55	7.24	7.76
Theory	Knüpfner ⁸⁾						
	$\alpha_n = \alpha_p$	28.2	32.7	25.5	7.64	7.40	7.81
	$\alpha_n \neq \alpha_p$	34.2	32.7	35.2	7.93	7.40	8.25

ST: Standard procedure ³⁾, MVN: Modified vibrational model form for the neutron transition density

Table 2: Comparison of various results for transition rates G_3 and radii R_{trans} for ^{208}Pb

microscopically calculated transition densities into the expression generating the transition potential. The procedure can be considered to be a further way specifying the quantity $\rho_{if}(r)$, in addition to the more phenomenological forms used above.

(iii) The transition densities are calculated in the framework of RPA on the basis of the model of a separable effective interaction ⁸⁾. The proton part ρ_{if} agrees fairly well with all what we know from electron scattering in this case. For the calculations of the neutron part we allow some variation of the radius parameter α_n of the oscillator well generating the single particle basis.

The various theoretical neutron transition densities displayed in fig. 3 influence clearly the predicted cross sections and match the experimental cross section with $\alpha_n = 0.39 \text{ fm}^{-1}$ (see the χ^2/F dependence of α_n in the inset of fig. 3). The corresponding neutron distribution leads to an enhancement in mass and neutron transition rate, to a larger value of the transition radius and to a shape of the relevant radial region consistent with the result from the purely phenomenological analysis.

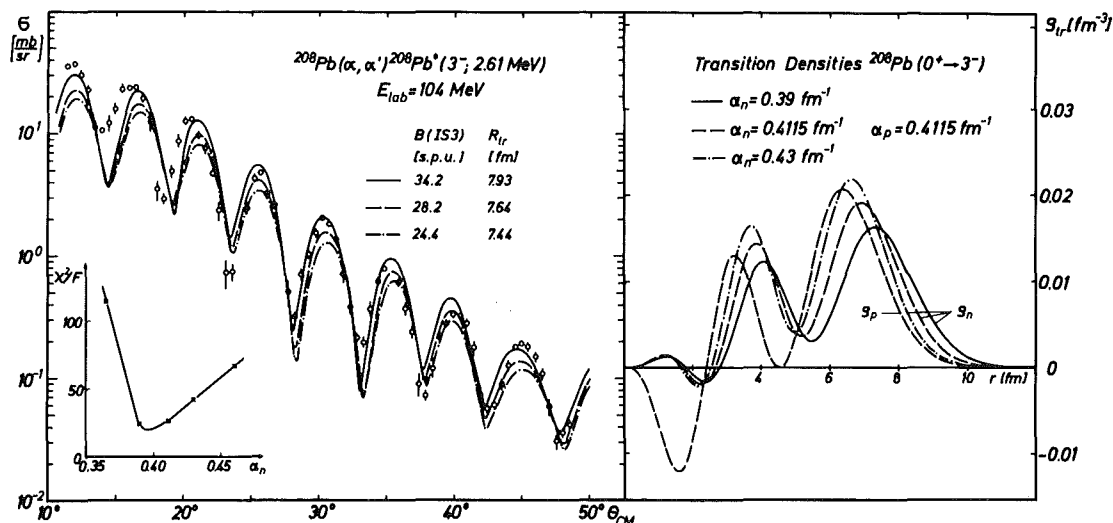


Fig. 3: Effects of the radius parameter of the neutron oscillator well on the transition densities and differential cross sections of inelastic α -particle scattering

References

- 1) H. Rebel, Proceedings of the Int. Summer School of Nucl. Phys. (Predeal Romania, Sept. 1974); KFK-Report 2065 (1974)
- 2) H.J. Gils, H. Rebel, H. Klewe-Nebenius, G.P. Nowicki, W. Nowatzke, Z. Physik A279 (1976) 55
- 3) H.J. Gils, H. Rebel and W. Knüpfer, Nuovo Cim. 36A (1976) 258
- 4) H.J. Gils and H. Rebel, Z. Physik A274 (1975) 259
- 5) H. Rebel, Z. Physik A277 (1976) 35
- 6) H. Rothhaas, J. Friedrich, K. Merle, B. Dreher, Phys. L. 51B (1974) 23
- 7) P. Fröbrich, J. Speth, Phys. L. 44B (1973) 477, Proceedings of the Symposium on Nuclear Structure, Balatonfured, Hungary, 1.-6. Sept. 1975
- 8) E. Grecksch, W. Knüpfer and M.G. Huber, Lett. Nuov. Cim. 14 (1975) 505

3.3.5 $(\alpha, \alpha_1 \gamma)$ Angular Correlation Measurements on sd-Shell Nuclei

W. Eyrich, A. Hofmann, U. Scheib, S. Schneider, F. Vogler,
Physikalisches Institut der Universität Erlangen-Nürnberg

H. Rebel

Institut für Angewandte Kernphysik des Kernforschungszentrums Karlsruhe

Particle- γ angular correlations provide more detailed information about reaction mechanisms and nuclear structure than differential cross sections. In the special case of $(\alpha, \alpha_1 \gamma)$ angular correlations on even-even nuclei it is possible to determine the individual reaction amplitudes, which describe the transitions to the various magnetic substates of the excited residual state. Therefore $(\alpha, \alpha_1 \gamma)$ angular correlation measurements are especially suitable for the study of reaction- and structure-models and their parameters.

The "in-plane" angular correlation function for α -particle scattering and the spin sequence $0^+ - 2^+ - 0^+$ is given by

$$W(\Theta_\alpha = \frac{\pi}{2}, \phi_\alpha; \Theta_\gamma = \frac{\pi}{2}, \phi_\gamma) = A(\phi_\alpha) + C(\phi_\alpha) \cdot \sin^2 2(\phi_\gamma - \phi_2(\phi_\alpha))$$

The quantities A, C and ϕ_2 , which depend on the α -particle scattering angle ϕ_α are simply related to reaction amplitudes ¹⁾.

For the reaction $^{24}\text{Mg} (\alpha, \alpha_1 \gamma)$ -angular correlation it has been shown ²⁾, that coupled channels calculations based on the extended optical model (EOM) as well as on a semimicroscopic folding model ³⁾ which fit the differential cross sections, can also describe the individual reaction amplitudes. Moreover it turned out that compared with the differential cross section especially the correlation amplitude C is very sensitive to the sign of the nuclear quadrupole deformation. This is demonstrated for the EOM-analyses in fig. 1 and 2. In fig. 1 the experimental differential cross sections are shown together with the best fits for prolate ($\beta_2 > 0$) and oblate ($\beta_2 < 0$) deformation. Both fits can reproduce the data, favouring the positive sign of β_2 . In fig. 2 the experimental values of the correlation amplitude C are compared with the calculations for $\beta_2 > 0$ and $\beta_2 < 0$ using the best fit parameters of the cross section analysis. There are large differences between both calculations and only the calculation with $\beta_2 > 0$ can reproduce the data.

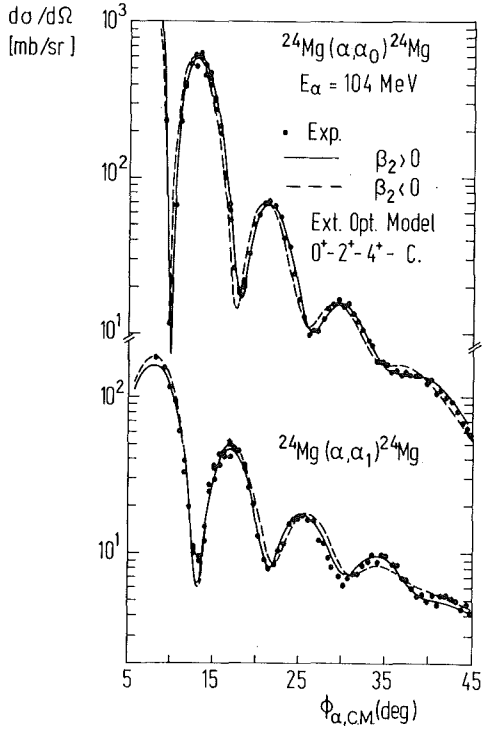


Fig. 1: Coupled channels analysis of the $^{24}\text{Mg}(\alpha, \alpha')$ differential cross section

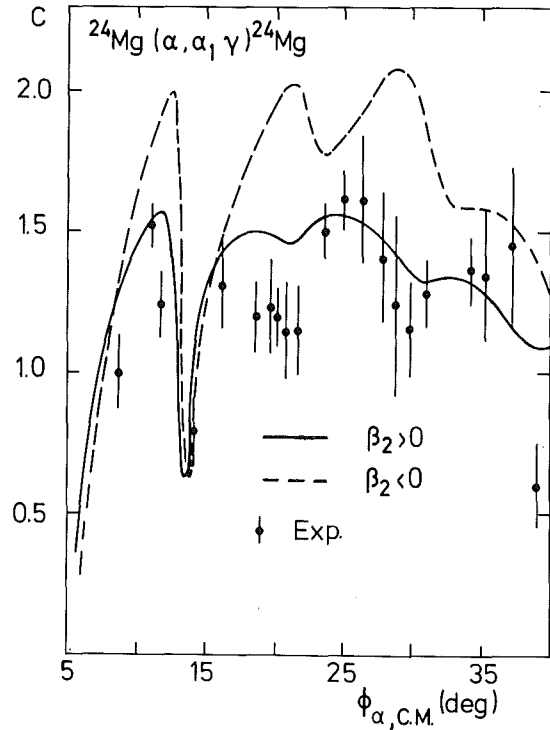


Fig. 2: The experimental correlation amplitude C of the reaction $^{24}\text{Mg}(\alpha, \alpha_1 \gamma)$ and coupled channels predictions for prolate and oblate deformation

We have continued these studies measuring the $^{28}\text{Si}(\alpha, \alpha' \gamma)$ -angular correlation. The sign of the quadrupole deformation of ^{28}Si was not as clearly assigned ⁴⁾ as in the case of ^{24}Mg , although in most publications oblate deformation is favoured. Our experimental set-up was similar as in the case of the ^{24}Mg -correlation experiment, which is described in detail in ²⁾. In contrast to this measurement however, the energy analysed beam has been used and the data have been acquired twodimensionally.

Again the analyses have been performed in terms of coupled channels on the basis of the symmetric rotator using the extended optical model (EOM) and the semimicroscopic folding model. The experimental cross sections are shown in fig. 3 together with the best fits for prolate and oblate deformation in the framework of the EOM. Both fits can reproduce the data favouring slightly the oblate deformation. In fig. 4 the correlation amplitude C is shown. Like in the case of ^{24}Mg large difference between both calculation occur. The experimental data allow an unambiguous decision for oblate deformation of ^{28}Si . Similar results are obtained from the folding model analyses where at least in the diffraction region the correlation data can be well reproduced by the

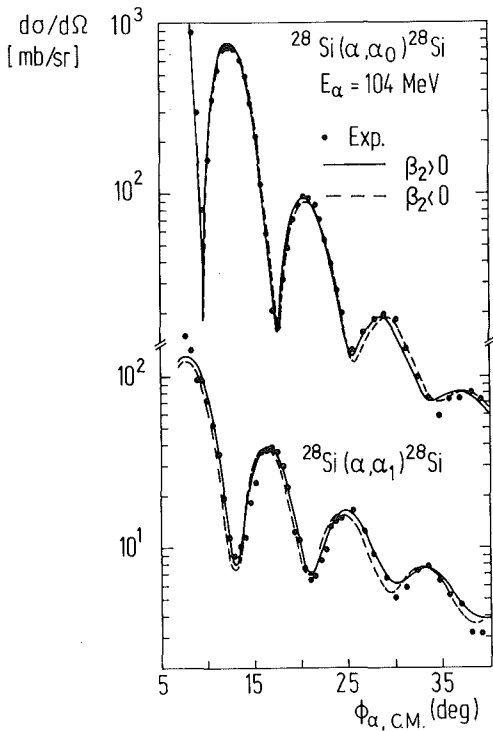


Fig. 3: Coupled channels analysis of the $^{28}\text{Si}(\alpha, \alpha')$ differential cross section

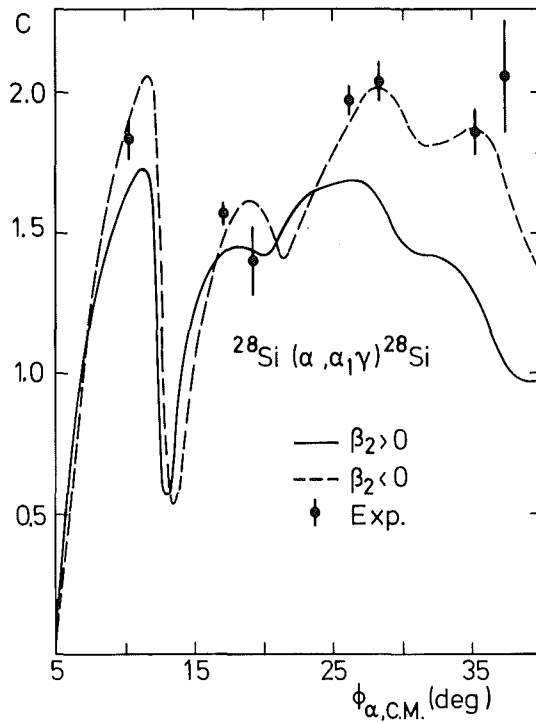


Fig. 4: The experimental correlation amplitude C of the reaction $^{28}\text{Si}(\alpha, \alpha_1 \gamma)^{28}\text{Si}$ and coupled channels predictions for prolate and oblate deformation

calculations assuming oblate deformation for ^{28}Si . In all analyses done so far the characteristic differences between prolate and oblate deformation prove to be independent of the potential parameters. They can be explained in the framework of Blair's diffraction model ⁵⁾ as shown in ²⁾. Therefore α - γ -angular correlations should provide a powerful tool to determine the sign of the quadrupole deformation of nuclei also in critical cases. Under this aspect work is in progress to study the α - γ -angular correlation on ^{26}Mg .

References

- 1) H. Wagner et al., Phys. Lett. 47B (1973) 497
- 2) W. Eyrich et al., Phys. Lett. 63B (1976) 406 and submitted to Nucl. Phys.
- 3) H. Rebel, Proceedings of the Intern. Summer School of Nucl. Phys. Predeal Romania (1974), ed. by A. Ciocanel KFK-2065 (1974), and further references therein
- 4) A. Nakada and Torizuka, H. Phys. Soc. (Japan) 32 (1972) 1,
H. Rebel et al., Nucl. Phys. A182 (1972) 145
C.E. Ahlfeld et al., Nucl. Phys. A191 (1972) 137
- 5) N. Austern and J.S. Blair, Ann. Phys. 33 (1965) 15

3.4 Nuclear Spectroscopy

3.4.1 Experimental Study of the Enhanced L=4 Transition in ^{140}Ce

A. Hanser, H. Rebel, J. Buschmann and H.J. Gils

Institut für Angewandte Kernphysik des Kernforschungszentrum Karlsruhe

H. Klewe-Nebenius

Institut für Radiochemie des Kernforschungszentrums Karlsruhe

H. Faust

Physikalisches Institut der Universität Heidelberg

L=4 transition probabilities are often deduced from inelastic scattering of electrons, protons, or α -particles in order to get information on hexadecapole motion in quasispherical or deformed nuclei. In many cases, however, a comparison of the results is influenced either by the model dependence of the analyses (especially when regarding earlier α -scattering data) or by the fact that α -scattering cross sections are determined by the isoscalar mass transition probabilities, while electron and proton scattering data imply electromagnetic isovectorial transition contributions. Therefore, the measurement of a quantity, which provides model independent information, is highly desirable.

Such a quantity informing on the charge transition is given by the probability of the direct $4_1^+ \rightarrow 0^+$ γ -decay, which in cases of strong enhancement can be measured despite of the strongly competing E2-cascade.

We have observed this E4 γ -ray transition in ^{140}Ce following the β -decay of ^{140}La . The competing lower energy E2 transitions were strongly reduced by means of a 5 cm lead absorber. In addition, the peak to background ratio in the γ -ray spectrum was increased by using an anticompton arrangement and electronic pile-up rejection. In fig. 1 the measured γ -ray spectrum together with a linear plotted part showing the 2083 keV E4 transition, the actual efficiency curve (including lead absorber, compton suppression, and pile-up rejector), and the relevant part of the ^{140}Ce level scheme are shown. The contribution of pile-up to the 2083 keV γ -ray was estimated from other pile-up peaks to be less than 1.5 %.

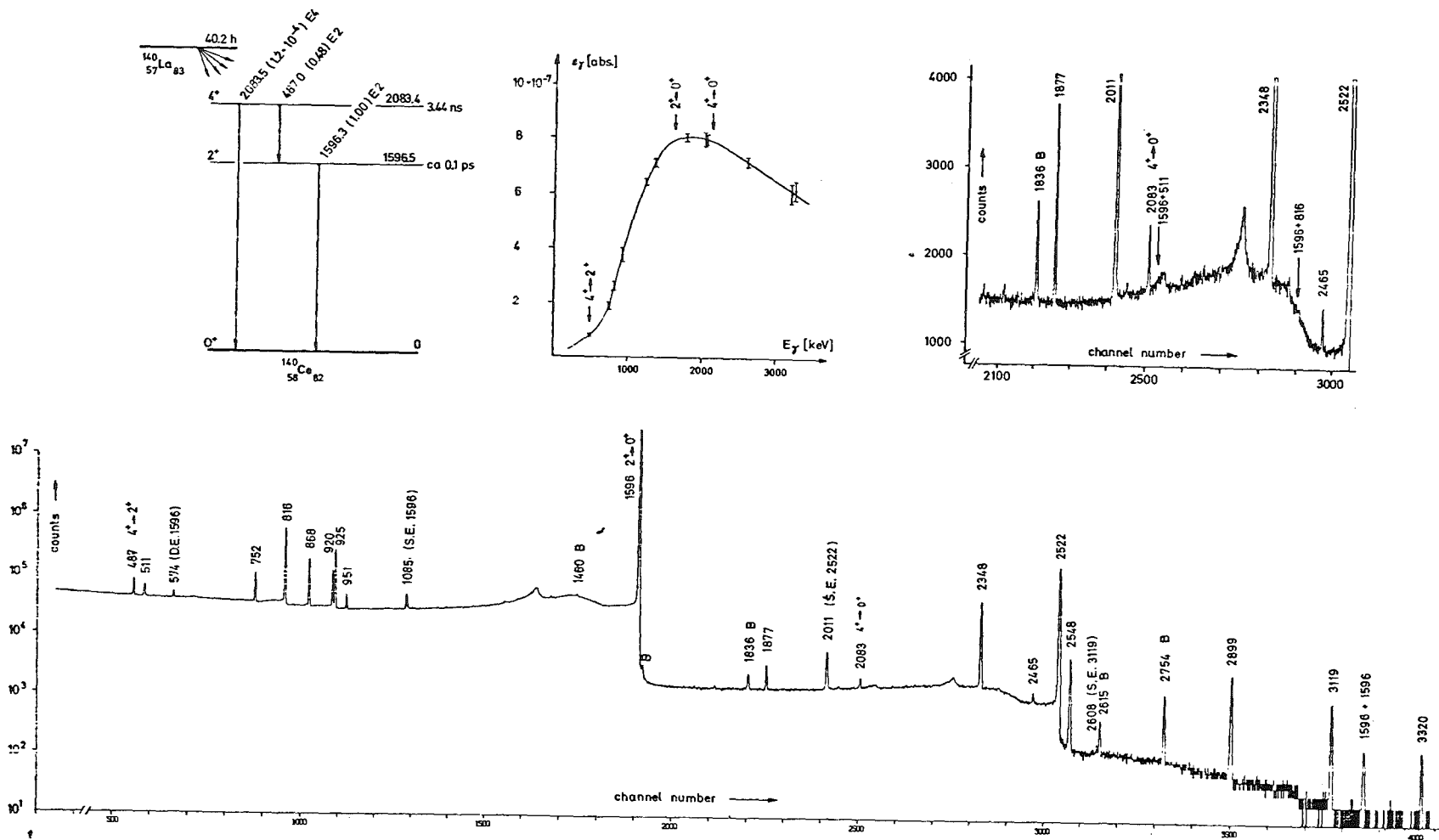


Fig. 1: γ -ray spectrum (logarithmic scale) of the decay of ^{140}La . The insets on top show the relevant part of the ^{140}Ce level scheme, the actual efficiency curve of the detector arrangement, and a linearly plotted part of the spectrum in the region of the E4 transition, respectively

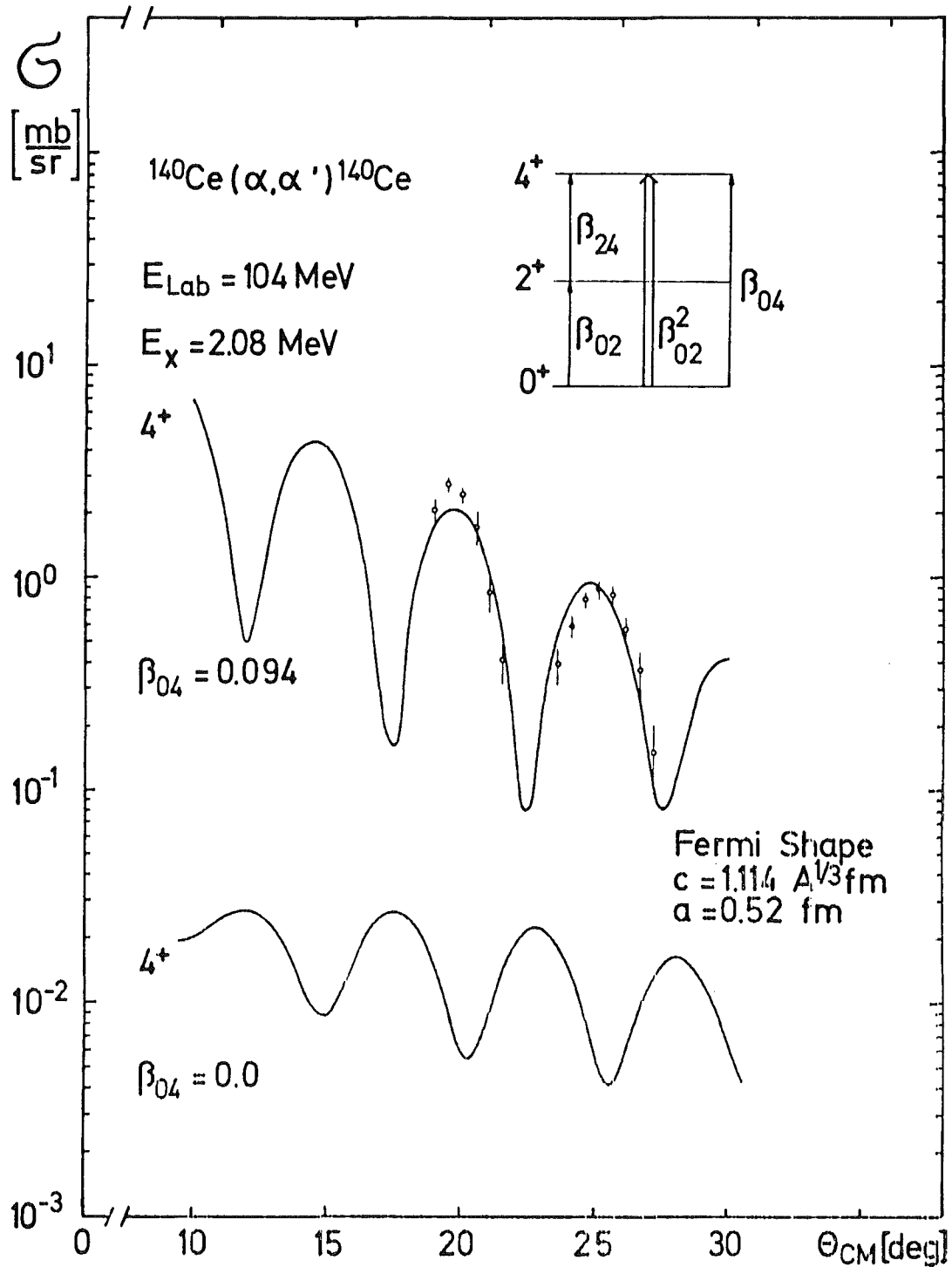


Fig. 2: Angular distribution of α -particles of 104 MeV scattered to the ^{140}Ce 4^+ state. The upper solid curve is the result of fitting the theoretical calculations. The lower curve shows the calculated angular distribution when no $L=4$ component is adopted. The inset demonstrates the excitation scheme on which the coupled channel calculations are based

From the intensity of the 2083 keV γ -ray a branching ratio of

$$\frac{I_{\gamma}(E4)}{I_{\gamma}(E2)} = (2.52 \pm 0.14) \cdot 10^{-4}$$

was obtained. Together with the half-life of (3.44 ± 0.03) ns of the ^{140}Ce 4^+ level an enhancement factor of

$$(11.9 \pm 0.7) \text{ s.p.u.}$$

is deduced for the $4_1^+ \rightarrow 0^+$ transition.

For comparison to (mass-sensitive) α -scattering data we have measured the angular distribution of inelastically scattered α -particles at $E_{\alpha} = 104$ MeV. The data were analyzed by use of a coupled channel code with a folding procedure for the optical potential. The results are shown in fig. 2. The 4^+ peak could only be analyzed for scattering angles $\geq 18^{\circ}$ since at smaller angles it was superimposed by strong peaks originating from O- and C-impurities of the target. For the same reason the 2^+ peak could not be evaluated. Thus, the R_{02} transition matrix element (see fig. 2) necessary for the analysis of the 4^+ angular distribution, had to be taken from literature ¹⁾. Its absolute value, however, does not strongly affect the 4^+ analysis.

We deduced an enhancement factor of

$$(13 \pm 2) \text{ s.p.u.}$$

for the $L = 4$ excitation which agrees well with the enhancement factor of the γ -ray transition and also with the value of (14 ± 2) s.p.u. obtained from a reanalysis of earlier 45 MeV α -scattering data ¹⁾ but differs clearly from electron scattering results ²⁾ which revealed

$$(20 \pm 4) \text{ s.p.u.}$$

We conclude that in the case of ^{140}Ce no difference between charge and mass transition probability exists and that the model used for the analysis of the α -scattering data describes them very well and consistently.

References

- 1) F.T. Baker and T. Tickle, Phys. Rev. C5 (1972) 182
- 2) R. Pitthan, Z. Physik 260 (1973) 283

3.4.2 Shape Factor Measurements on Short Lived β -Emitters

W. Thies, H. Appel, R. Pesl

Institut für Experimentelle Kernphysik des Kernforschungszentrums Karlsruhe

H. Behrens

Zentralstelle für Atomkernenergie-Dokumentation des Kernforschungszentrums
Karlsruhe

There is certainly need of new and improved measurements of β -spectra shapes. The motivations are, e.g.:

- to test the conserved vector current hypothesis and its degree of correctness. Theory offers definite predictions on the energy dependence of the shape factors in Gamow-Teller transitions
- to measure the shape factors of superallowed $0^+ \rightarrow 0^+$ transitions which should be constant. While the ft-values for some of these decays have again been thoroughly investigated recently by measuring half lives and Q-values (for the inverse reaction) no shape factor determination has been published so far. For principle reasons and with regard to the correctness of radiation corrections the shapes of $0^+ \rightarrow 0^+$ spectra should be reliably analysed
- to proof that the scalar interaction does not contribute in addition to the vector interaction in allowed vector β -decay. Otherwise it could cause deviations from the statistical spectrum shape. Results from the observation of superallowed spectra allow a considerable improvement on the limit of the Fierz interference term.

Apart from these more principle aspects which refer to allowed transitions only, valuable information on the details of the relevant nuclear structure can be taken from the shape factors of forbidden transitions ¹⁾.

Since the lifetimes of $0^+ \rightarrow 0^+$ transitions lie typically in the range between some hundreds of milliseconds and seconds the investigations have to be carried out in beam. An iron free intermediate image spectrometer of the type described by Alburger ²⁾ has been installed at the Cyclotron (see fig. 1). Intermediate image spectrometers are very suitable for shape factor measurements, particularly with respect to background radiation at the detector. The iron free type offers the additional advantage of strict linearity between current and electron momentum. The energy range has been extended up to 17 MeV.

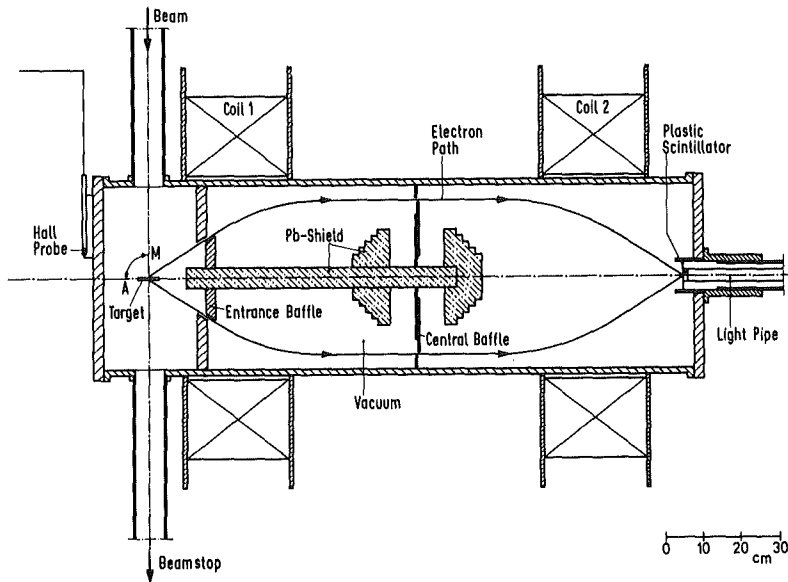


Fig. 1: Schematic diagram of the iron free intermediate image beta-spectrometer

A momentum resolution of about 2 % has been chosen together with a transmission rate of approximately 1 %.

Activation period (target position A in fig. 1) and measurement period are chosen with respect to the relevant half lives investigated. For the latter period the target is switched from position A to M. During each measurement period the whole range of β momenta is recorded. Since the current increase in the spectrometer coils is not sufficiently linear in time it is necessary to gain information on the time-momentum relation. This is achieved by measuring the in- or decreasing field with a Hall-probe with respect to a periodic pulse sequence. More details on the spectrometer and on some earlier results can be taken from former publications ^{3,4,5}.

Recently the superallowed $0^+ \rightarrow 0^+$ transition in $K^{38m} \rightarrow Ar^{38}$ ($\tau = 926$ ms) has been investigated. The production process $K^{39}(p,pn)K^{38m}$ has been chosen. The Fermi-plot of the data is presented in fig. 2. A three parameter fit (K , E_0 , and a or b) has been applied to the data (the quantities are explained in detail, e.g., in ref. (3)), and, of course, the model independent radiation corrections. The extracted end point energy of $E_0 = (5026.5 \pm 11.5)$ keV agrees well with the (necessarily more accurate) result from Q-value measurements, which is $E_0 = (5021.2 \pm 3.4)$ keV ⁶.

The other parameters determined are

$$a = -0.0007 \pm 0.0018 \quad \text{and}$$

$$b = -0.03 \pm 0.09 \quad .$$

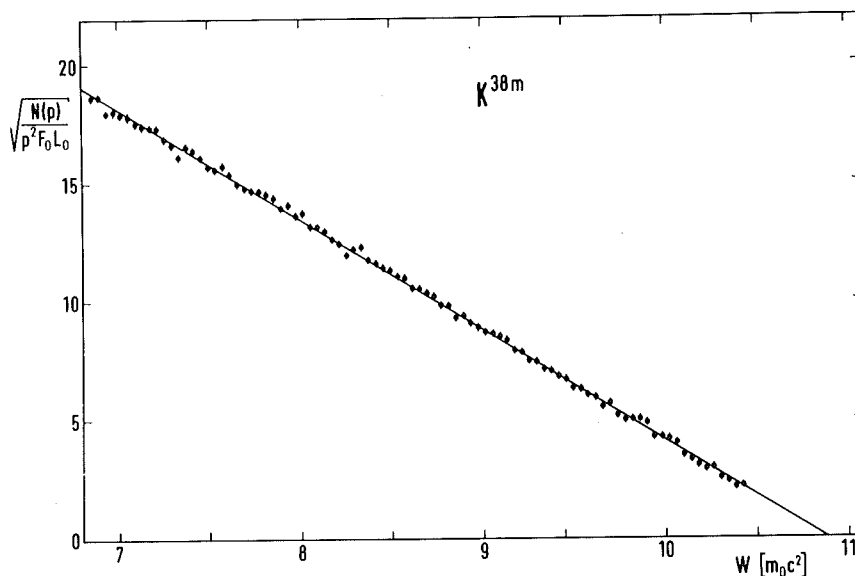


Fig. 2: The linearized beta-spectrum of the $0^+ \rightarrow 0^+$ transition $K^{38m} \rightarrow Ar^{38}$

Within the error, the quantity a turns out to be zero, the shape factor is consequently constant. The theoretical expectations on the shape factor are confirmed, including the influence of the radiative corrections.

In addition the $3^+ \rightarrow 2^+$ Gamow-Teller-transition in $K^{38} \rightarrow Ar^{38}$ has been investigated. An exact model calculation on the basis of the CVC hypothesis including nuclear structure effects results in a change of the shape factor of $-0.42 \text{ \%}/m_0 c^2$. With a determined end point energy of $E_0 = (2730.5 \pm 6.3) \text{ keV}$ the experimental value for the shape factor is $(-0,0064 \pm 0.0025) \text{ \%}/m_0 c^2$.

It is particularly advantageous that the latter results can be referred to the measurements of the $0^+ \rightarrow 0^+$ transitions, which guarantee that the transmission of the spectrometer is constant and independent of the momentum. No effects of instrumental origin larger than the statistical error can therefore enter the results.

References

- 1) H.J. Gehrhardt, Thesis, University of Karlsruhe, 1977
- 2) D.E. Alburger, Rev. Sci. Instr. 27 (1956) 991
- 3) H. Behrens, M. Kobelt, W.G. Thies, and H. Appel, Z. Physik 252 (1972) 349
- 4) H. Behrens, M. Kobelt, L. Szybisz, and W.G. Thies, Nucl. Phys. A246 (1975) 317
- 5) H. Behrens, M. Kobelt, L. Szybisz, and W.G. Thies, Nucl. Phys. A245 (1975) 515
- 6) G.T.A. Squier, W.E. Burcham, J.M. Freeman, R.J. Petty, S.D. Hoath, and J.S. Ryder, Nucl. Phys. A242 (1975) 62

3.5. Measurements of Nuclear Magnetic Moments

3.5.1 Determination of the Quadrupolemoment of the (25/2⁺) Isomer in ¹¹⁷Sb

M. von Hartrott, K. Nishiyama, D. Quitmann, J. Rossbach and E. Weihreter
 Institut für Atom- und Festkörperphysik, Freie Universität Berlin

The measurement of nuclear quadrupole moments for isomeric states in the life time range between about 1s and 10⁻⁵s offers particular experimental problems. Therefore only few values have been determined combining several favourable circumstances prevailing for just the special cases. An example of this kind is the moment Q^{117m} of the 340 μs isomer in ¹¹⁷Sb. This can be deduced from the quadrupolar part T_Q⁻¹ of the spin lattice relaxation observed by perturbed angular correlations after production and alignment by the reaction ¹¹⁵In(α,2n)^{117m}Sb in a liquid InSb target. The explicit derivation of Q^{117m} rests on additional information in the following way:

Due to the proportionality T_Q⁻¹ ∝ f(I) · Q² (1), the ratio R of the quantities f(I) · Q² belonging to two different isotopes can be measured directly by comparing their respective quadrupolar relaxation rates in the same matrix at the same temperature (f(I) spin factor, see 1)). If one of the moments is unknown (here: ^{117m}Sb) it can be obtained by inserting the spins of both isotopes and the quadrupole moment of the reference isotope.

The quadrupolar rates for stable ¹²¹Sb and ¹²³Sb in liquid InSb have been determined in a conventional NMR experiment for a series of temperatures by isotopic separation 2). In the present experiment, T_Q⁻¹ was determined for ^{117m}Sb over almost the same range of temperatures. The ratio R averaged over temperature is

$$R(^{117m}\text{Sb}/^{121}\text{Sb}) = 0.30(3) ;$$

the quoted error is mainly due to the systematic difference of the T_Q⁻¹ curves in both experiments. With I(^{117m}Sb) = 25/2 as proposed in ref. 3), the ratio of the quadrupole moments becomes

$$Q(^{117m}\text{Sb})/Q(^{121}\text{Sb}) = 2.1(1) .$$

Unfortunately, the ground state quadrupole moment of ¹²¹Sb is not known very accurately 4); with Q(¹²¹Sb) = 0.26(10) barn, we obtain |Q(¹¹⁷Sb)| = 0.54(20) barn. This result may be compared with the prediction based on a three quasi-particle state with the configuration {(νh_{11/2})²10⁺, πd_{5/2}} $\frac{25}{2}$ 3). For the

quadrupole moment of the neutron part of the configuration we take that of the $(\nu h_{11/2})^2 10^+$ isomeric state of the nucleus ^{116}Sn , which is $-0.50(5)$ barn ⁵⁾. For the $d_{5/2}$ proton moment one would as a first guess take that of the ground-state ^{117}Sb which is -0.30 barn ⁶⁾. It is, however, to be noted that the quadrupole moment of this state does not fit into the systematics of the moments of the $d_{5/2}$ groundstates in the odd neutron deficient Sb isotopes. One obtains the value $-0.20(4)$ barn by interpolating between the ground states of ^{115}Sb and ^{119}Sb . Because of the stretched coupling, the moments of the two components add up, yielding for the isomer ^{117m}Sb a theoretically expected value of $-0.60 \dots -0.80$ barn. Since the absolute value agrees within the limits of error with experiment, we adopt the negative sign and get as the final experimental result:

$$Q(^{117m}\text{Sb}) = (-)0.54(20) \text{ barn.}$$

References

- 1) A. Abragam and R.V. Pound, Phys. Rev. 92 (1953) 943
- 2) W.W. Warren Jr. and W.G. Clark, Phys. Rev. 177 (1969) 600
- 3) W.D. Fromm, H.F. Brinckmann, F. Dönau, C. Heiser, F.R. May, V.V. Pashkevich and H. Rotter, Nucl. Phys. A243 (1975) 9
- 4) S.L. Ruby, G.M. Kalvius, G.B. Beard and R.E. Snyder, Phys. Rev. 159 (1967) 239
- 5) F. Dimmling, D. Riegel, K.G. Rensfelt and C.J. Herrlander, Phys. Lett. 55B (1975) 293
- 6) V.S. Shirley, Hyperfine Interactions in Excited Nuclei IV, Editor G. Goldring and R. Kalish; Gordon and Breach, New York, London, Paris, 1970, p. 1255-1336

3.5.2 Spins and Magnetic Moments of Neutron Deficient Rb Isotopes by In-Beam Optical Pumping

J. Collignon, F. Buchinger, R. Neugart
 Institut für Physik der Universität Mainz

H. Schweickert
 Institut für Angewandte Kernphysik/Zyklotron des Kernforschungszentrums
 Karlsruhe

The method of in-beam optical pumping ¹⁾ has been applied to ⁸⁰Rb and ⁸²Rb. Fig. 1 shows the principle of the experimental set up. Both isotopes are produced from enriched Kr targets by the respective (p,n) reactions. The target cell containing free Rb atoms in a Kr atmosphere is simultaneously used for the optical pumping experiment. Polarization achieved by irradiating the circularly polarized D₁ resonance line is detected by the asymmetry in the β decay. Rf resonances between the hfs levels of the atomic ground state yield the spins, hfs splittings and magnetic moments.

The following results have been obtained

⁸⁰Rb (30 s) : I = 1 μ_I = -0.0836(6) nm
⁸²Rb (1.3 m) : I = 1 μ_I = 0.554(3) nm

(including diamagnetic correction)

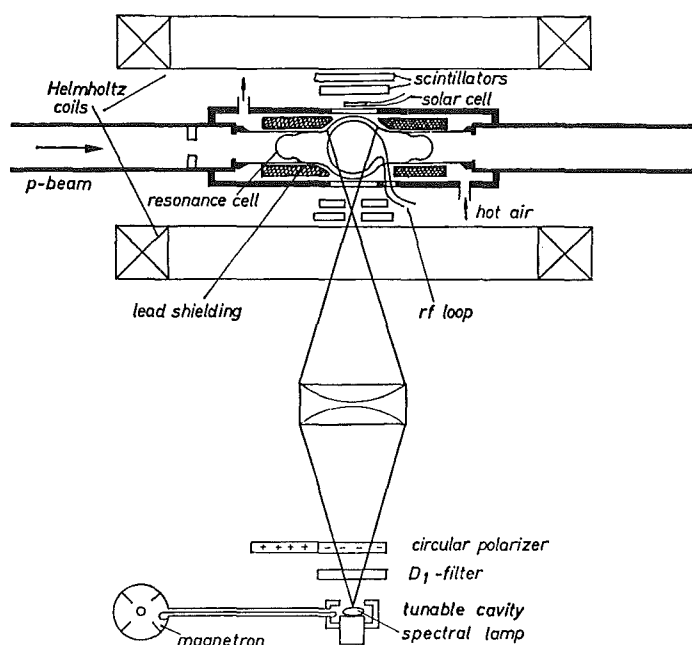


Abb. 1: Experimental setup for on-line optical pumping

In the case of ^{80}Rb a precision measurement of the hfs splitting has been performed yielding $\Delta\nu = 233.936(2)$ MHz. This result combined with the direct measurement of the nuclear moment gives an upper limit of 1 % for the hfs anomaly between ^{80}Rb and the stable ^{87}Rb .

Both isotopes considered here lie in the transition region between the stable isotopes near the neutron shell closure and a region of strong nuclear deformation. Ekström et al. ²⁾ have contributed important information on the more neutron-deficient isotopes by using the atomic-beam magnetic resonance method. An optical pumping experiment has been performed on ^{76}Rb at ISOLDE/CERN ²⁾. A rather comprehensive set of nuclear ground state properties in the region of light Rb isotopes has thus been obtained.

References:

- 1) H. Schweickert, J. Dietrich, R. Neugart, E.W. Otten
Nucl. Phys. A246 (1975) 187-209
- 2) C. Ekström, S. Ingelman, G. Wannberg, M. Skarestad, Proc. 3rd Int.
Conference on Nuclei far from Stability, Cargèse, France, CERN 76-13
(1976) p.193
- 3) H. Fischer, P. Dabkiewicz, P. Freiling, H.-J. Kluge, H. Kremmling,
R. Neugart, E.-W. Otten, Z. Physik, to be published

3.5.3 High Resolution Laser Spectroscopy of Radioactive Light Barium Isotopes

G. Nowicki, K. Bekk, S. Göring, A. Hanser, H. Rebel and G. Schatz

Institut für Angewandte Kernphysik des Kernforschungszentrums Karlsruhe

The development of narrow band tunable dye lasers has provided a tool for high resolution optical spectroscopy measurements on very small amounts of atoms. Thereby it has become possible to investigate optical isotope shifts in a long isotopic row, including short-lived radioactive atoms, in order to get information on the change of nuclear charge radii ^{1,2)}.

We have build up a laser spectrometer for high resolution atomic spectroscopy of short lived nuclides produced with the cyclotron beam. The principle of the experimental arrangement is shown in fig. 1. We measure the resonance fluorescence of the respective radioactive atoms in a well collimated beam, using a single mode cw-dye laser as light source. The fluorescence intensity was detected by photon counting. The exact frequency of the exciting light was determined by an optical heterodyn method using a second single mode dye laser, whose frequency was stabilized to the known resonance transition frequency of a stable Ba isotope, as an optical reference oscillator. We obtained an experimental resolution of 24 MHz (FWHM) which is comparable to the natural line width of 19 MHz.

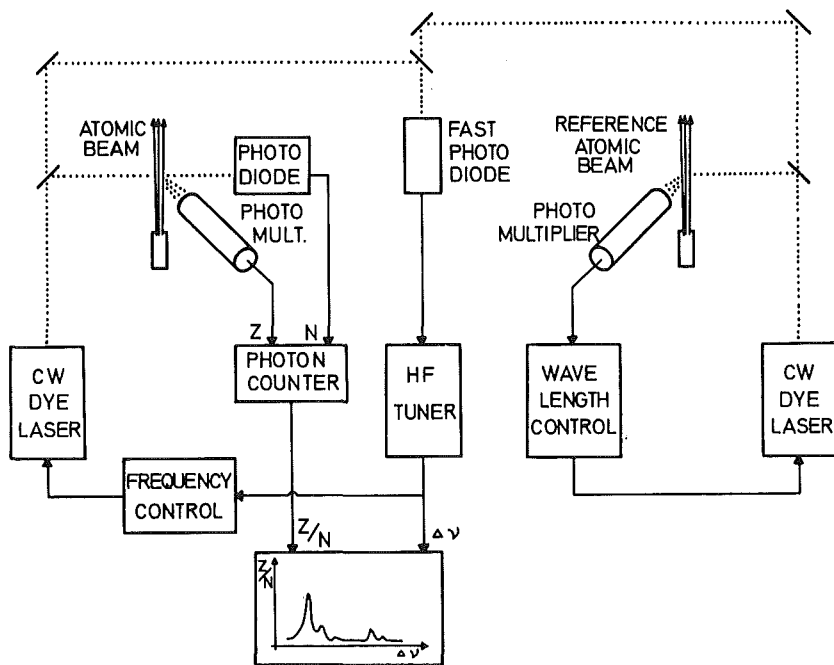


Fig. 1: Principle of the experimental arrangement

First we studied the isotope shifts and hyperfine structure of ^{128}Ba and ^{131}Ba . We produced ^{128}Ba ($T_{1/2} = 2.45$ d) and ^{131}Ba ($T_{1/2} = 11.5$ d) via (d,xn) reactions and subsequent β^+ decay from enriched ^{130}Ba and ^{134}Ba , respectively, at the Karlsruhe Isochronous Cyclotron. ^{131}Ba was also produced by neutron irradiations of enriched ^{130}Ba in the Karlsruhe Research Reactor FR2. The isotope in question was enriched using an electromagnetic mass separator. At the beginning of the measurements the atomic beam oven contained about 1 to 30 ng of the isotope to be investigated and an amount of stable Ba isotopes about 2 to 100 times as large.

We identified the $^1S_0 - ^1P_1$ transition of ^{128}Ba by observing its decrease due to radioactive decay because it lies very close to one hyperfine component of ^{137}Ba . The resulting isotope shift is $\Delta\nu (^{128}\text{Ba} - ^{130}\text{Ba}) = 2.08 \pm 0.04$ mK. The $^1S_0 - ^1P_1$ transition of ^{131}Ba should have two hyperfine components because of its nuclear ground state spin $I = 1/2$ ³⁾. As one of these components coincides with the transition of ^{138}Ba we measured the fluorescence spectrum changing the polarization direction of the incoming laser light in order to subtract the intensity of the ^{138}Ba line. The results we got are $\Delta\nu (^{131}\text{Ba} - ^{130}\text{Ba}) = 1.33 \pm 0.07$ mK and $A = -8.33 \pm 0.05$ mK. Using the well known hyperfine splittings of the stable isotopes $^{135}, ^{137}\text{Ba}$ ⁴⁾ and neglecting a possible hyperfine anomaly we obtain the magnetic moment of ^{131}Ba $\mu = - (0.714 \pm 0.006) \mu_N$.

The problem of determining differences of nuclear charge radii of Ba isotopes from optical isotope shifts is discussed in detail by Fischer et al. ⁵⁾. Following their procedure we obtain the radius differences $\delta \langle r^2 \rangle (^{130}\text{Ba} - ^{128}\text{Ba}) = 0.022 (3) \text{ fm}^2$ which are shown in the fig. 2 together with the values of other isotopes ^{5,6)}. It can be seen that the large odd-even staggering is remarkably reduced at neutron number 75.

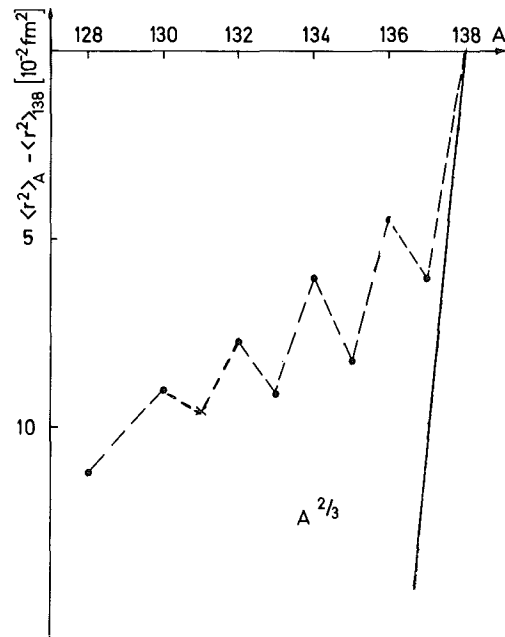


Fig. 2: $\delta \langle r^2 \rangle$ values of light Barium isotopes. The straight line represents the values expected for the standard uniform sphere

References

- 1) C. Duke, H. Fischer, H.-J. Kluge, H. Kremmling, Th. Kühl and E.W. Otten, Phys. Lett. 60A (1977) 303
- 2) R. Neumann, F. Träger, J. Kowalski and G. zu Putlitz, Z. Phys. A279 (1976) 249
- 3) D.J. Horen, J.M. Hollander and R.L. Graham, Phys. Rev. 135B (1964) 301
- 4) H.-J. Kluge and H. Sautter, Z. Phys. 270 (1974) 295
- 5) W. Fischer, M. Hartmann, H. Hühnermann and H. Vogg, Z. Phys. 267 (1974) 209
- 6) C. Höhle, H. Hühnermann, Th. Meier, H.R. Ihle and R. Wagner, Phys. Lett. 62B (1976) 390

3.5.4 Positron Trapping

G. Gräff and D. Richter

Institut für Physik der Universität Mainz

The aim of this experiment is the spectroscopic determination of Larmor frequency and cyclotron frequency of free positrons. In order to achieve a sufficient time of interaction between the rf field and the positrons, the latter must be trapped within a small volume under ultrahigh vacuum conditions. The trapping potential consists of an electrostatic quadrupole with superimposed homogeneous magnetic field. To confine a particle within the trap, the incoming particle has either to be decelerated or to be created inside the trap. We shall try the latter method. For this the trap is filled with radioactive positron emitting positive charged ions. Using strong magnetic fields (60 kG) a reasonable number of positrons have sufficiently low momenta so that they will be trapped.

The positron emitting isotope ^{84}Rb is produced by the reaction $^{84}\text{Kr}(p,n)^{84}\text{Rb}$. Those atoms are absorbed on the surface of a tungsten wire. The wire is then installed at one of the electrodes of the electrostatic quadrupole trap. When the wire is heated up to several hundred degrees most of the ^{84}Rb atoms leave the surface as ions and drift into the trapping region where they are stored. We expect that by this means up to several hundred positrons can be trapped within the storage region.

3.6 Measurements with the Large Neutron Spectrometer

3.6.1 Isospin Mixing of T = 3/2 Isobaric Analog States in Light T_z = 1/2 Nuclei

S. Cierjacks, I. Schouky

Institut für Angewandte Kernphysik des Kernforschungszentrums Karlsruhe

S.K. Gupta

Nuclear Physics Division, BARC, Bombay, India

The neutron decay of T = 3/2 states in light T_z = 1/2 nuclei is isospin forbidden and can proceed only via isospin impurities in either the initial or the final states. Thus the investigation of the neutron widths of T = 3/2 resonances provides a good means to obtain information about the isospin purity of such states. Furthermore isospin admixtures are connected with charge-dependence effects in the nuclear states, i.e. are due to the fact that the nuclear interaction contains also a small charge-dependent contribution, produced by the Coulomb interaction and a charge-dependent part of the nucleon-nucleon interaction. This latter fact demonstrates the gain of information also expected from such studies with respect to the charge-dependence of the nuclear force.

A first attempt to investigate isospin mixing of low lying T = 3/2 states in light nuclei was made for the ²⁸Si+n system. This study was initiated by a recent observation of Weigmann et al. ¹⁾ who demonstrated for a first time that T_{3/2} states can also be observed in neutron induced reactions.

By reanalyzing the measured total and differential scattering cross sections of ²⁸Si in the energy range from 1.05 - 1.40 MeV unambiguous resonance parameters were obtained for four resonances in this region. The experimental results and the calculations are shown in Fig. 1. This figure contains the total neutron cross section (top curve) and the differential elastic scattering cross sections at ten scattering angles between 20° ≤ θ_{c.m.} ≤ 151° (lower curves). Total neutron cross sections were measured with a total uncertainty of less than 2 %; data points are at about 0.6 keV apart from each other. The differential scattering cross sections having a statistical accuracy of ~ 3 % were measured in energy intervals of about 1 keV. All experimental data were obtained from measurement with the Karlsruhe fast neutron time-of-flight spectrometer. The solid lines in the figure are the results of a

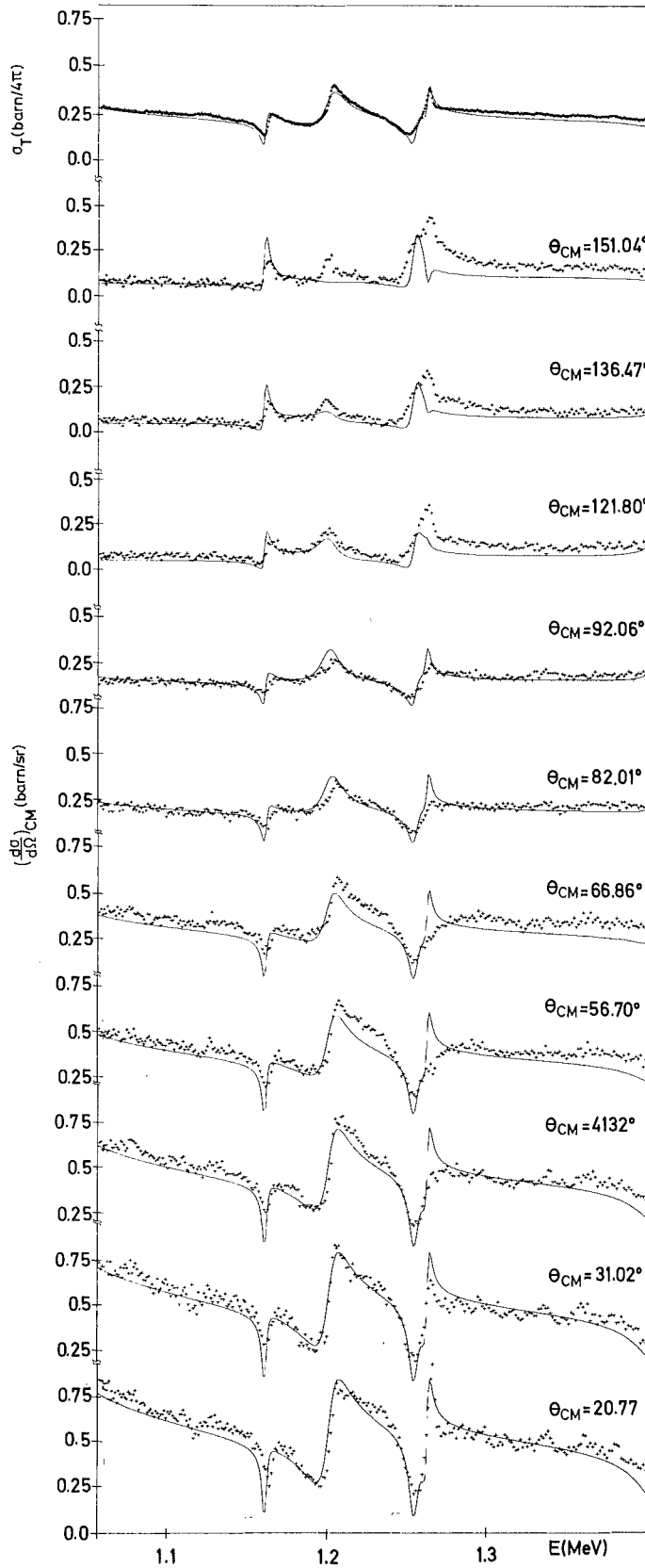


Fig. 1: The total neutron cross section and the differential scattering neutron cross section for natural silicon. The total cross section were measured with an accuracy of $\pm 2\%$ while the energy steps are ~ 0.6 keV. The differential cross section having statistical errors ranging below 3% and the energy steps are ~ 1 keV. All these data were measured with the Karlsruhe neutron time-of-flight-spectrometer using the 57 m flight path. The solid curves is the result of a single channel, multi-level R-matrix calculation

simultaneous R-matrix multilevel fit. In the present case the optimum fit was obtained by a visual comparison of the measured and the calculated cross sections. R-matrix calculations were made with the Nebe-Kirouac code ²⁾ starting with parameters given in BNL-325 ³⁾. From the analysis the resonance at 1254 keV was identified as the isobaric analog of the first excited state ($J = 1/2^+$ $E_x = 1.402$ MeV) in ²⁹Al. This identification took also into account experimental radiative neutron capture data ⁴⁾ and shell-model calculations for the radiative width ⁵⁾.

Using first order perturbation theory Weigmann et al. ¹⁾ have shown that a "zerth order" guess of the average mixing matrix element $\overline{\langle T=3/2 | V | T_i = 1/2 \rangle}_o$ is defined by the equation

$$\Gamma_n^o (T=3/2) = \left| \overline{\langle T=3/2 | V | T_i = 1/2 \rangle}_o \right|^2 \sum_i \frac{\Gamma_n(i)}{|E_i - E(T=3/2)|^2}$$

where Γ_n^o is the reduced width and the average is over all $T = 1/2$ states of the same J^π labelled by i .

A lower limit $\overline{\langle T=3/2 | V | T_i = 1/2 \rangle}_{\min}$ is obtained by assuming constructive interference of all resonances

$$\Gamma_n^o (T=3/2) = \left| \overline{\langle T=3/2 | V | T_i = 1/2 \rangle}_{\min} \right|^2 \left| \sum_i \frac{\Gamma_n^o(i)}{E_i - E(T=3/2)} \right|^2$$

The use of the results from our resonance analysis in addition to further results from BNL-325 for two $J=1/2^+$ resonance below 1 MeV provided the mixing matrix elements given in Tab. 1. From this table which also compares our

Quantity	²⁸ Si+n For the assigned IAR at 1254 MeV	²⁸ Si+n If 1160 keV le- vel would be the IAR	²⁴ Mg+n For 1567 keV J=1/2 ⁺ , T=3/2 le- vel from ref. 1
$\frac{\Gamma_n^o(T=3/2)}{\Gamma_n^o(T=1/2)}$	14 %	7 %	18 %
$\overline{\langle T=3/2 V i \rangle}_o$ in keV	112	58	150
$\overline{\langle T=3/2 V i \rangle}_{\min}$ in keV	77	42	90

Table 1: Estimate of isospin impurity for ²⁸Si+n and comparison with ²⁴Mg+n

results with Weigmann's data for the $T = 3/2$ s-wave resonance of ^{24}Mg , it can be seen that the isospin mixing matrix element for these two nuclei are comparable.

References

- 1) H. Weigmann, R.L. Macklin, J.A. Harvey, Phys. Rev. C14 (1976) 1328
- 2) G.J. Kirouac, J. Nebe, KFK 1069 (1969)
- 3) S.F. Mughabghab, D.I. Garber, BNL-325, Vol. 1 (1973)
- 4) J.W. Boldeman, B.J. Allen, A.R. de L. Musgrove, R.K. Macklin, Nucl. Phys. A252 (1975) 62
- 5) M.J.A. De Voigt, B.H. Wildenthal, Nucl. Phys. A206 (1973) 705

3.6.2 Precision Measurements of Fission Cross Section Ratios for
 ^{239}Pu and ^{240}Pu Relative to ^{235}U

K. Kari, S. Cierjacks, D. Erbe, B. Leugers, G. Schmalz

Institut für Angewandte Kernphysik des Kernforschungszentrums Karlsruhe

The fission cross sections of ^{239}Pu and ^{240}Pu are fundamental data in reactor technology. Precise values are important for optimizing the design of fast breeder reactors. Despite a large number of measurements, the cross sections for these nuclei are still insufficiently known. Individual measurements still show deviations ranging between 10 and 15 %. These discrepancies are mainly due to the fact that both nuclei have small α half-lives and thus are highly radioactive which complicates precise cross section measurements. A new measurement aiming at high precision was carried out for both Pu-isotopes between 0.5 - 20 MeV employing time-of-flight techniques ¹⁾. The measurements were conducted using gas scintillation counters of a special design, capable to measure fission events in the presence of extremely high α -background. Since flux measurements in fast neutron spectra are difficult to perform, fission cross sections were measured relative to the fission cross section of ^{235}U , the internationally recommended standard. As a typical result Fig. 1 shows the fission cross section ratio for ^{239}Pu in the energy region from 0.1 - 20 MeV on a semilogarithmic scale. In this diagram our data are compared with the values of a recent measurement in the Lawrence Livermore Laboratory, carried out by Behrens et al. ²⁾. It can be seen that rather good agreement exists between the two data sets, except in the range above about 16 MeV, which is, however, unimportant for a fast reactor spectrum. In the decay regions around 6 and 12 MeV there seems to exist also a small discrepancy between in both energy scales.

References

- 1) S.W. Cierjacks, B. Leugers, K. Kari, B. Brotz, D. Erbe, D. Gröschel, G. Schmalz, F. Voß, Proc. NEA-Specialist Meeting on Fast-Neutron Fission Cross Sections, Argonne, June 1976, Report ANL-76-90, p.96
- 2) J.W. Behrens, C.W. Carlson, Proc. NEA-Specialists Meeting on Fast Neutron Fission Cross Sections, Argonne, June 1976, Report ANL-76-90, p. 47

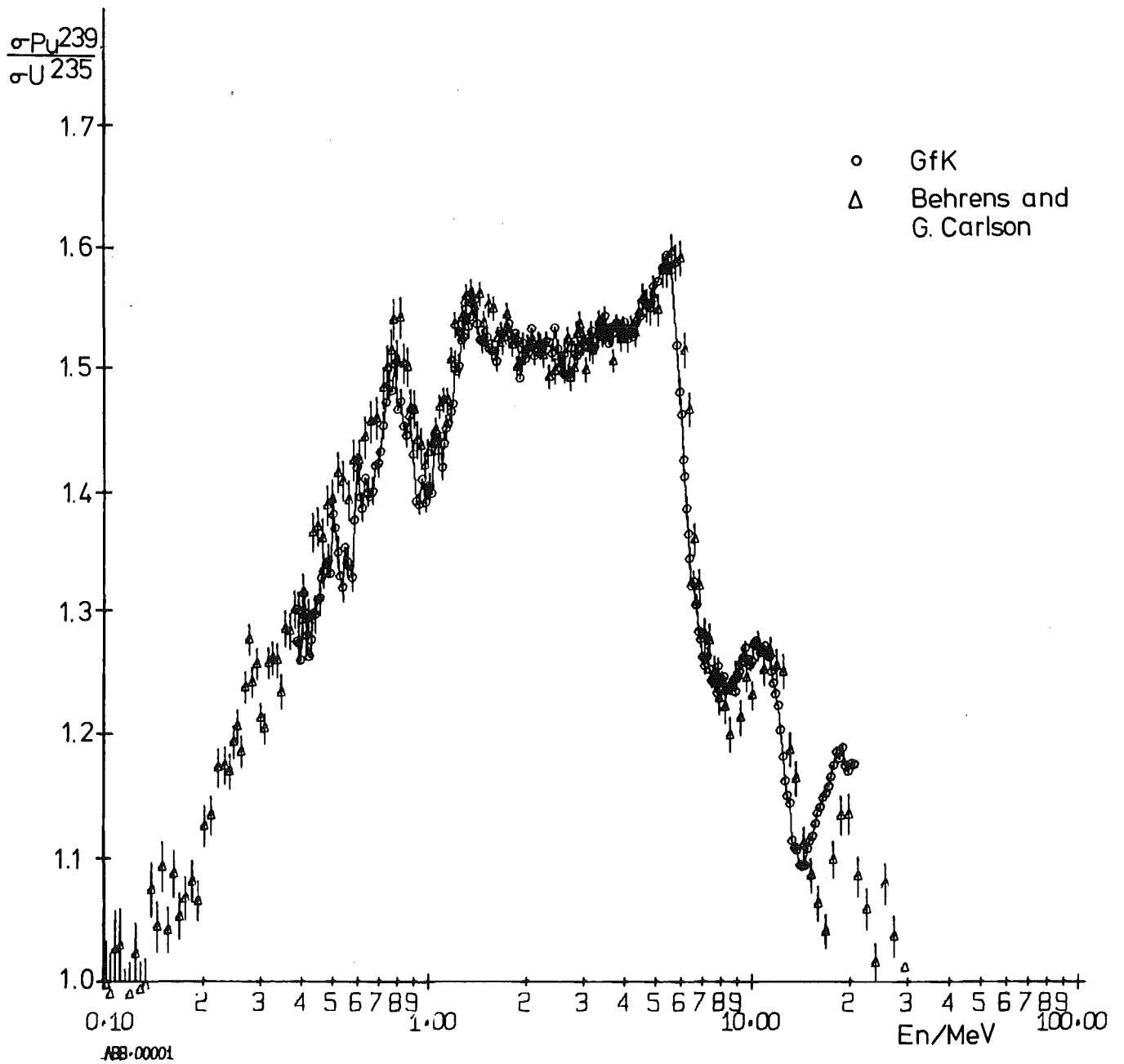


Fig. 1: The fission cross section ratio of $^{239}\text{Pu}/^{235}\text{U}$. The present results (open circles) are compared with data obtained in a recent experiment at the Lawrence Livermore Laboratory, ref. 2 (open triangles). There is good agreement between both data sets except above ~ 16 MeV. A slight difference in both absolute energy scales appears in the decay regions near 6 and 12 MeV

3.7 Measurements on Nuclear Fission

3.7.1 Determination of the Fission Barrier of ^{232}Pu from β -Delayed Fission

D. Habs, H. Klewe-Nebenius, B. Neumann and H.J. Specht
 Physikalisches Institut der Universität Heidelberg and
 V. Metag, Max-Planck-Institut für Kernphysik, Heidelberg

The investigation of β -delayed fission ¹⁾ allows to determine fission barrier heights in nuclei far off the stability line.

In the irradiation of ^{237}Np with α -particles of 104 MeV a delayed fission activity with a half-life of (55 ± 7) s and a cross section of (5 ± 1) nb has been observed. Reaction products recoiling from a $100 \mu\text{g}/\text{cm}^2$ thick target were stopped 5 mm downstream in a $100 \mu\text{g}/\text{cm}^2$ thick carbon foil. After an irradiation of 200 s the catcher foil was moved pneumatically in between two closely spaced surface barrier detectors positioned 60 cm away from the activated target for registration of correlated fission fragments and α -particles.

From a detailed α -spectroscopy involving α - α coincidences to clarify mother-daughter relations the production cross sections of all final nuclei have been determined. A comparison with calculated cross sections using an evaporation model code allows to assign the observed activity to the fission of ^{232}Pu following the electron capture decay of ^{232}Am ²⁾.

The fission probability can be determined experimentally by measuring the cross section for the delayed fission activity and the cross section for the electron capture decay of the precursor nucleus. The latter has been inferred from the observation of the α -decay chain of ^{232}Am using predicted α/EC branching ratios ³⁾.

On the other hand, the probability for fission following electron capture decay may also be calculated from

$$(1) P_{\text{EC},\text{F}} = \frac{\sigma_{\text{EC},\text{F}}}{\sigma_{\text{EC}}} = \frac{\int_0^{Q_{\text{E}}} f(Q_{\text{E}} - E) S_{\text{E}}(E) \frac{\Gamma_{\text{f}}}{\Gamma_{\text{f}} + \Gamma_{\gamma}} dE}{\int_0^{Q_{\text{E}}} f(Q_{\text{E}} - E) S_{\text{E}}(E) dE} = f(Q_{\text{E}}, E_{\text{A},\text{B}}, \omega_{\text{A},\text{B}})$$

The product of the integrated Fermi function f and the β -strength function S_{β} accounts for the population of excited states in the daughter nucleus, and the ratio $\frac{\Gamma_f}{\Gamma_{\gamma} + \Gamma_f}$ describes the competition between fission and γ cascades leading to the ground state.

Considering the near constancy of Γ_{γ} and S_{ϵ} together with the weak (quadratic) energy dependence of the Fermi function the main energy dependence of the integrand in (1) stems from the exponential variation of Γ_f for subbarrier fission. Thus, the folded fission probability is essentially determined by the barrier parameters (heights E_A , E_B and curvature energies $\hbar\omega_A$, $\hbar\omega_B$) and Q_{ϵ} -value for the electron capture decay which is rather reliably predicted by mass formulae.

The fission probability $P_{EC,F} = (1.3 \pm 0.8)^4$ % found for the observed fission activity yields a fission barrier height of (5.3 ± 0.4) MeV for ^{232}Pu according to eq. (1). The systematic and smooth trend of experimentally determined barrier heights shows that this value refers to the inner barrier. The newly determined fission barrier height exceeds theoretical predictions using the shell correction approach of Strutinsky by about 2 MeV. The discrepancy between theoretical and experimental fission barrier heights previously observed in particular for U and Th isotopes ⁴⁾ points to severe defects in the procedure of calculating static fission barriers and, at the same time, rises doubts in the predicted stability of superheavy nuclei.

References

- 1) N.K. Skobelev, Sov. J. Nucl. Phys. 15 (1972) 249
- 2) B. Neumann, Diplomarbeit, Universität Heidelberg (1977)
- 3) H. Münzel and K.A. Keller, KFA Report 1059 (1969)
- 4) H.J. Specht, Nukleonika 20 (1975) 717

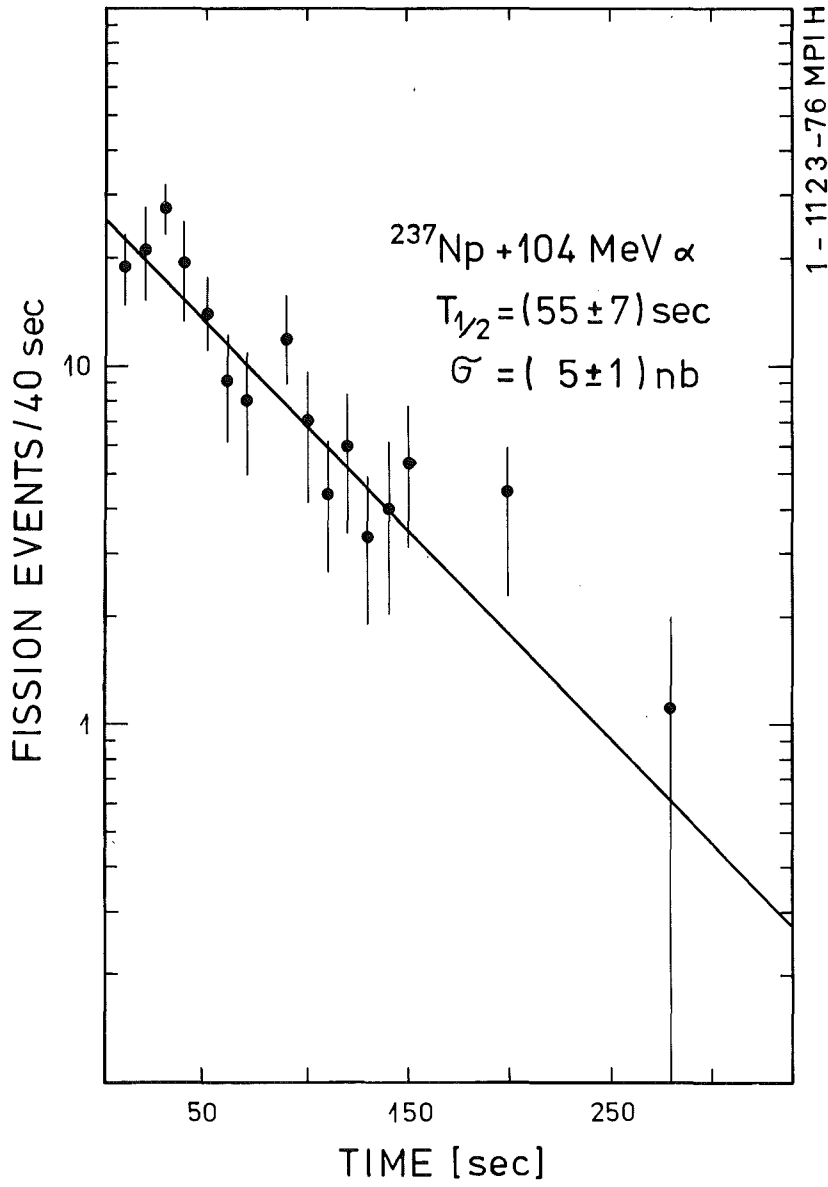


Fig. 1: Decay curve of a fission activity produced in the irradiation of ^{237}Np with 104 MeV α -particles

Publications in 1976 using the Karlsruhe Isochronous Cyclotron

Nuclear Reactions

Eyrich, W.; Hofmann, A.; Scheib, U.; Schneider, S.; Vogler, F.; Rebel, H.
Study of Prolate-Oblate Effects by Use of Particle - γ Angular Correlations
in the Reaction $^{24}\text{Mg}(\alpha, \alpha')^{24}\text{Mg}$
2. Conference on Radial Shape of Nuclei, Cracow, Poland, June 22-25, 1976

Gils, H.J.
Isoskalare Übergangswahrscheinlichkeiten aus Streuexperimenten mit
 α -Teilchen und Untersuchungen der Neutronenkollektivität in ^{208}Pb
Expertentreffen der Kernphysiker, Schleching, 2.-12. März, 1976

Rebel, H.; Gils, H.J.; Knüpfer, W.
Experimental Studies of Neutron Collectivities by α -particle Scattering and
Some Implications for Giant Resonance Excitations
14. Internat. Winter-Meeting on Nuclear Physics, Bormio/Italien, Januar 19-24,
1976

Rebel H.
Realistische Coulomb-Potentiale bei Coupled-Channel-Rechnungen für die
Streuung von α -Teilchen und ^{16}O -Ionen an deformierten Kernen
KFK-2247 (Januar 1976)

Gils, H.J.; Rebel, H.; Buschmann, J.; Klewe-Nebenius, H.; Nowicki, G.;
Nowatzke, W.
Experimentelle Untersuchungen der Unterschiede zwischen den kollektiven
Eigenschaften von Protonen und Neutronen in $^{204}, ^{206}, ^{208}\text{Pb}$ durch α -Teilchen-
Streuung: RMS-Radien und Oktupol-Übergangsraten
Frühjahrstagung DPG und OEPG, Kernphysik, Baden/Oesterr., 29. März - 2. April
1976. Verhandlungen der Deutschen Physikalischen Gesellschaft, R.6,
Bd 11 (1976) S. 857-58

Bechtold, V.; Friedrich, L.; Strassner, G.; Breuer, H.; Doll, P.;
Knöpfle, K.T.; Mairle, G.; Sessler, A.; Wagner, G.J.
Spinbestimmung von $1p$ -Lochzuständen in ^{15}N mit vektorpolarisierten Deuteronen
Frühjahrstagung DPG und OEPG, Kernphysik, Baden/Österr., 29. März-2. April
1976. Verhandlungen der Deutschen Physikalischen Gesellschaft, R.6, Bd 11
(1976) S. 860

Kropp, J.; Buschmann, J.; Wisshak, K.; Faust, H.; Klewe-Nebenius, H.;
Rebel, H.
Anregungsfunktionen von $(^6\text{Li}, xn+p)$ -Reaktionen bei Energien bis $E(\text{Li})=156$ MeV
Frühjahrstagung DPG und OEPG, Kernphysik, Baden/Österr., 29. März - 2. April
1976. Verhandlungen der Deutschen Physikalischen Gesellschaft, R.6, Bd 11
(1976) S. 891

Eyrich, W.; Gerbig, V.; Hofmann, A.; Scheib, U.; Schneider, S.; Vogler, F.; Rebel, H.
Teilchen- γ -Winkelkorrelationen als Mittel zur Untersuchung von Kernreaktionen
Frühjahrstagung DPG und OEPG, Kernphysik, Baden/Österr., 29. März - 2. April
1976. Verhandlungen der Deutschen Physikalischen Gesellschaft, R.6, Bd 11
(1976) S. 895

Abdel-Wahab, M.S.; Bialy, J.; Junge, M.; Schmidt, F.K.; Bechtold, V.; Friedrich, L.
Experimentelle Untersuchung der Aufbruchreaktion $dp \rightarrow ppn$ am vektorpolarisierten
Deuteronenstrahl des Karlsruher Isochronzyklotrons
Frühjahrstagung DPG und OEPG, Kernphysik, Baden/Österr., 29. März - 2. April
1976. Verhandlungen der Deutschen Physikalischen Gesellschaft, R.6, Bd 11
(1976) S. 965

Abdel-Wahab, M.S.; Bechtold, V.; Bialy, J.; Friedrich, L.; Junge, M.; Schmidt, F.K.; Strassner, G.
Vektoranalysierstärken der elastischen Deuteron-Proton- und Deuteron-Deuteron-
Streuung bei 52 MeV.
Frühjahrstagung DPG und OEPG, Kernphysik, Baden/Österr., 29. März - 2. April
1976. Verhandlungen der Deutschen Physikalischen Gesellschaft, R.6, Bd 11
(1976) S. 966

Gils, H.J.; Rebel, H.
Differences between neutron and proton density RMS-radii of $^{204,206,208}\text{Pb}$
determined by 104 MeV α -particle scattering
2. Conference on Radial Shape of Nuclei, Cracow, Poland, June 22-25, 1976
Physical Rev. C, 13 (1976) S. 2159-165

Kropp, J.; Klewe-Nebenius, H.; Buschmann, J.; Rebel, H.; Faust, H.; Gils, H.J.; Rieder, J.; Wisshak, K.
Excitation functions of $^{191+193}\text{Ir}$, ^{197}Au ($^6\text{Li}, xn+yp$) compound nuclear reactions
at $E(\text{Li}) = 48 - 156$ MeV
KFK 2342 (August 76)

Eyrich, W.; Hofmann, A.; Scheib, U.; Schneider, S.; Vogler, F.; Rebel, H.
Alpha-gamma angular correlation measurements as a sensitive method determining
the sign of the nuclear quadrupole deformation
Phys. Lett. 63B (1976) S. 406-8

Gils, H.J.; Rebel, H.; Buschmann, J.; Klewe-Nebenius, H.; Nowicki, G.; Nowatzke, W.
Nuclear matter sizes and isoscalar octupole transition rates of $^{204,206,208}\text{Pb}$
from 104 MeV α -particle scattering
Zeitschrift für Physik A, 279 (1976) S. 55-68

Boschitz, E.T.; Hefter, E.F.; Heidt, V.; Weddigen, Ch.
Die $^{14}\text{N}(d,p)^{15}\text{N}$ Reaktion
Frühjahrstagung DPG und OEPG, Kernphysik, Baden/Österr., 29. März - 2. April
1976, Verhandlungen der Deutschen Physikalischen Gesellschaft, R.6, Bd 11
(1976) S. 932

Kluge, W.; Matthaey, H.; Sakamoto, Y.; Schlüfter, R.; Schneider, H.
Experimentelle und theoretische Analyse der Deuteronenaufbruchreaktion
 ${}^2\text{H}(d, pd)n$ bei $T(d) = 52$ MeV
Frühjahrstagung DPG und OEPG, Kernphysik, Baden/Österr., 29. März - 2. April
1976. Verhandlungen der Deutschen Physikalischen Gesellschaft, R.6, Bd 11
(1976) S. 966

Neutron Physics

Voss, F.
Neutron Energy Calibration at the Karlsruhe Time-of-Flight Facility
Neutron Interlab. Seminar CBNM, Geel/Belgien, November 12-14, 1975

Cierjacks, S.; Schouky, I.
Elastische Neutronenstreuung an ${}^{16}\text{O}$ und ${}^{28}\text{Si}$
Frühjahrstagung DPG und OEPG, Kernphysik, Baden/Österr., 29. März - 2. April
1976. Verhandlungen der Deutschen Physikalischen Gesellschaft, R.6, Bd 11
(1976) S. 823-24

Leugers, B.; Kari, K.
Eine Gasszintillator-Anordnung zur Messung von Spaltfragmenten bei hohem
 α -Untergrund
Frühjahrstagung DPG und OEPG, Kernphysik, Baden/Österr., 29. März - 2. April
1976, Verhandlungen der Deutschen Physikalischen Gesellschaft, R.6, Bd 11
(1976) S. 843

Voss, F.; Schmalz, G.
Präzisionsmessungen der Energien von Neutronenresonanzen im MeV-Bereich
Frühjahrstagung DPG und OEPG, Kernphysik, Baden/Österr., 29. März - 2. April
1976. Verhandlungen der Deutschen Physikalischen Gesellschaft, R.6, Bd 11
(1976) S. 917

Cierjacks, S.; Leugers, B.; Kari, K.; Brotz, B.; Erbe, D.; Gröschel, D.;
Schmalz, G.; Voss, F.
Measurements of neutron induced fission cross section ratios at the Karlsruhe
Isochronous Cyclotron.
Specialists Meeting on Fast Neutron Fission Cross Sections, Argonne, Ill.,
June 28-30, 1976

Leugers, B.; Cierjacks, S.; Brotz, P.; Erbe, D.; Gröschel, D.; Schmalz, G.;
Voss, F.
The ${}^{235}\text{U}$ and ${}^{238}\text{U}$ neutron induced fission cross sections relative to the
 $\text{H}(n, p)$ cross section
Specialists Meeting on Fast Neutron Fission Cross Sections, Argonne, Ill.,
June 28-30, 1976

Cierjacks, S.; Erbe, D.; Kari, K.; Leugers, B.; Schmalz, G.; Schouky, O.;
Voss, F.
Messung von Wirkungsquerschnitten
In: Projekt Schneller Brüter. 2. Vierteljahresbericht 1976.
KFK-1276/2 (November 1976) S. 121/1-5

Materials research

Ehrlich, K.; Gross, R.
Zyklotronbestrahlungen zur Simulation der Porenbildung in metallischen Werkstoffen
Frühjahrstagung DPG, Festkörperphysik, Freudenstadt, 5.-9. April 1976.
Verhandlungen der Deutschen Physikalischen Gesellschaft, R.6, Bd 11 (1976) 632

Herschbach, K.
Simulationsversuche am Zyklotron zum In-Pile-Kriechen von metallischen Werkstoffen
Frühjahrstagung DPG, Festkörperphysik, Freudenstadt, 5.-9. April 1976.
Verhandlungen der Deutschen Physikalischen Gesellschaft, R.6, Bd 11 (1976) S. 632-33

Maier, P.; Ruoss, H. Seibt, E.
Strahlenresistenzverhalten von Al₅ Supraleitern
Frühjahrstagung DPG, Festkörperphysik, Freudenstadt, 5.-9. April 1976.
Verhandlungen der Deutschen Physikalischen Gesellschaft, R.6, Bd 11 (1976) S. 712-13

Seibt, E.; |HRSG. |; Dustmann, C.H.; Jüngst, K.P.; Komarek, P.; Krafft, G.; Krauth, H.; Maier, P.; Ries, G.; Schauer, W.; Schmidt, C.; Seibt, E.; Turowski, P.; |MITARB. |
Supraleitertechnologie für Fusionsmagnete
KFK-2359 (November 76)

Solid State Physics

Krill, G.; Lapierre, M.F.; Gautier, F.; Robert, C.; Czjzek, G.; Fink, J.; Schmidt, H.
Electronic and Magnetic Properties of the Pyrite-Structure Compound NiS₂: Influence of Vacancies and Copper Impurities
Journal of Physics C, 9 (1976) S. 761-82

Czjzek, G.; Fink, J., Schmidt, H.; Blanckenhagen P. von; Krill, G.; Lapierre, M.F.; Robert, C.; Panissod, P.; Gautier, F.
Untersuchungen von magnetischen Strukturen und Phasenübergängen in NiS(2-x)Se(x) durch Moessbauerspektroskopie an ⁶¹Ni und Neutronenbeugung
Frühjahrstagung DPG, Festkörperphysik, Freudenstadt, 5.-9. April 1976.
Verhandlungen der Deutschen Physikalischen Gesellschaft, R.6, Bd 11 (1976) 533

Czjzek, G.; Fink, J.; Schmidt, H.; Krill, G.; Lapierre, M.F., Panissod, P.; Gautier, F.; Robert, C.
An investigation of magnetic structures and phase transitions in NiS(2-x)Se(x) by ⁶¹Ni-Moessbauer spectroscopy
Journal of Magnetism and Magnetic Materials, 3 (1976) S. 58-60

Fink, J.; Czjzek, G.; Schmidt, H.; Krill, G.; Lapierre, M.F.; Gautier, F.; Robert, C.
An investigation of NiS₂ by ⁶¹Ni-Moessbauer spectroscopy: influences of vacancies and copper impurities
Journal of Magnetism and Magnetic Materials, 3 (1976) S. 202-203

Hartrott, M. von; Hadijuana, J.; Nishiyama, K.; Quitmann, D.; Riegel, D.; Schweickert, H.
Nuclear spin relaxation of Xe in liquid Te
Zeitschrift für Physik A278 (1976) S. 303-308

Crececius, G.; Maletta, H.; Hauck, J.; Institut für Festkörperforschung der Kernforschungsanlage Jülich GmbH
Fink, J.; Czjzek, G.; Schmidt, H.; Morariu, M.
Elektronische Struktur und Hyperfeinfeldwechselwirkungen in der Mischreihe $Dy(Fe(x)Ni(1-x))_3$
Frühjahrstagung DPG, Festkörperphysik, Freudenstadt, 5.-9. April 1976.
Verhandlungen der Deutschen Physikalischen Gesellschaft, R.6, Bd 11 (1976) 625

Krill, G.; Panissod, P.; Lapierre, M.F.; Czjzek, G.; Fink, J.; Schmidt, H.; Küntzler, R.
Physical properties of the $NiS(2-x)Se(x)$ compounds with pyrite structure: occurrence of an antiferromagnetic metallic phase.
5. Internat. Conference on Solid Compounds of Transition Elements, Uppsala, June 21-25, 1976

Krill, G.; Lapierre, M.F.; Panissod, P.; Robert, C.; Gautier, F.; Czjzek, G.; Fink, K.; Schmidt, H.; Blankenhagen, P. von;
Covalency effects and the metal-insulator transition in $NiS(2-x)Se(x)$
Internat. Conference on the Applications of the Moessbauer Effect, Corfu, September 13-17, 1976

Engineering

Essig, G.
Zur Aktivierung von Maschinenteilen für Abtragsmessungen
Kerntechnik, 18 (1976) S. 470-74

Nuclear Medicine

Michel, F.; Münzel, H.; Schulz, F.; Schweickert, H.
Statusbericht über die ^{123}J -Produktion am Karlsruher Isochron Zyklotron
Jod-123-Panel, Jülich, 13. Februar, 1976

Nuclear Spectroscopy

Faust, H.; Wisshak, K.; Klewe-Nebenius, H.; Rebel, H.; Gils, H.J.; Hanser, A.
Die $L=4$ Übergangswahrscheinlichkeit aus der inelastischen α -Streuung an ^{60}Ni und der direkten Beobachtung des $4_1^+ \rightarrow 0^+$ -Übergangs nach dem Zerfall von ^{60}Co
Frühjahrstagung DPG und OEPG, Kernphysik, Baden/Österr., 29. März - 2. April 1976. Verhandlungen der Deutschen Physikalischen Gesellschaft, R.6, Bd 11 (1976) S. 840-41

Wisshak, K.; Hanser, A.; Klewe-Nebenius, H.; Buschmann, J.; Rebel, H.; Faust, H.; Toki, H.; Faessler, A.
Das Niveauschema von ^{143}Eu
Frühjahrstagung DPG und OEPG, Kernphysik, Baden/Österr., 29. März - 2. April 1976. Verhandlungen der Deutschen Physikalischen Gesellschaft, R.6, Bd 11 (1976) S. 912

Wisshak, K.; Hanser, A.; Klewe-Nebenius, H.; Buschmann, J.; Rebel, H.; Faust, H.; Toki, H.; Faessler, A.
Experimental studies of the level scheme of ^{143}Eu and a generalized decoupling model description
Zeitschrift für Physik A277 (1976) S. 129-39

Collignon, J.

Messung der HFS-Aufspaltung und des $g(I)$ -Faktors zur Bestimmung der HFS-Anomalie von ^{80}Rb
Diplomarbeit, Universität Mainz, 1976

Nuclear Chemistry

Misaelides, P.

Untersuchung der Anregungsfunktionen für ^3He - und α -Reaktionen mit ^{107}Ag und ^{109}Ag
Dissertation, Universität Karlsruhe 1976; KFK-2311 (June 76)

Münzel, H.; Michel, F.; Coetzee, P.P.; Krivan, V.

Utilization of cyclotron produced fast neutrons for the activation analysis of oxygen
1976 Internat. Conference: Modern Trends in Activation Analysis, München, September 13-17, 1976

Technical Development

Kappel, W.; Karbstein, W.; Kneis, W.; Möllenbeck, J.; Schweickert, H.; Volk, B.

CICERO, ein interaktives Programmsystem für den rechnerunterstützten Zyklotronbetrieb unter Verwendung von CAMAC
Frühjahrstagung der Studiengruppe für Nukleare Elektronik, Arbeitsgemeinschaft der Großforschungseinrichtungen, Stuttgart, 22.-24. März, 1976

Haushahn, G.; Möllenbeck, J.; Schatz, G.; Schulz, F.; Schweickert, H.
Status Report of the Axial Injection System at the Karlsruhe Isochronous Cyclotron

Frühjahrstagung DPG und OEPG, Kernphysik, Baden/Österr., 29. März - 2. April 1976. Verhandlungen der Deutschen Physikalischen Gesellschaft, R.6. Bd 11 (1976) S. 809

Cierjacks, S.; Schmalz, G.; Erbe, D.; Voss, F.

Das verbesserte Neutronen-Flugzeitspektrometer am Karlsruher Isochronzyklotron

Frühjahrstagung DPG und OEPG, Kernphysik, Baden/Österr., 29. März - 2. April 1976. Verhandlungen der Deutschen Physikalischen Gesellschaft, R.6, Bd 11 (1976) S. 916-17

Schweickert, H.

Status report on the Karlsruhe isochronous cyclotron

13. European Cyclotron Progress Meeting, Milano, May 6-8, 1976

Schulz, F.; Schweickert, H.; |HRSG.|

Operation of the Karlsruhe Isochronous Cyclotron in 1975
KFK-2298 (June 76)